AFRL-SN-RS-TR-2000-30 Vol I (of two)
Final Technical Report
March 2001

INCREASING SECONDARY DATA OR ENHANCED ADAPTIVE DISPLACED PHASE CENTERED ANTENNA APPROACHES

Capraro Technologies, Inc.

Rick S. Blum

APPROVED FOR PUBLIC RELEASE; DISTRIBUTION UNLIMITED.

AIR FORCE RESEARCH LABORATORY
SENSORS DIRECTORATE
ROME RESEARCH SITE
ROME, NEW YORK

Although this report references (*) limited document(s) on pages 35 and 54 no limited information has been extracted.

This report has been reviewed by the Air Force Research Laboratory, Information Directorate, Public Affairs Office (IFOIPA) and is releasable to the National Technical Information Service (NTIS). At NTIS it will be releasable to the general public, including foreign nations.

AFRL-SN-RS-TR-2001-30 Vol I (of two) has been reviewed and is approved for publication.

APPROVED: David B. Bunker

DAVID B. BUNKER
Project Engineer

FOR THE DIRECTOR: Robert G. Polce

ROBERT G. POLCE, Chief
Rome Operations Office
Sensors Directorate

If your address has changed or if you wish to be removed from the Air Force Research Laboratory Rome Research Site mailing list, or if the addressee is no longer employed by your organization, please notify AFRL/SNRT, 26 Electronic Pky, Rome. NY 13441-4514. This will assist us in maintaining a current mailing list.

Do not return copies of this report unless contractual obligations or notices on a specific document require that it be returned.

REPORT DOCUMENTATION PAGE	Form Approved OMB No. 0704-0188

1. AGENCY USE ONLY *(Leave blank)*	2. REPORT DATE	3. REPORT TYPE AND DATES COVERED
	MARCH 2001	Final Mar 97 - Feb 98

4. TITLE AND SUBTITLE
INCREASING SECONDARY DATA OR ENHANCED ADAPTIVE DISPLACED PHASE CENTERED ANTENNA APPROACHES

5. FUNDING NUMBERS
C - F30602-97-C-0065
PE - 62702F
PR - 4506
TA - 11
WU - PJ

6. AUTHOR(S)
Rick S. Blum

7. PERFORMING ORGANIZATION NAME(S) AND ADDRESS(ES)
Prime: Capraro Technologies, Inc.
311 Turner Street - Suite 410
Utica NY 13501

Sub: Leigh University
EECS Department
19 Memorial Drive West
Bethlehem PA 18015

8. PERFORMING ORGANIZATION REPORT NUMBER
N/A

9. SPONSORING/MONITORING AGENCY NAME(S) AND ADDRESS(ES)
Air Force Research Laboratory/SNRT
26 Electronic Pky
Rome NY 13441-4514

10. SPONSORING/MONITORING AGENCY REPORT NUMBER
AFRL-SN-RS-TR-2001-30
Vol I (of two)

11. SUPPLEMENTARY NOTES
Air Force Research Laboratory Project Engineer: David B. Bunker/SNRT/(315) 330-2345

12a. DISTRIBUTION AVAILABILITY STATEMENT
APPROVED FOR PUBLIC RELEASE; DISTRIBUTION UNLIMITED.

12b. DISTRIBUTION CODE

13. ABSTRACT *(Maximum 200 words)*

A study of space-time adaptive processing in nonhomogeneous environments is presented. The results produced are logically organized as investigations into three different but related topics. The first topic can be summarized as an investigation of the performance of partially adaptive space-time adaptive processing schemes using measured (MCARM) data. The second topic considers the development of a new set of space-time processing algorithms, which use prior knowledge to reduce the number of parameters, which need to be adapted. The new schemes were tested using MCARM data. The final topic provides analytical realistic cases where the reference or training data may have different statistics from the data in the cell under test. Such equations have not yet appeared in the literature and they are useful for understanding the performance of space-time adaptive processing (STAP) schemes when they are tested with MCARM data.

14. SUBJECT TERMS
Space Time Adaptive Processing (STAP), Adaptive Array Processing (ASAP), Estimation Using Mismatched Statistics, Airborne Radar Signal Processing

15. NUMBER OF PAGES
120

16. PRICE CODE

17. SECURITY CLASSIFICATION OF REPORT	18. SECURITY CLASSIFICATION OF THIS PAGE	19. SECURITY CLASSIFICATION OF ABSTRACT	20. LIMITATION OF ABSTRACT
UNCLASSIFIED	UNCLASSIFIED	UNCLASSIFIED	UL

Table of Contents

List of Figures

Chapter 1

Chapter 2

List of Tables

INTRODUCTION

This report documents the work done by Lehigh University under contract F30602-97-C-0065-01. This work involved completing tasks 4.1.1 and 4.1.2 of the original contract. The results produced are logically organized as investigations into three different but related topics. Each of these topics forms one chapter in this report. Each of these chapters is self-contained and includes an introduction and a conclusion. The first chapter includes an expanded version of work proposed under task 4.1.1. This work can be summarized as an investigation of the performance of partially adaptive space-time adaptive processing schemes using MCARM data. The second chapter includes an expanded version of work proposed under task 4.1.2. This work can be summarized as the development of a new set of space-time processing algorithms which use prior knowledge to reduce the number of parameters which need to be adapted. The new schemes were tested using MCARM data. The final chapter provides analytical expressions for evaluating the performance of space-time processing schemes in realistic cases where the reference or training data may have different statistics from the data in the cell-under-test. Such equations have not yet appeared in the literature and they are useful for understanding the performance of space-time adaptive processing schemes when they are tested with MCARM data. The final chapter has results which are applicable to both task 4.1.1 and task 4.1.2.

Chapter 1 : Task 4.1.1

1. INTRODUCTION

In airborne radar, target detection is often limited by ground clutter and other forms of interference. Platform motion causes Doppler shifts in interference returns, making Doppler filtering alone ineffective. In such cases Space-Time Adaptive Processing (STAP) offers a potential solution.

STAP has been an active research topic for at least the last two decades. Much of the interest was generated by the research in [1] and [2]. Since then several algorithms have been proposed and evaluated using simulated radar data. With the recent improvements in phased array antenna and digital signal processing technology, a STAP-based airborne radar system is becoming an attractive alternative for detection of airborne targets competing with strong clutter returns and jamming, as compared to classical low-sidelobe beamforming [3].

Current STAP research efforts [4] are focused on a number of interesting issues. Performance evaluation of several competing STAP approaches is the topic of this report. In most previous research, STAP algorithms were evaluated using optimistic simulated data or by manipulating stationary platform measurements to emulate motion. While simulated data is very useful in the development and analysis of algorithms, a more complete evaluation includes using actual recorded radar data. Thus, in this report, we compare various STAP schemes using measured airborne data. A general formulation of a useful class of STAP processing approaches is developed. This formulation, which includes most linear processing schemes, unifies the techniques considered.

Assume the radar transmits a coherent burst of $\mathbf{M}$ pulses at a constant pulse repetition frequency $f_r = \mathbf{1/T_r}$, where $\mathbf{T_r}$ is the pulse-repetition-interval (PRI). The time interval over which the waveform returns are collected is commonly referred to as the coherent-processing-interval (CPI). The radar antenna used is an array antenna with $\mathbf{N}$ identical elements. Denote the observation corresponding to the $\mathbf{i^{th}}$ antenna element, the

j^{th} pulse and the k^{th} range cell as $x_{i,j,k}$. It is convenient to denote the data associated with the k^{th} range cell as

$$\mathbf{X}_k = \left[x_{1,1,k}, x_{2,1,k}, \cdots, x_{N,1,k}, x_{1,2,k}, \cdots, x_{N,M,k}\right]^T \quad (1)$$

where $\mathbf{a}^T$ denotes the transpose of the vector **a.** We will refer to $\mathbf{X}_k$ as a space-time snapshot.

A simple set of STAP schemes that have been suggested can be represented as an inner product of the conjugate of a weight vector **w** and the vector $\mathbf{X}_k$. This inner product

$$z = \mathbf{w}^H \mathbf{X}_k \quad (2)$$

produces the complex quantity **z** whose magnitude is often compared to a threshold to make a decision regarding target presence or absence. The weight vector **w** may depend on the estimated interference-plus-noise environment and on the target of interest. In the well-know sample matrix inversion (SMI) algorithm [2] for example, a popular fully adaptive algorithm, the weight vector is given, to within a scale factor, as

$$\boldsymbol{w} = \boldsymbol{R}^{-1}\boldsymbol{V} \quad (3)$$

where **R** is the estimated interference-plus-noise covariance matrix. The estimate is based on a set of reference data, typically chosen from the surrounding range cells. **V** is the normalized target response ($\mathbf{X}_k$ for a target observed without clutter or noise) [5]. In the case where the interference statistics are known or the estimated covariance matrix is exactly equal to the true covariance matrix, SMI can achieve optimal performance. A fully adaptive STAP scheme, like SMI, requires the formation of an **NM** by **NM** covariance matrix. For moderate **M** and **N**, the computational cost of the computation of $\mathbf{R}^{-1}$ becomes excessive for real-time implementation. Further, schemes which estimate **R** typically require a large set of independent and identically distributed (iid) reference data

vectors to achieve an accurate estimate for moderate **M** and **N**. This requirement may be unrealistic, since measurements [6] indicate that multi-channel airborne radar clutter data is often severely non-homogeneous. For this reason the reference data set available for estimation of clutter statistics is usually quite small. As a result, reduced complexity approaches called partially adaptive STAP (PASTAP) have been developed whose computational cost and reference data requirements are more realistic. Some examples of reduced complexity approaches are given in the next section.

It is important to know how different PASTAP algorithms perform for realistic cases. This issue is studied in this report. In Section 2 we define a general PASTAP scheme and give a detailed description of several specific approaches. Performance comparisons based on measured airborne radar data are presented in Section 3. Conclusions are given in Section 4.

2. Some Reduced Complexity STAP Schemes

STAP is an active research area and new schemes are continually being developed. In order to compare schemes, a standard terminology is useful. Here, we will mainly follow the terminology used in [5]. We caution the reader that other terminology also appears in the literature. We first define a general formulation of a PASTAP approach which encompasses many existing algorithms. Next we describe eight specific approaches which are included in the general formulation. They are

1. Adaptive Displaced Phase-Centered Antenna (ADPCA)
2. subarrayed ADPCA (BDPCA)
3. Beamspace ADPCA (BeamAD)
4. Factored Post Doppler (FTS)
5. subarrayed FTS (BFTS)
6. Extended Factored Approached (EFA)
7. subarrayed EFA (BEFA)

8. Joint-Domain Localized Approach (JDL)

2.1 General STAP Approach

Consider the transformations

$$\tilde{\mathbf{X}}_k(p) = (\mathbf{A}_p \otimes \mathbf{B}_p)^H \mathbf{X}_k ; \qquad p=0,1,2,\ldots,P-1 \tag{4}$$

where $\mathbf{X}_k$ is the space-time snapshot from the $\mathbf{k}^{th}$ range cell and $\mathbf{A}_p$ and $\mathbf{B}_p$ are scheme-dependent matrices. The operations in (4) can be interpreted as a pre-processor applied to the received signals. This pre-processing generates data for the adaptive processing to follow. Note that **P** vectors are produced by the operations in (4). Typically, the pre-processing in (4) performs a coordinate transformation and a selection operation.

We describe the adaptive processing on the $\mathbf{p}^{th}$ vector as

$$y_k(p) = \mathbf{S}^H \mathbf{R}_k^{-1}(p) \tilde{\mathbf{X}}_k(p) / \Phi \tag{5}$$

where

$$\mathbf{R}_k(p) = \frac{1}{Q} \sum_{i=k-Q/2-1, i\neq k-1,k,k+1}^{k+Q/2+1} \tilde{\mathbf{X}}_i(p) \tilde{\mathbf{X}}_i(p)^H \tag{6}$$

and **S** is a scheme-dependent steering vector. $\mathbf{R}_k(p)$ is the interference-plus-noise covariance matrix estimated from **Q** adjacent range cells, excluding the cell-under-test and the two closest range cells. The estimate in (6) is the maximum likelihood estimate if the data samples from the **Q** adjacent range cells are independent and identically distributed with the same complex Gaussian distribution as the interference-plus-noise in the cell-under-test. It is straight-forward to generalize (6) to allow the range cells to be selected differently, including selections which are non-symmetric about the cell-under-test. We do not discuss these generalizations here since we use only the approach suggested in (6) in our tests. The term Φ in the denominator of (5) is the normalization to provide CFAR in homogeneous clutter and is given by

$$\Phi = \sqrt{\mathbf{S}^H \mathbf{R}_k^{-1} \mathbf{S}} \tag{7}$$

In different schemes, $y_k(p)$ may or may not be the final output of interest. If $y_k(p)$ is the final output of interest, its magnitude will be compared to a threshold to decide if target is present. For cases where $y_k(p)$ will be processed further, we assemble the complex outputs from each adaptive processor as

$$\tilde{Y}_k = [y_k(0), y_k(1), \ldots, y_k(P-1)]^T \quad (8)$$

and compute

$$\tilde{Z}_{k,m} = f_m^H \tilde{Y}_k \quad (9)$$

which we call post-processing (after adaptive processing). Typically, f_m is the m^{th} column of a $P \times P$ filter matrix F, and $Z_{k,m}$ is the final output whose magnitude will be compared to a threshold to produce a decision.

2.2 ADPCA and its beamspace version

Define a set of P sub-CPIs $X_k(p)$, $p=0,\ldots,P-1$ in the k^{th} snapshot. Each sub-CPI contains possible target returns from K_s pulses and all N elements. Fig. 1 shows two different ways to form the sub-CPIs. As indicated in Fig. 1, implementation (a) does not overlap pulses. Given M pulses in a CPI where M can be divided by K_t, implementation (a) generates $P=M/K_t$ sub-CPIs. The 0^{th} sub-CPI consists of pulses $0, \ldots, K_t-1$ and the p^{th} sub-CPI consists of pulses $pK_t, \ldots, pK_t+K_t-1$. Implementation (b) forms the sub-CPIs by using the same pulse returns in several sub-CPIs. Given M pulses in a CPI, implementation (b) generates $P=M-K_t+1$ sub-CPIs. The 0^{th} sub-CPI consists of pulses $0, \ldots, K_t-1$ and the p^{th} sub-CPI consists of pulses $p, \ldots, p+K_t-1$. In Fig.1, K_t is set to 3 and in implementation (b), neighboring sub-CPIs overlap 2 pulses. Of course, other overlaping pulse configurations are possible.

The pre-processing we have just described can be put into the framework of (4). B_p is set to I_N which is an $N \times N$ identity matrix and

$$\mathbf{A}_p = \begin{bmatrix} \mathbf{0}_{p(K_t-h)\times K_t} \\ \mathbf{I}_{K_t} \\ \mathbf{0}_{(M-K_t-pK_t+ph)\times K_t} \end{bmatrix} \qquad (10)$$

where the notation $0_{q\times m}$ refers to an $q\times m$ matrix of zeros. **h** indicates the number of pulses which are overlapped. In implementation (a) **h** is set to be zero and in implementation (b) **h** is set to be $\mathbf{K_t-1}$. $\mathbf{A_p}$ is an $\mathbf{M\times K_t}$ selection matrix.

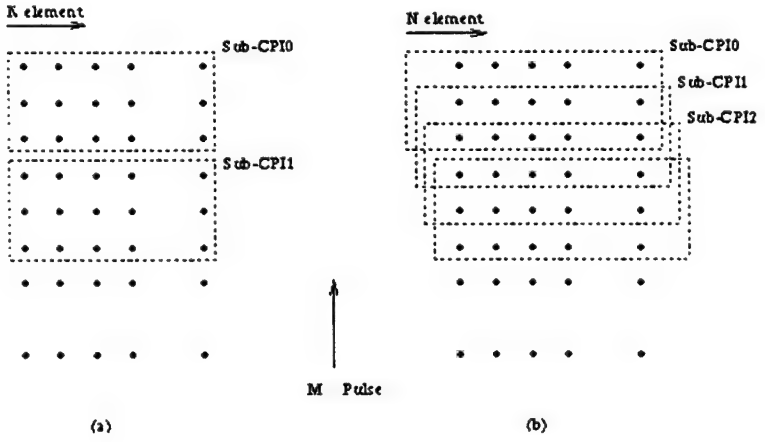

Figure 1) ADPCA sub-CPI formation

The adaptive processing in ADPCA is described by (5) with the steering vector

$$\mathbf{S} = \mathbf{S}_t \otimes \mathbf{S}_s \qquad (11)$$

where $\mathbf{S_s}$ is the $\mathbf{N\times 1}$ spatial steering vector [5] and $\mathbf{S_t}$ is a $\mathbf{K_t\times 1}$ vector, which is composed of the binomial coefficients, with each coefficient altered in sign (start with positive). As a particular example, we have

$$\mathbf{S}_t = (1,-2,1)^T \qquad (12)$$

for a three pulse case.

Typically, post-processing as described in (8) and (9) is employed in ADPCA. In ADPCA **F** is a matrix corresponding to a Doppler filter bank, and $\mathbf{f_m}$ is the filter corresponding to the $\mathbf{m^{th}}$ Doppler frequency. A DFT matrix implements the Doppler filter bank. Thus, a fast fourier transform efficiently computes (9) for all **m**. $|\mathbf{Z_{k,m}}|$, the magnitude of the final output for Doppler bin **m**, is compared to a threshold to test for a target in Doppler bin **m**.

Subarrayed ADPCA and beamspace ADPCA are both beamspace versions of ADPCA. $\mathbf{B_p}$ is used as a beamformer matrix to produce $\mathbf{K_s} \leq \mathbf{N}$ beams. We focus on **Ks**=3 in this report.

In subarrayed ADPCA the beamformer matrix

$$\mathbf{B_p} = \mathbf{G} = \begin{bmatrix} g_0 & 0 & & 0 \\ g_1 & g_0 & & \\ \vdots & g_1 & \ddots & \\ g_{N'-1} & \vdots & & g_0 \\ & g_{N'-1} & \ddots & g_1 \\ & & & \vdots \\ 0 & 0 & & g_{N'-1} \end{bmatrix} \qquad (13)$$

is employed in (4) , where $g = (g_0, g_1, g_2, \ldots, g_{N'-1})^T$ is an **N'x1** vector and $\mathbf{N' = N - K_s + 1}$. The vector **g** can be any of the popular window functions from the DSP or radar literature [7,8]. Only results which use the uniform window are provided here. In our preliminary tests, the uniform window appeared to outperform the other windows we tried so we focused on this choice.

Each vector produced by (4) will be adaptively processed as in (5) where

$$\mathbf{S} = (\mathbf{I_{Kt}} \otimes \mathbf{G})^H \mathbf{S_e} \qquad (14)$$

with $\mathbf{S_e}$ chosen as the steering vector defined by (11). The post processing is the same as in ADPCA.

Beamspace ADPCA is identical to subarrayed ADPCA, but with $\mathbf{B_p = G = [\, f_{N,1}, f_{N,2}, \ldots, f_{N,K_s}\,]}$, where $\mathbf{f_{N,j}}$ $\mathbf{j=1, \ldots, K_s}$ are those columns of $\mathbf{N \times N}$ DFT matrix corresponding to $\mathbf{K_s}$ particular angle bins.

2.3 FTS and subarrayed FTS

In factored post-Doppler STAP [5], Doppler processing is first performed on each spatial channel. Let the Doppler filter applied to the $\mathbf{p^{th}}$ spatial channel be $\mathbf{f_p}$ and assume $\mathbf{f_p}$ is chosen from the set of possible Doppler filters in the $\mathbf{M \times M}$ matrix $\mathbf{F_M = [\, f_0, f_1, \ldots, f_{M-1}]}$. Then the pre-processing is described by (4) with $\mathbf{A_p = f_p}$, $\mathbf{P = M}$, and $\mathbf{B_p = I_N}$. This pre-processing transforms the signal into Doppler space. In this case $\mathbf{p}$ indicates the index of Doppler bin in question. Next, the adaptive processing in (5) is employed with the steering vector defined as in (11) with $\mathbf{K_t = 1}$. Here $\mathbf{S = S_s}$, since $\mathbf{K_t}$ is 1. As for most of the STAP schemes we discuss, tapering could be applied to the steering vector [5]. Post-processing is not usually employed and $\mathbf{|y_k(p)|}$ is compared to a threshold to test for a target in the $\mathbf{p^{th}}$ Doppler bin.

Subarrayed FTS is identical to FTS but with $\mathbf{B_p = G}$ as described in (13). The adaptive processing is as in FTS with the steering vector defined in (14). Here $\mathbf{S_e}$ is the steering vector that is used in the adaptive processing of FTS. Post processing is not employed.

2.4 EFA andsubarrayed EFA

The extended factored approach (EFA) [9] is a slight extension of the factored post-Doppler approach. In EFA, adaptive processing is applied to several adjacent Doppler bins instead of just one. Thus, the pre-processing performs both transformation and selection. In the case considered here, where the scheme adapts over 3 adjacent bins, the pre-processing can be described as in (4) with $\mathbf{A_p = J_p = [\, f_{p-1}, f_p, f_{p+1}]}$ and $\mathbf{B_p = I_N}$.

The other quantities are set in a similar manner as for factored post-Doppler STAP but with the new $\mathbf{A_p}$. For example, the steering vector is obtained from

$$\mathbf{S} = \left(\mathbf{A_p} \otimes \mathbf{B_p}\right)^H \mathbf{V} \qquad (15)$$

where $\mathbf{V}$ is the normalized target response as used in (3). For example, if $\mathbf{f_p}$ correspond to the target Doppler frequency under consideration, the steering vector can be defined as in (11) with $\mathbf{S_t} = [0, 1, 0]^T$.

In subarrayed EFA, the pre-processing is the same as with EFA but with $\mathbf{B_p}$ set as in (13). The adaptive processing is defined as in (5) with $\mathbf{S}$ as in (15).

2.5 Joint-Domaint Localized approach (JDL)

In JDL [10], the pre-processor performs two dimensional transformation and selection. The data is transformed from the space-time domain into the angle-Doppler domain. This pre-processing can be described as in (4), with $\mathbf{A_p}=[\mathbf{f_{m,1}}, \mathbf{f_{m,2}}, \ldots, \mathbf{f_{m,Kt}}]$, where $\mathbf{f_{m,j}}$ $\mathbf{j=1, \ldots, K_t}$ are $\mathbf{K_t}$ columns of an $\mathbf{M \times M}$ **DFT** matrix and with $\mathbf{B_p = G}=[\mathbf{f_{n,1}}, \mathbf{f_{n,2}}, \ldots, \mathbf{f_{n,Ks}}]$, where $\mathbf{f_{n,j}}$ $\mathbf{j=1, \ldots, K_s}$ are $\mathbf{K_s}$ columns of $\mathbf{N \times N}$ **DFT** matrix. As for FTS and EFA, only the post processing corresponding to a single $\mathbf{p}$ must be calculated to test for a target at a particular normalized Doppler and spatial frequency.

If we focus on $\mathbf{K_t} = \mathbf{K_s} = 3$ and consider the case where the target to be detected has the Doppler frequency corresponding to $\mathbf{f_{m,2}}$ and the spatial frequency corresponding to $\mathbf{f_{n,2}}$, then the adaptive processing in (5) is used with

$$\mathbf{S} = [0 \;\; 1 \;\; 0] \otimes [0 \;\; 1 \;\; 0] \qquad (16)$$

More precisely, the steering vector has all its entries equal to zero except for the one corresponding to the spatial and Doppler frequency of the target. No post-processing is employed for JDL.

3. MEASURED DATA RESULTS

To test the STAP algorithms described in section 2, we use data from the Multi-Channel Airborne Radar Measurements (MCARM) database, flight 5, acquisition 575. See [11,12] for detailed information about the MCARM program and the data. For each experiment, a single target signal with amplitude 0.05, a particular normalized Doppler frequency and a particular spatial frequency was inserted in a particular range bin. Reference data are selected from consecutive range cells on each side of the cell-under-test, excluding the cell-under-test and the two closest cells. We employ normalized test statistics as in (5), which provide a constant false alarm rate (CFAR) characteristic for homogenous clutter [13]. The parameters used in each of the STAP algorithms studied are given in the Appendix.

For each example, we provide plots of the magnitude of the normalized test statistics for a set of range bins including the target range. We judge a scheme by how large the test statistic is at the target range in comparison to other ranges.

In the first example, we inserted a target at range bin 150 for the cases shown in Table 1. The location of the targets and an estimate of the clutter (plus noise) power spectral density (psd) are illustrated in Fig. 2. As visible from Fig. 2, the psd estimate used is rather crude and is provided to give a rough description of the clutter environment. In the estimate, the periodogram method [14] is used with blackman windowing. The operations are applied just on the cell-under-test data (no neighboring range cells are averaged). We found that some of the artifacts can be removed by averaging, but this was not considered necessary in this case.

Case	Normalized Doppler Frequency	Spatial Frequency
a	-0.2656	-0.2656
b	-0.0312	-0.0312
c	0.125	0.203
d	-0.0312	-0.1875
e	-0.0312	0.203
f	0.3593	-0.1875
g	-0.1875	0.3593

Table 1) Test cases for each example.

A summary of the results is given in Table 2. Fig. 3 through Fig. 9 present the results for most of the schemes tested. FTS and subarrayed FTS generally perform poorly, so their results are not shown. In this example, generally JDL provides best results. JDL is best in every case except cases d and e. In case d, BeamAD slightly outperforms JDL and ADPCA, but the difference is quite small. In case e, EFA outperforms the others, however JDL also performs well. The apparently large interference indicated by Fig. 2 near the normalized Doppler frequency -0.0312 could be the reason why JDL is not best in these two cases. These are apparently difficult cases where no scheme can really excel. Table 2 shows that case b is also quite difficult, but here JDL performs much better than the other schemes. The extra clutter ridges in Fig. 2 are discussed in [15] and [16].

In the second example, we inserted a target at range bin 350. We present results for the same cases in Table 1. The best three schemes for all the cases are given in Table 3. The location of the targets and an estimate of the clutter psd is given in Fig. 10. The normalized test statistics for the six best schemes tested for each case in Table 1 are given

in Figures 11 through 17. The results indicate that none of the schemes always outperforms all the others. However, post-Doppler algorithms are generally better than pre-Doppler algorithms. Either JDL or EFA were best in all but case b. In case b, where the target is inserted in the largest clutter of all cases, BEFA is only slightly better than EFA and JDL.

Next, we inserted a target at range bin 415. We present results for the same cases as in previous examples. The location of the targets and an estimate of the clutter psd is given in Fig. 18. A summary of the results is provided in Table 4. Here, for cases b, c, d, f, and g either JDL, or BEFA provide best performance. In the other cases, EFA is best and JDL also performs well. JDL performs well in every case except case b. Even in this case, its performance is adequate. EFA and its beamspace version are best in some cases and near-best in others. ADPCA and its beamspace version give good performance in number of cases, but these schemes were never best in this example.

Finally, we test the same cases as before when the target is inserted in range bin 500. The locations of the targets and an estimate of the clutter psd is given in Fig. 19. A summary of the results is given in Table 5. Again JDL, EFA and BEFA outperform the other algorithms except for case e where ADPCA is best.

4. CONCLUSIONS

In our tests, JDL and EFA generally perform very well. Subarrayed EFA also shows good performance in many situations. The common element these schemes share is post Doppler processing. This type of processing, used in the correct way, appears to be superior when using measured data. This appears to be the major result of this study. When there is a strong interference near the target, case d and e in Table 5 for example, ADPCA performs well and sometimes outperforms all the other schemes. The reason appears to be related to the extra whitening provided by its steering vector.

This is one of the few STAP studies we have seen which uses real airborne radar measurements and thus we feel these results are interesting. Judging performance using

measured data is difficult since one can't directly extract probability of detection and probability of false alarm, the accepted measure of performance for radar signal detection problems. However, measured data studies are still important to obtain a more complete assessment of performance. In the current study we present comparisons only for a particular configuration of each algorithm. We have tried to pick the most popular or at least a reasonable configuration for each algorithm. The results may be different for different configurations. Further we have tested the algorithms for many different range bins for two different data sets (flights) and based on these cases the results given here appear to be representative. However, the results could be much different for some data sets we have not tested.

We have obtained results for a fairly large number of different cases. Due to space limitations we have provided only a limited set of these in this report. We believe that further study using measured data is needed and we hope to see more papers by other research groups on this topic. Hopefully other data sources will become available and these can be compared to results obtained using the MCARM database. Most importantly, we believe that techniques for assessing performance with measured data is itself a topic which deserves attention.

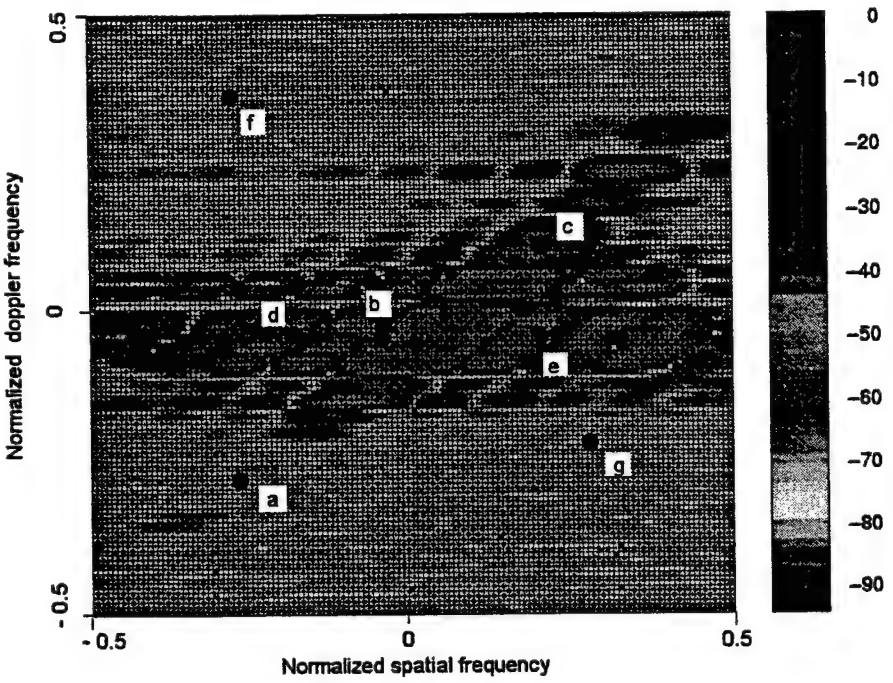

Figure 2) Power spectrum plot of range 150

Case	Normalized Doppler Frequency	Spatial Frequency	The 3 best schemes	D	Figure
a	-0.2656	-0.2656	JDL BEFA BeamAD	36 25 16	3
b	-0.0312	-0.0312	JDL	10	4
c	0.125	0.203	JDL EFA	30 12	5
d	-0.0312	-0.1875	BeamAD JDL ADPCA	8 7 6	6
e	-0.0312	0.203	EFA JDL BeamAD	20 12 5	7
f	0.3593	-0.1875	JDL EFA BeamAD	43 38 30	8
g	-0.1875	0.3593	JDL BEFA BeamAD	38 18 7	9

Table 2) The three best schemes for all the cases when the target is inserted at range 150 (D is the approximate difference between the normalized test statistic at the target and the largest peak in the normalized test statistic at some other range).

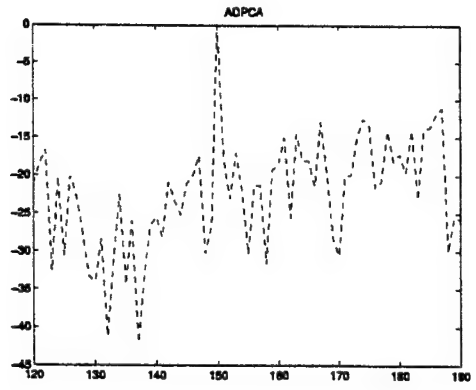

a) ADPCA

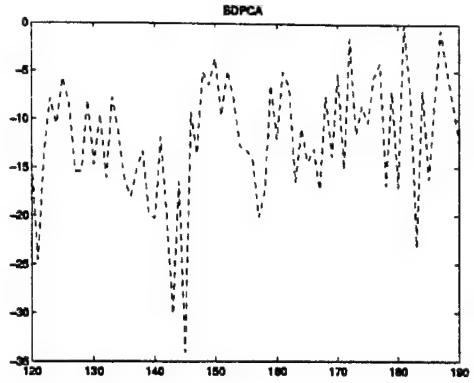

b) BDPCA

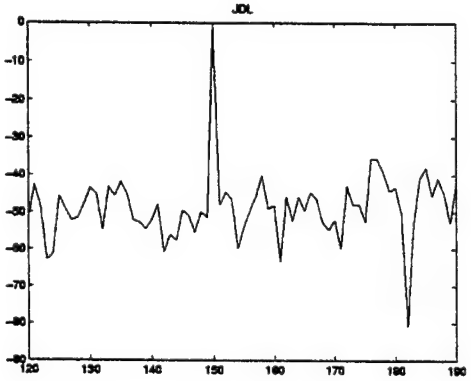

c) JDL

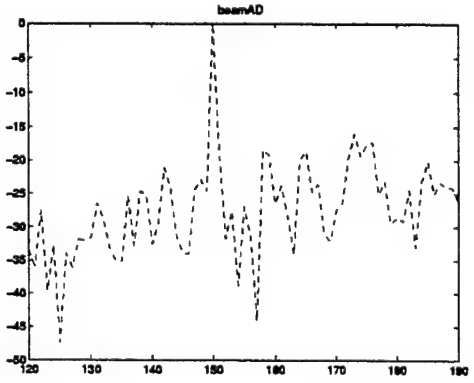

d) BeamAD

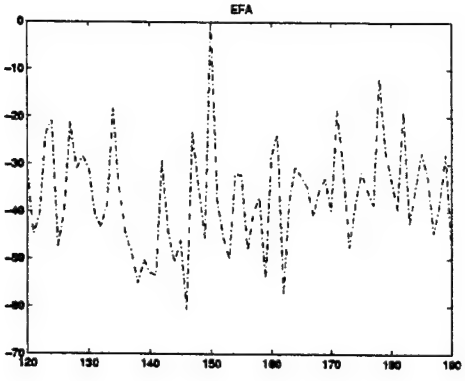

e) EFA

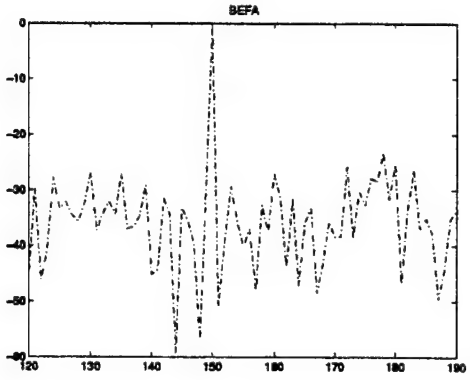

f) BEFA

Figure 3) Performance comparison when target is inserted at range150, case a.

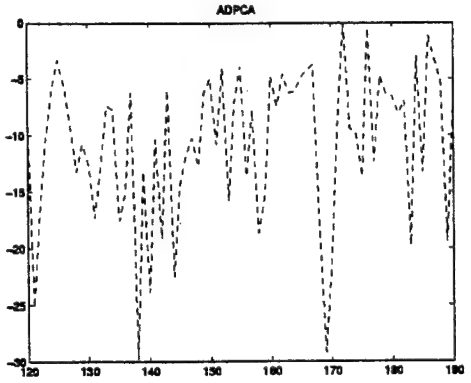

a) ADPCA

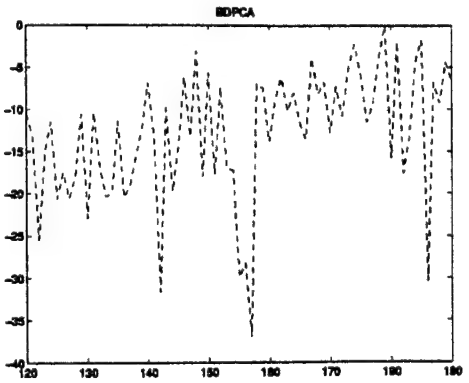

b) BDPCA

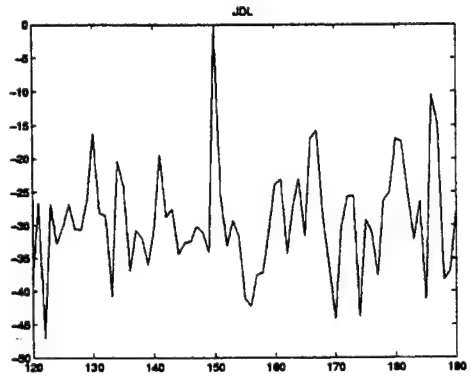

c) JDL

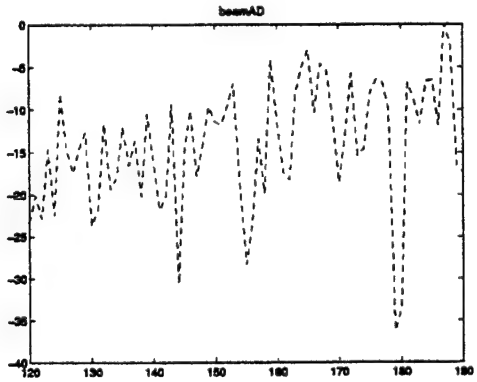

d) BeamAD

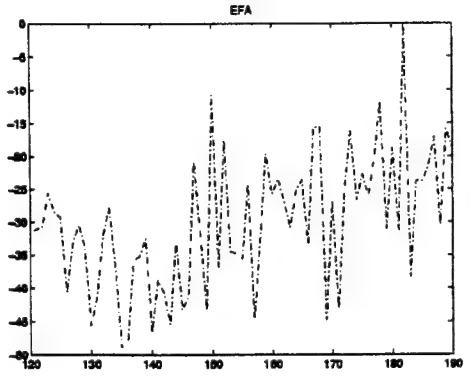

e) EFA

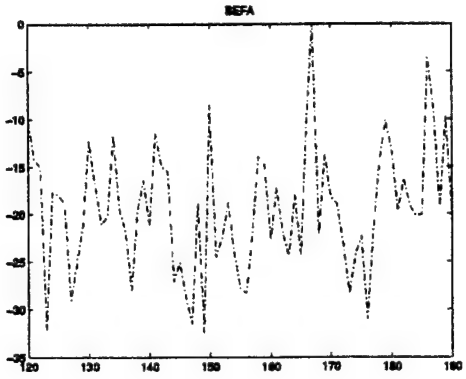

f) BEFA

Figure 4) Performance comparison when target is inserted at range 150, case b.

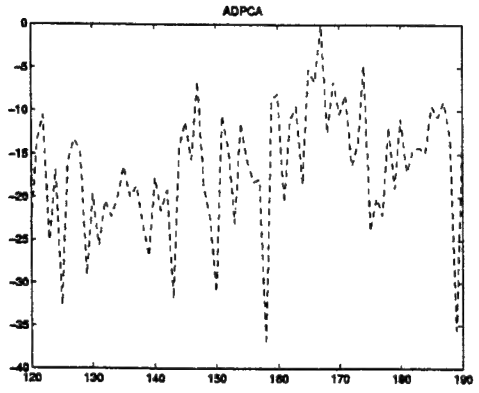

a) ADPCA

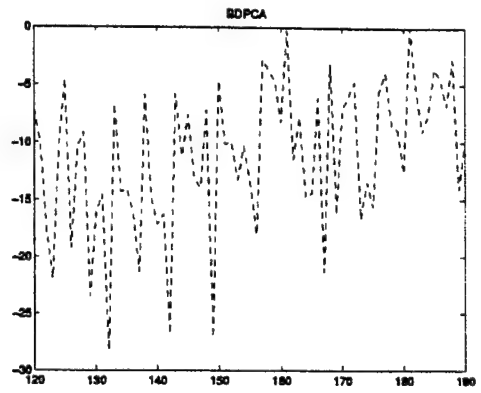

b) BDPCA

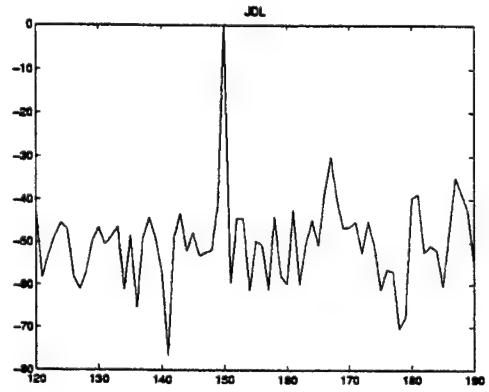

c) JDL

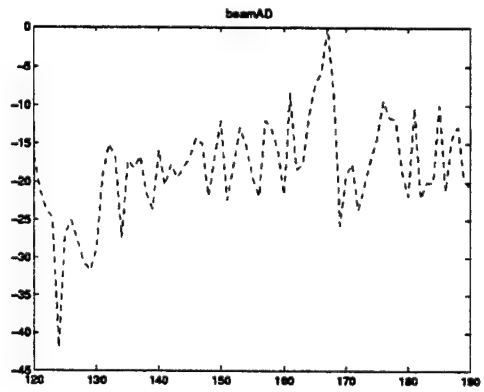

d) BeamAD

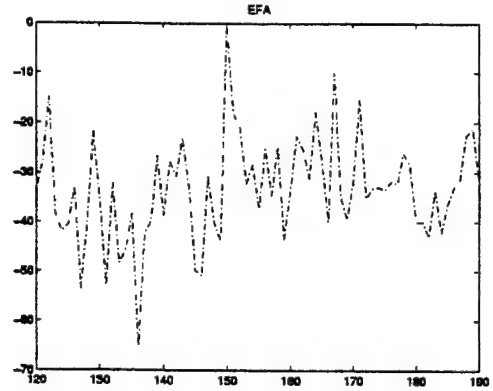

e) EFA

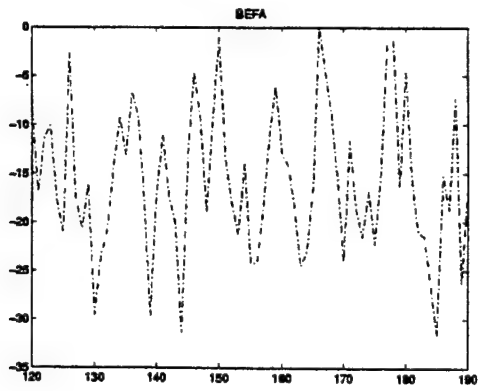

f) BEFA

Figure 5) Performance comparison when target is inserted at range 150, case c.

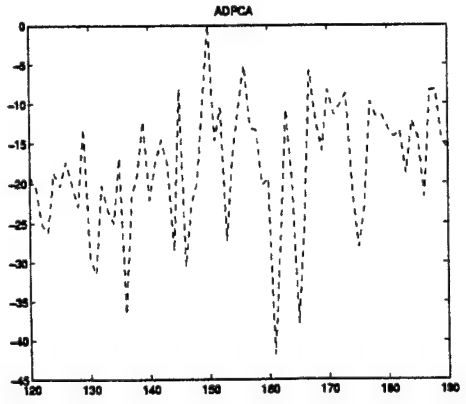

a) ADPCA

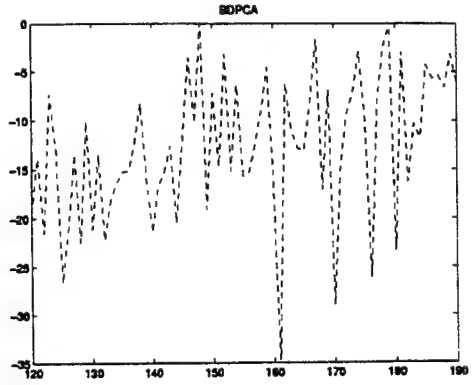

b) BDPCA

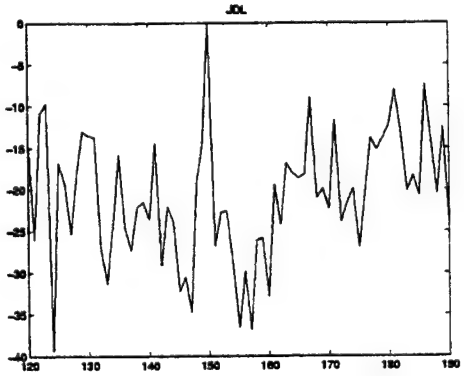

c) JDL

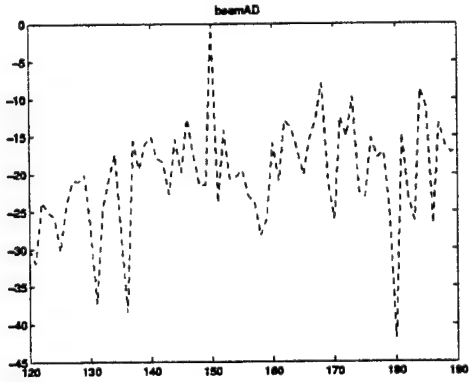

d) BeamAD

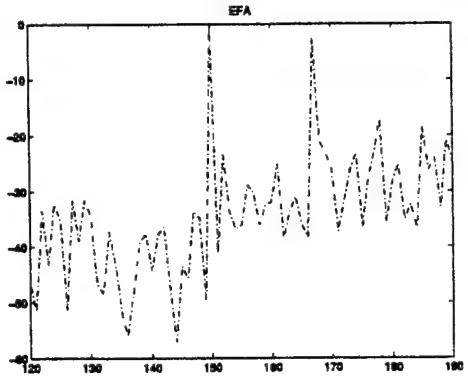

e) EFA

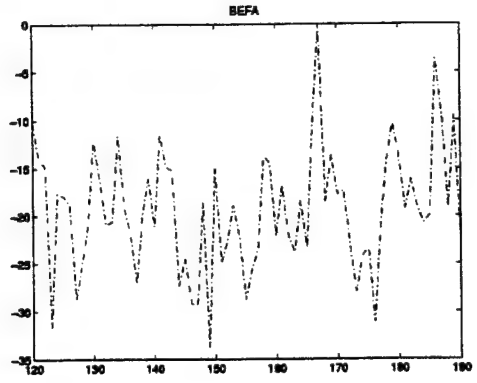

f) BEFA

Figure 6) Performance comparison when target is inserted at range 150, case d.

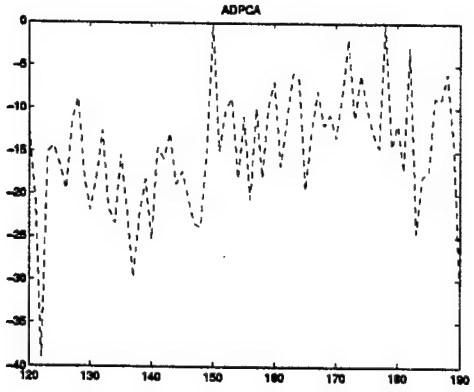

a) ADPCA

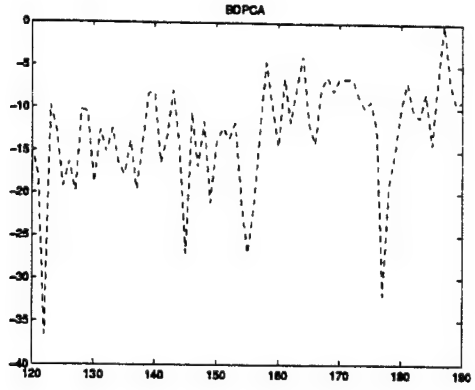

b) BDPCA

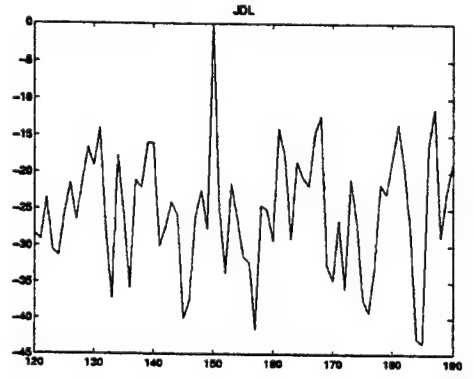

c) JDL

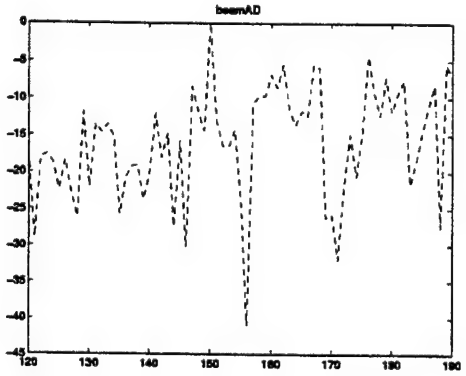

d) BeamAD

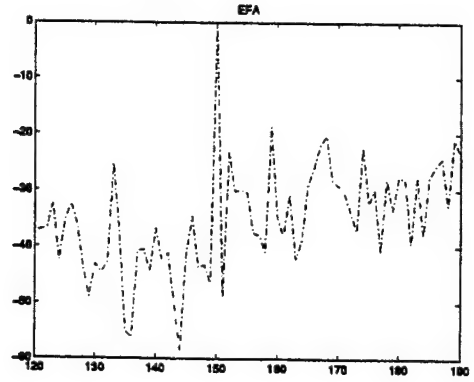

e) EFA

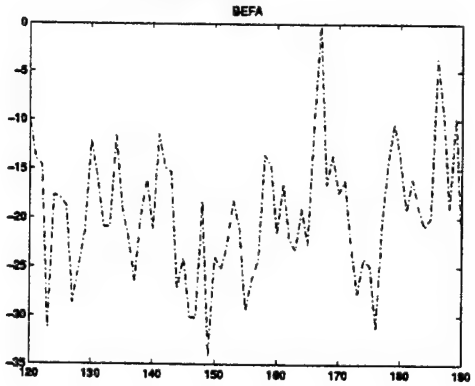

f) BEFA

Figure 7) Performance comparison when target is inserted at range 150, case e.

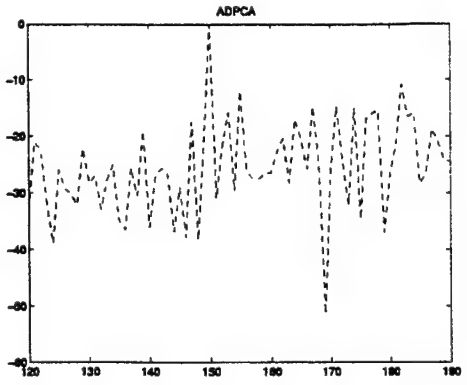

a) ADPCA

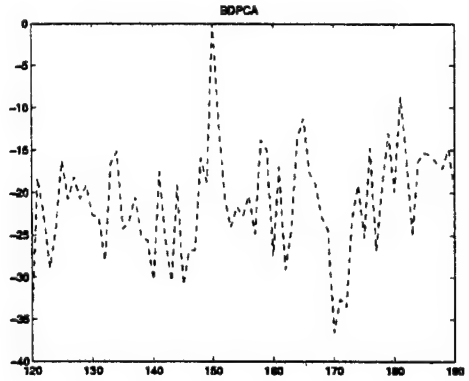

b) BDPCA

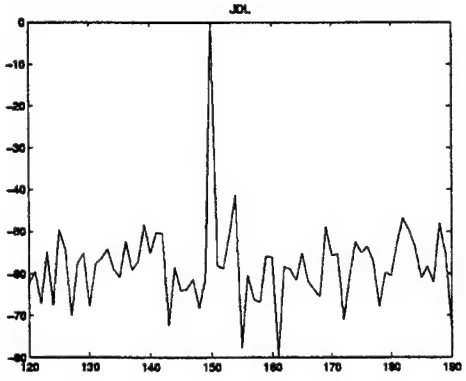

c) JDL

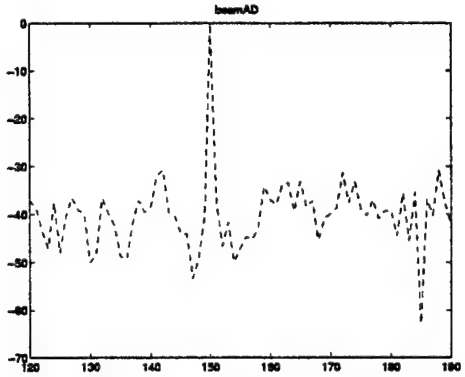

d) BeamAD

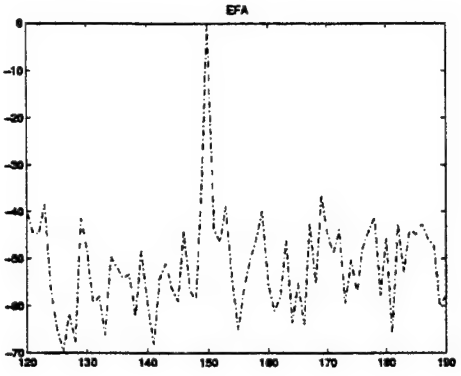

e) EFA

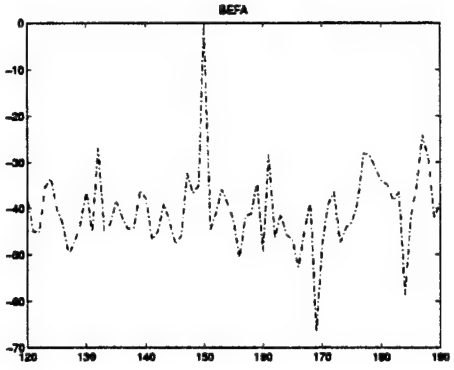

f) BEFA

Figure 8) Performance comparison when target is inserted at range 150, case f.

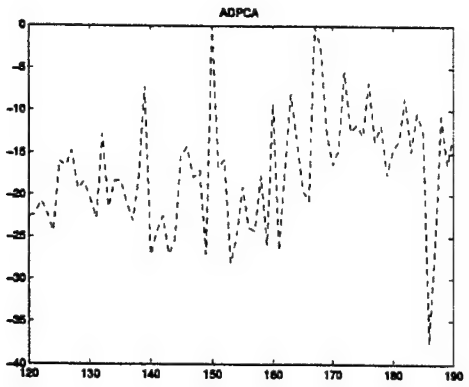

a) ADPCA

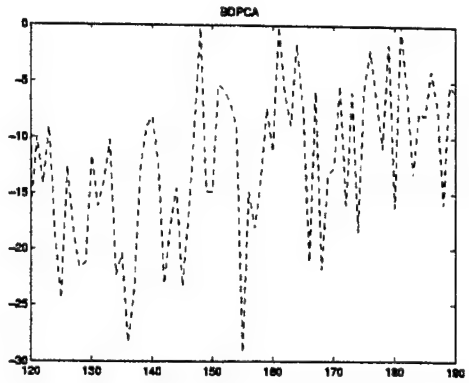

b) BDPCA

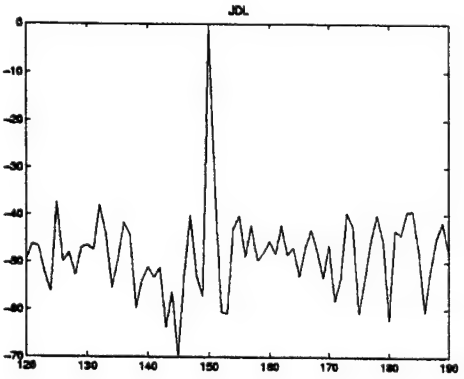

c) JDL

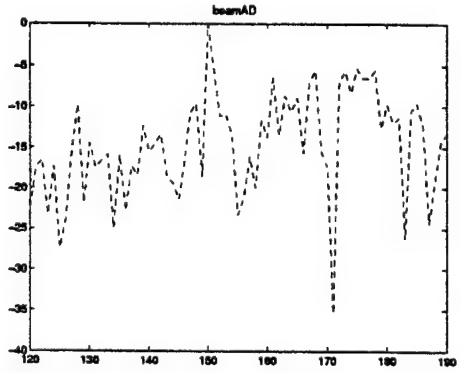

d) BeamAD

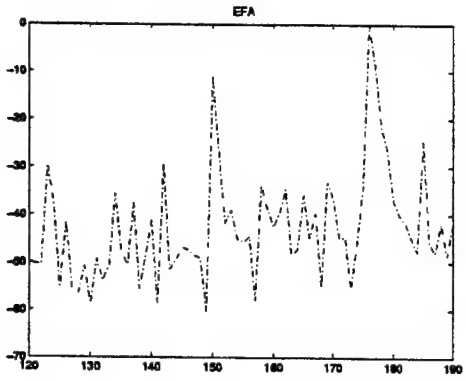

e) EFA

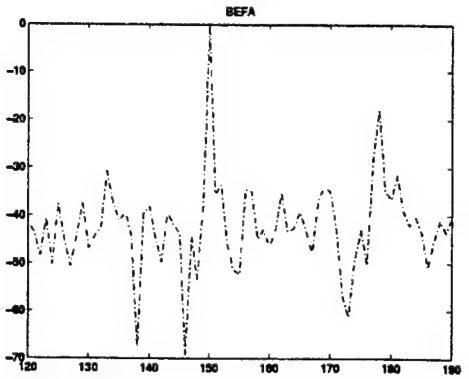

f) BEFA

Figure 9) Performance comparison when target is inserted at range 150, case g.

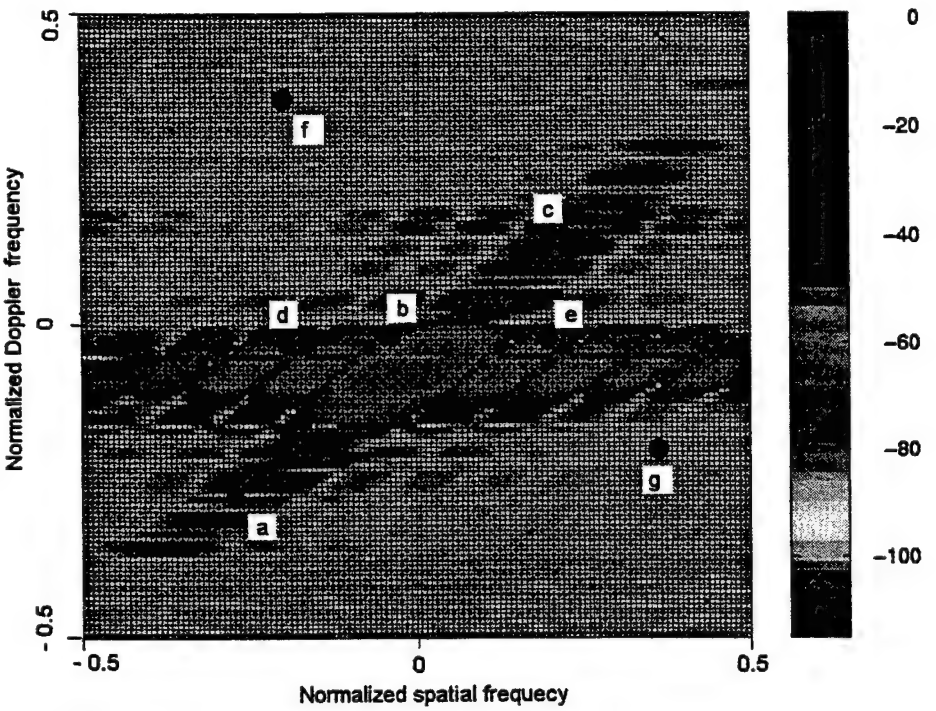

Figure 10) Power spectrum plot of range 350.

Case	Normalized Doppler Frequency	Spatial Frequency	The 3 best schemes	D	Figure
a	-0.2656	-0.2656	EFA JDL BEFA	24 18 5	11
b	-0.0312	-0.0312	BEFA EFA JDL	15 12 10	12
c	0.125	0.203	JDL EFA BEFA	34 25 13	13
d	-0.0312	-0.1875	EFA JDL ADPCA	28 20 12	14
e	-0.0312	0.203	EFA JDL ADPCA	22 18 7	15
f	0.3593	-0.1875	EFA JDL BeamAD	48 43 24	16
g	-0.1875	0.3593	JDL BEFA BeamAD	33 18 14	17

Table 3) The three best schemes for all the cases when the target is inserted at range 350. (D is the approximate difference between the normalized test statistic at the target and the largest peak in the normalized test statistic at some other range.).

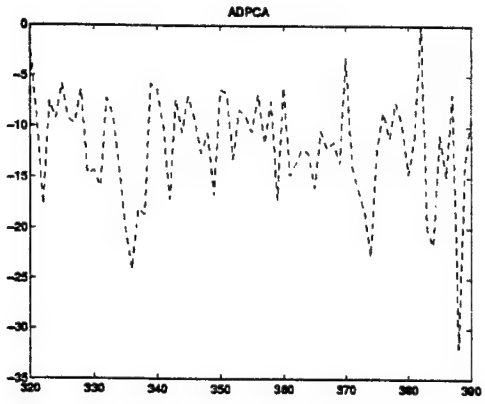

a) ADPCA

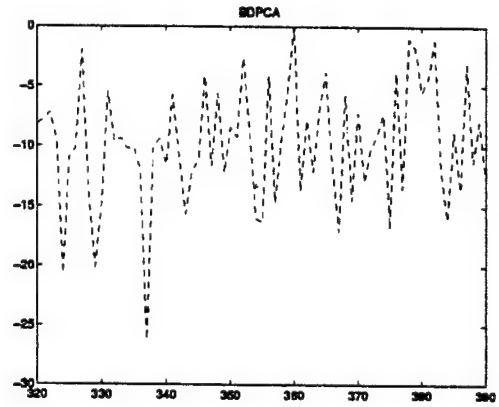

b) BDPCA

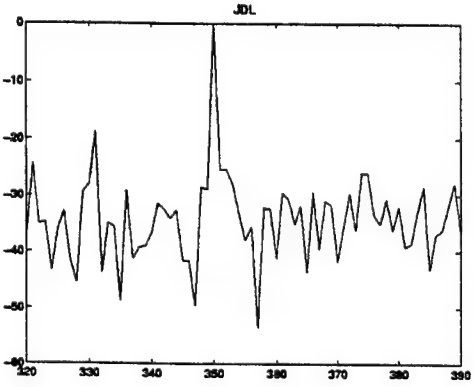

c) JDL

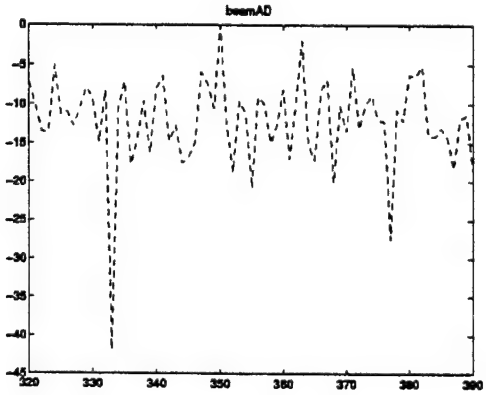

d) BeamAD

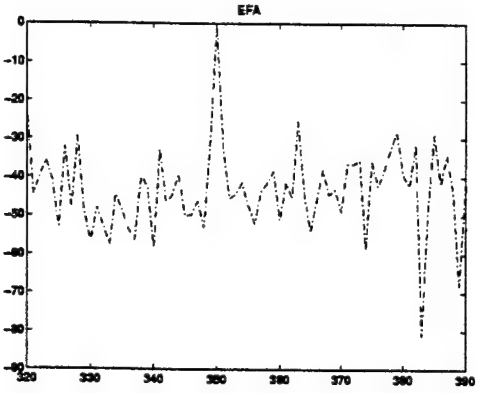

e) EFA

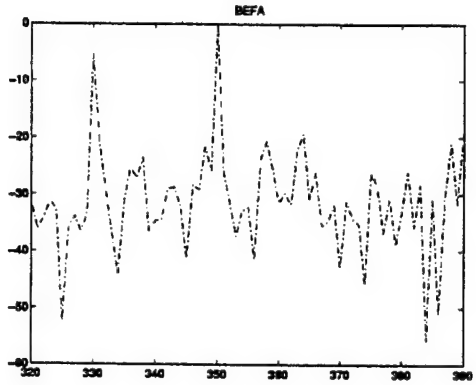

f) BEFA

Figure 11) Performance comparison when target is inserted at range 350, case a.

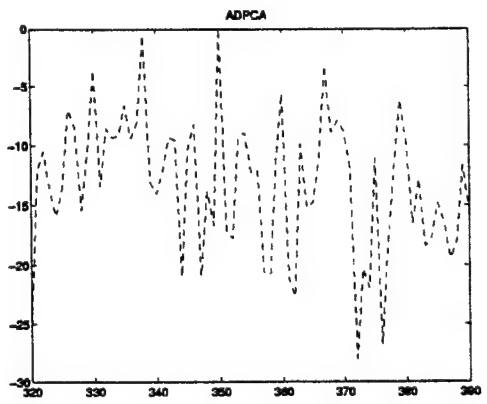

a) ADPCA

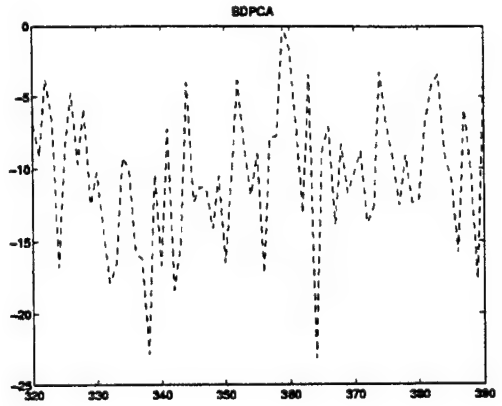

b) BDPCA

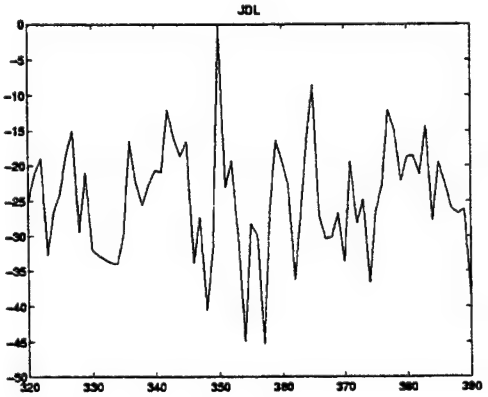

c) JDL

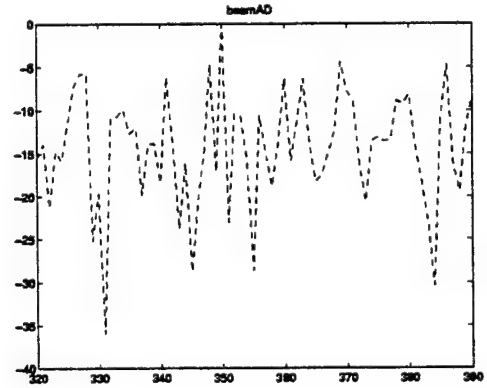

d) BeamAD

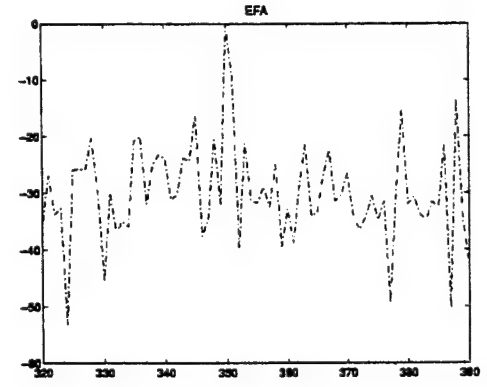

e) EFA

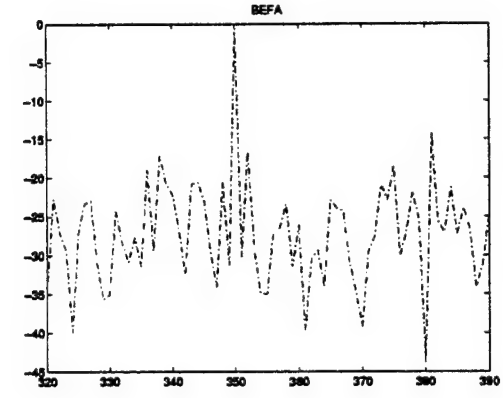

f) BEFA

Figure12) Performance comparison when target is inserted at range 350, case b.

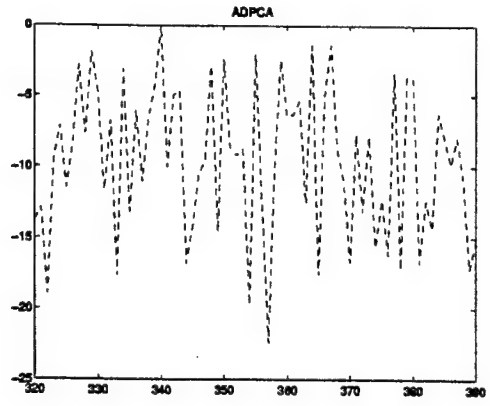

a) ADPCA

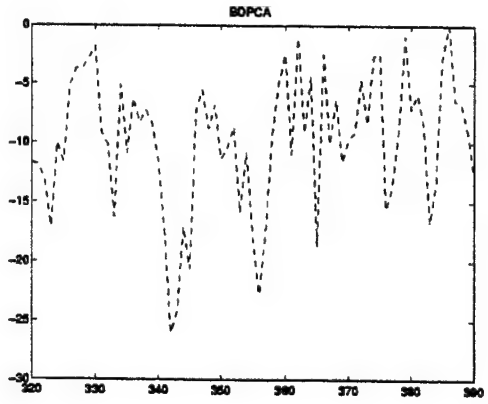

b) BDPCA

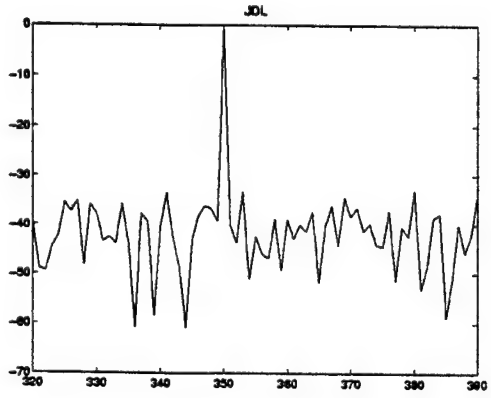

c) JDL

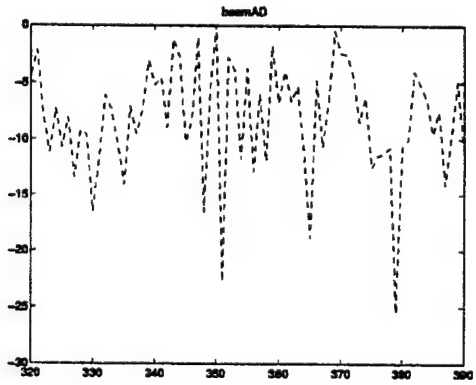

d) BeamAD

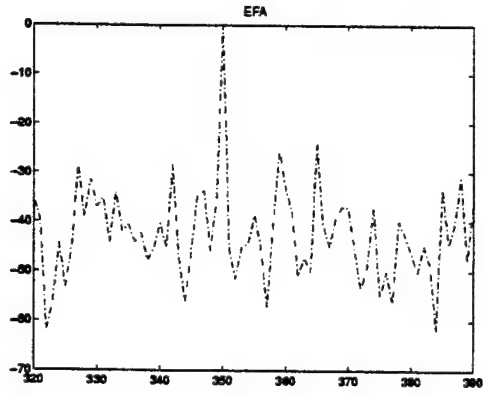

e) EFA

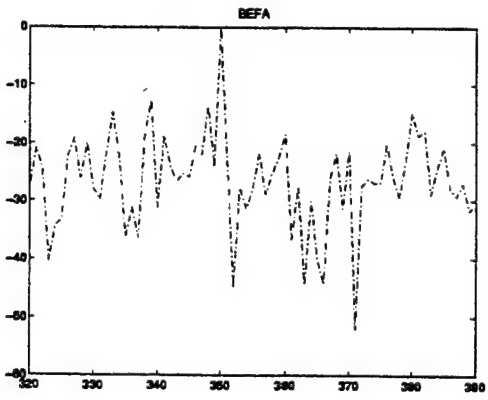

f) BEFA

Figure 13) Performance comparison when target is inserted at range 350, case c.

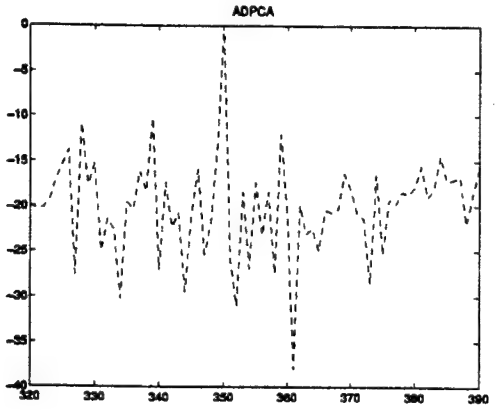

a) ADPCA

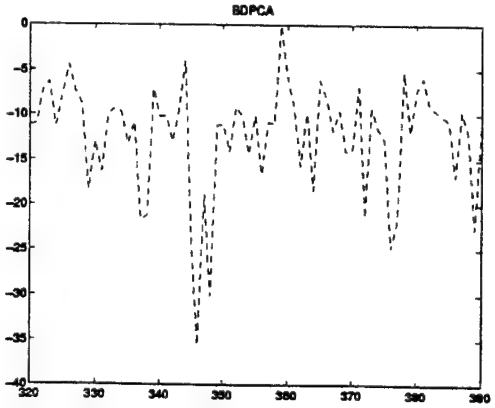

b) BDPCA

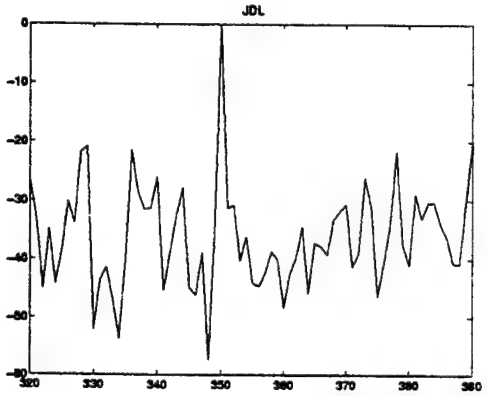

c) JDL

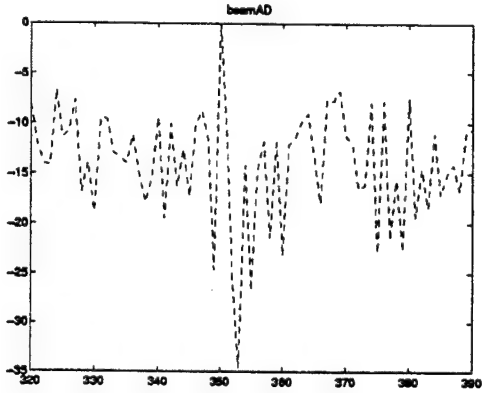

d) BeamAD

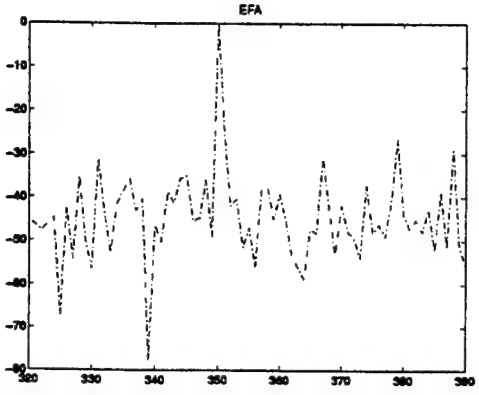

e) EFA

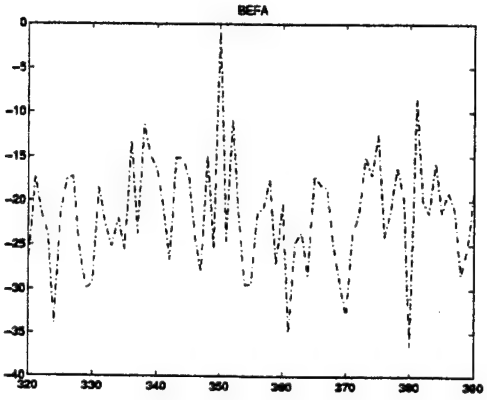

f) BEFA

Figure 14) Performance comparison when target is inserted at range 350, case d.

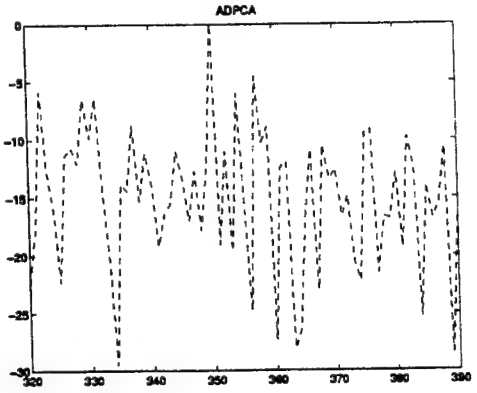

a) ADPCA

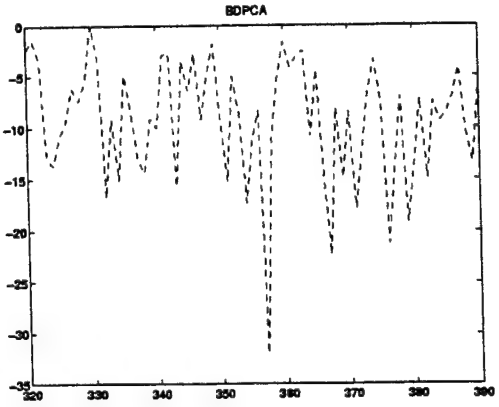

b) BDPCA

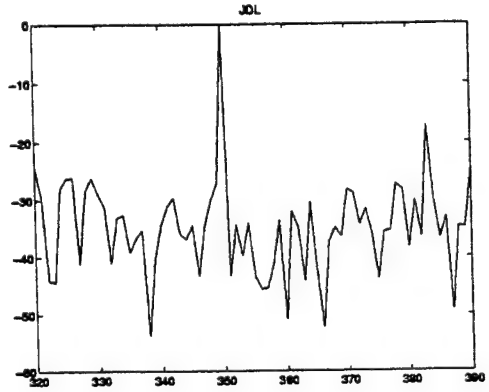

c) JDL

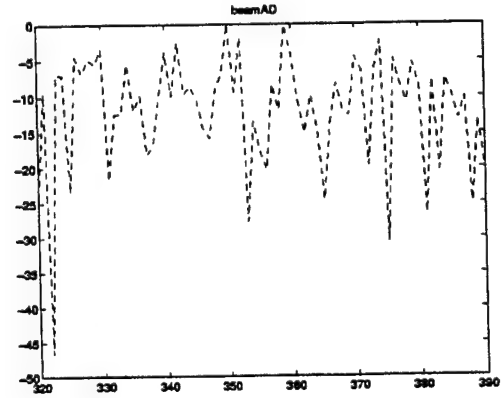

d) BeamAD

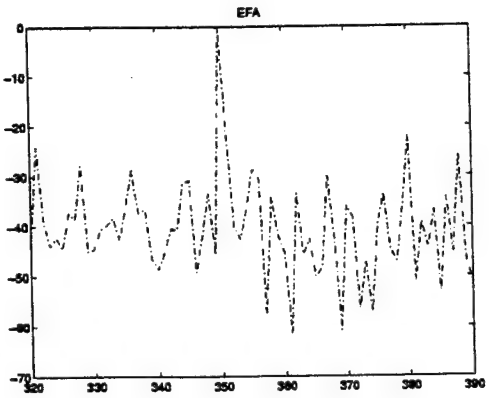

e) EFA

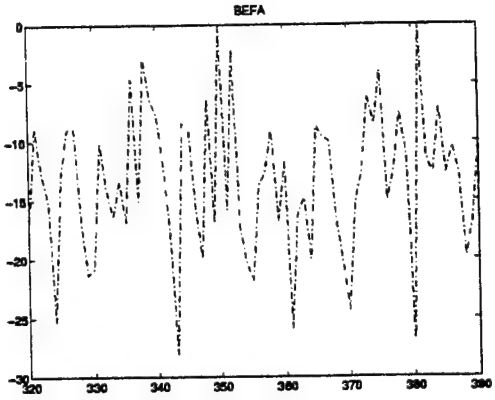

f) BEFA

Figure 15) Performance comparison when target is inserted at range 350, case e.

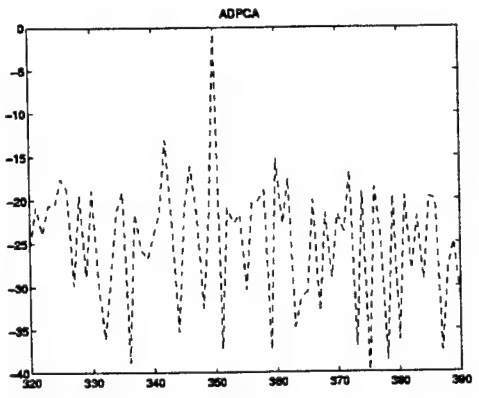

a) ADPCA

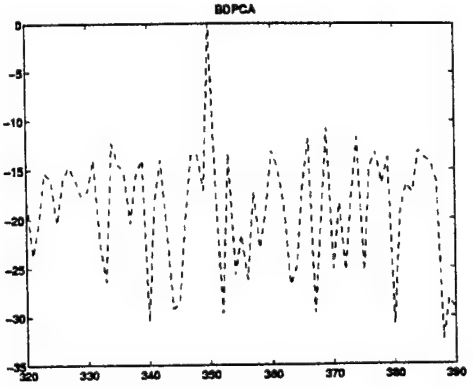

b) BDPCA

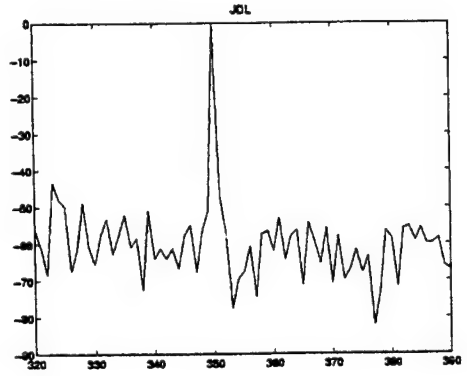

c) JDL

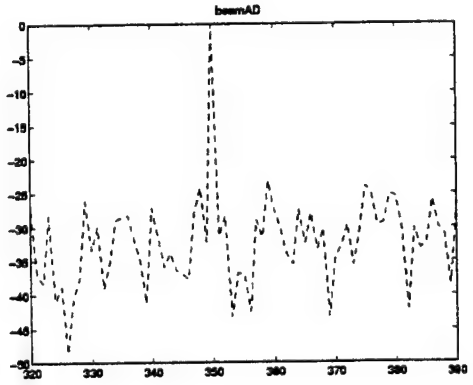

d) BeamAD

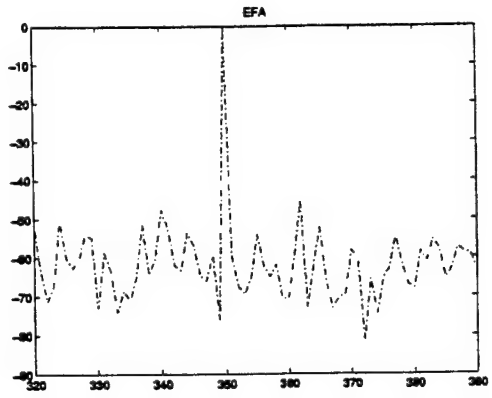

e) EFA

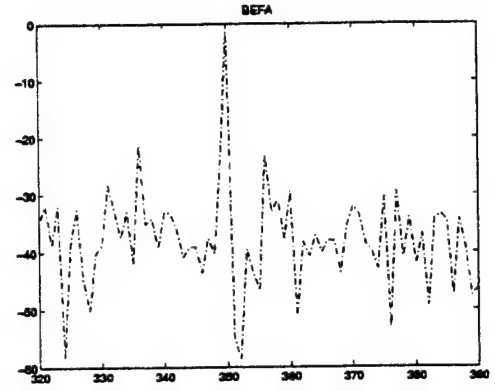

f) BEFA

Figure 16) Performance comparison when target is inserted at range 350, case f.

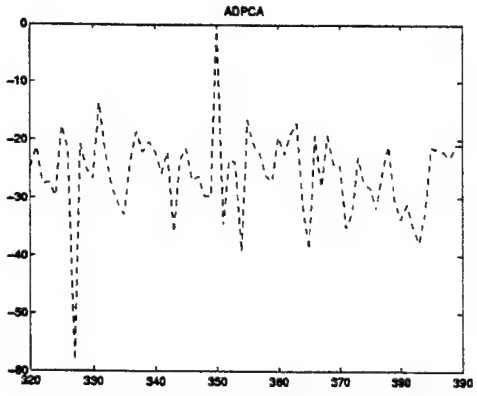

a) ADPCA

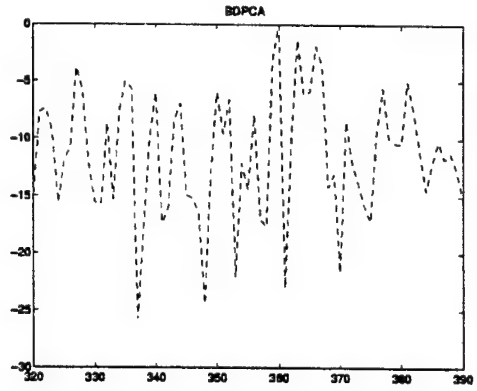

b) BDPCA

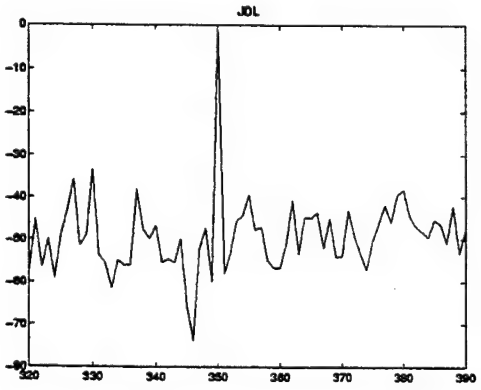

c) JDL

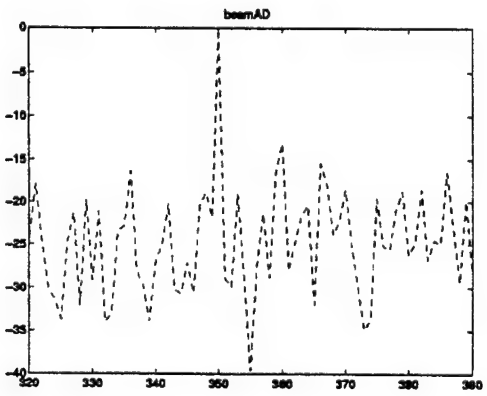

d) BeamAD

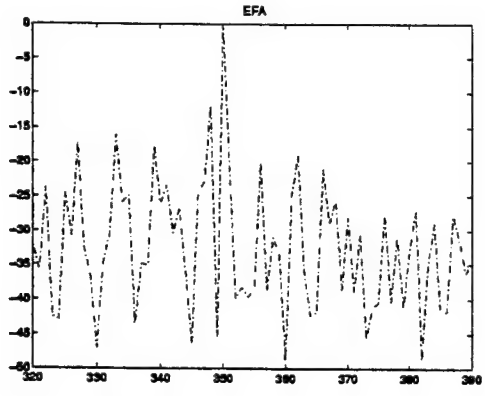

e) EFA

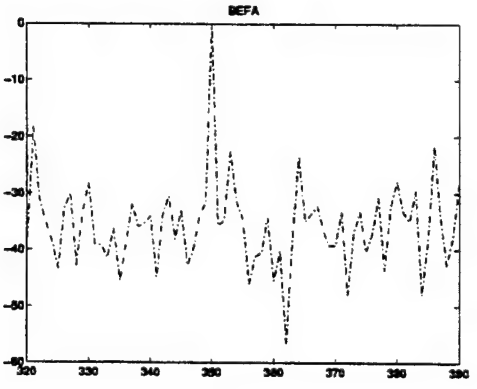

f) BEFA

Figure17) Performance comparison when target is inserted at range 350, case g.

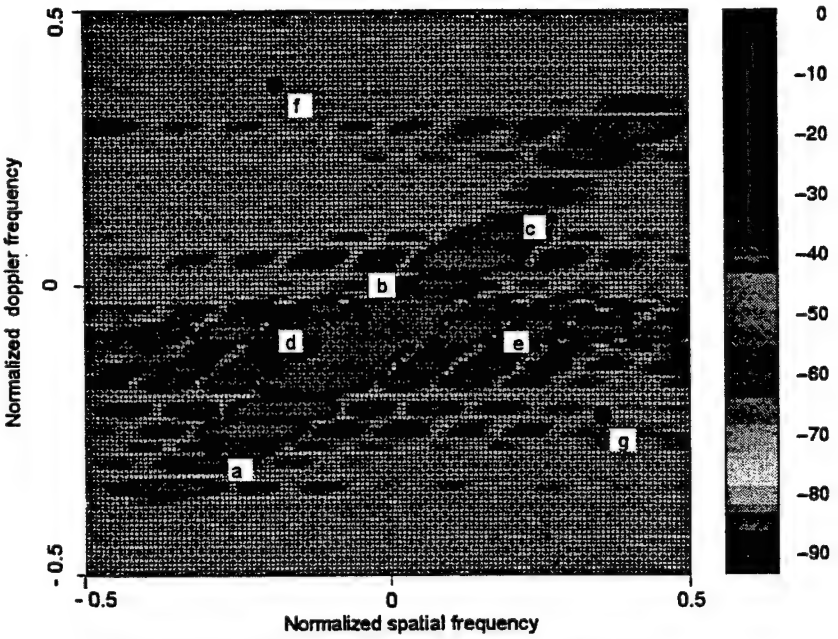

Figure 18) Power spectrum plot of range 415

Case	Normalized Doppler Frequency	Spatial Frequency	The 3 best schemes	D
a	-0.2656	-0.2656	EFA JDL ADPCA	25 22 12
b	-0.0312	-0.0312	BEFA BeamAD EFA, ADPCA	25 18 15
c	0.125	0.203	BEFA JDL BeamAD	30 23 12
d	-0.0312	-0.1875	JDL, BEFA BeamAD EFA, ADPCA	20 18 16
e	-0.0312	0.203	EFA JDL ADPCA	28 24 15
f	0.3593	-0.1875	JDL BeamAD BEFA	45 35 32
g	-0.1875	0.3593	JDL EFA BeamAD	42 20 18

Table 4) The three best schemes for all the cases when the target is inserted at range 415. (D is the approximate difference between the normalized test statistic at the target and the largest peak in the normalized test statistic at some other range)

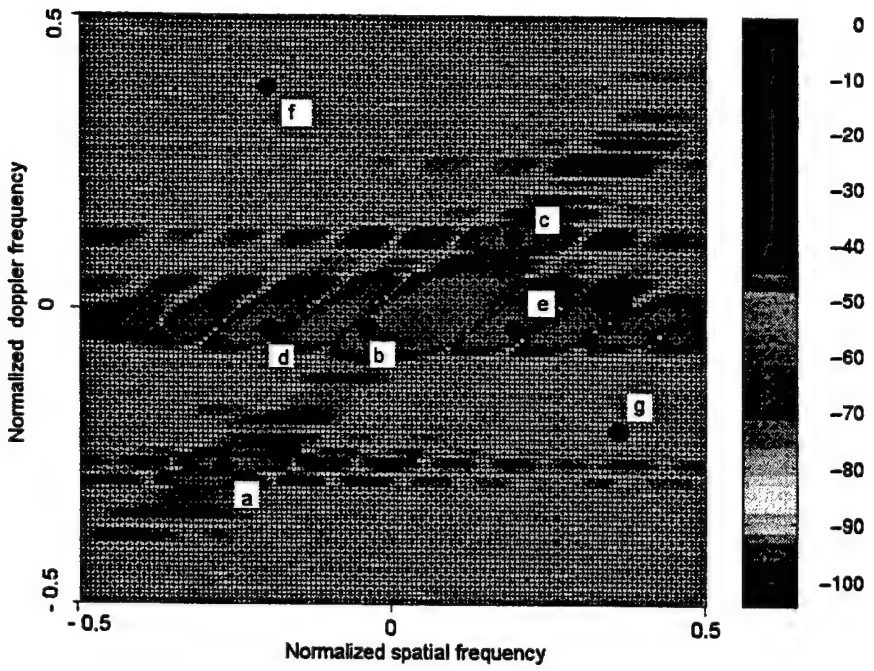

Figure 19) Power spectrum plot of range 500

Case	Normalized Doppler Frequency	Spatial Frequency	The 3 best schemes	D
a	- 0.2656	- 0.2656	JDL EFA ADPCA	32 13 7
b	-0.0312	-0.0312	JDL EFA BEFA	22 20 15
c	0.125	0.203	JDL BEFA EFA, BeamAD	36 12 7
d	- 0.0312	- 0.1875	JDL EFA ADPCA	26 20 10
e	- 0.0312	0.203	ADPCA JDL EFA	22 18 15
f	0.3593	- 0.1875	JDL EFA, BEFA BeamAD	38 28 23
g	- 0.1875	0.3593	BEFA, JDL BeamAD EFA	33 17 15

Table 5) The three best schemes for all the cases when the target is inserted at range 500. (D is the approximate difference between the normalized test statistic at the target peak and the largest peak in the normalized test statistic at some other range)

5. REFERENCES

1. L.E. Brennan and I. S. Reed, " Theory of Adaptive Radar", *IEEE Trans. On Aerospace and Electronic Systems*, vol. AES-9, no. 2, pp. 237-252, March 1973.
2. I.S. Reed, J. D Mallett and L.E. Brennan, " Rapid convergence rate in adaptive arrays", IEEE Transactions on Aerospace and Electronic Systems, AES-10, no.6, November 1974.
3. Alfonso Farina, *Antenna-based Signal Processing Techniques for Radar Systems*, (Artech House: MA, 1992).
4. H. Wang, Y. Zhang and Q. Zhang, "A view of current of space-time processing algorithm research", *IEEE International Radar Conference*, Alexandria, Virginia, May 1995, pp. 635-640.
5. J. Ward, *Space-Time Adaptive Processing for Airborne Radar*, Technical Report 1015, Lincoln Laboratory, 1995.
6. W. L. Melvin and B. Himed, "Comparative Analysis of Space –Time Adaptive Algorithms with Measured Airborne Data", *Proc. of the 7th International Conference on Signal Processing Applications and Technology*, pp. 1479-1483, October 7-10, 1996.
7. A. Oppenheim and R. Schafer, *Discrete-Time Signal processing*, Prentice Hall, Englewood Cliffs, New Jersey, 1989.
8. M. D. Zoltowski, "*Beamspace M.L. Bearing Estimation for Adaptive Phased Array Radar*", In Adaptive Radar Detection and Estimation, S. Haykin and A. Steinhardt Editors, John Wiley and Sons, New York, 1992.
9. R. C. Dipietro, "Extended Factored Space-Time Processing for Airborne Radar", Proceedings of the 2th Asilomar Conference, Pacific Grove CA, October 1992, pp. 425-430.
10. H. Wang and L. Cai, "On adaptive spatial-temporal processing for airborne surveillance radar systems", *IEEE Transactions on Aerospace and Electronic Systems*, Vol. 30, pp. 660-669, July 1994.
* 11. D. Sloper et. al., *MCARM Final Rept.*, Rome Laboratory Technical Report, RL-TR-96-49, April 1996.

* Although this report references the above limited report, no limited information has been extracted.

12. MCARM database web site - Rome Laboratory USAF, 'http://128.132.2.

13. A. M. Chen and I. S. Reed, "A New CFAR detection test for radar," Digital Signal Processing, Vol. 4, Oct. 1991, pp. 198-214.

14. S. L. Marple, Digital Spectral Analysis with Applications, Prentice Hall, Englewood Cliffs, New Jersey, 1986.

15. W. Melvin, H.Wang and M. Wicks, "*Multi-channel Airborne Radar Array Data Analysis*", Record of the 41st Annual Tri-Service radar symposium, pp. 303-317, June 1995.

16. H. Wang, "*Space-Time Processing and Its Radar Applications*", notes used for the class ELE 891 at Syracuse University, Summer 1995.

APPENDIX

Scheme	M	N	Kt	Ks	A_p	G	DOF
ADPCA	128	22	3	-	$[\ 0_{p\times3},\ I_3,\ 0_{(125-p)\times3}\ ]^T$	I_{22}	66
EFA	128	22	3	-	$[f_{128,Dp-1}, f_{128,Dp}, f_{128,Dp+1}]$	I_{22}	66
FTS	128	22	1	-	$f_{128,Dp}$	I_{22}	22
Beamspace ADPCA	128	22	3	3	$[\ 0_{p\times3},\ I_3,\ 0_{(125-p)\times3}\ ]^T$	See Note	9
Subarraying ADPCA	128	22	3	3	$[\ 0_{p\times3},\ I_3,\ 0_{(125-p)\times3}\ ]^T$	*G	9
Subarraying EFA	128	22	3	3	$[f_{128,Dp-1}, f_{128,Dp}, f_{128,Dp+1}]$	* G	9
Subarraying FTS	128	22	3	3	$f_{128,Dp}$	* G	3
JDL	128	22	3	3	$[f_{128,Dp-1}, f_{128,Dp}, f_{128,Dp+1}]$	See Note	9

Table 6) Parameters for comparison tests in this study.

DOF: number of degrees of freedom. It is equal to the Q in (6) in this paper.

* **G** is the beamforming matrix which is formed as described in (13).

Note: MCARM data is not collected by a uniformly spaced linear antenna array, so its beamforming matrix is relatively complicated. This G matrix used in beamspace ADPCA and JDL can be obtained by using measured steering vector information provided with the MCARM database. See the discussion on modSA at [11].

Chapter 2: Task 4.1.2

1. Introduction

Adaptive space-time processing schemes for airborne radar have received significant attention recently [1]. Typically these schemes involve using observations from neighboring range cells, called reference data, to estimate the covariance matrix of the clutter-plus-interference in the range cell-under-test. The estimated covariance matrix is then used to define a weight vector in a linear processing scheme. The weight vector is chosen with the hope that it will suppress the clutter-plus-interference in the range cell-under-test. If the estimated covariance matrix accurately represents the true covariance matrix for the cell-under-test then most STAP schemes perform well. There are many reasons why, in practice, this may not occur. The data taken from surrounding range cells often have different statistics from data taken from the cell-under-test. Further, the amount of reference data available which can be used in the estimation is usually quite limited. Often this is a consequence of nonstationarity.

To overcome these difficulties, reduced-dimension STAP schemes [1, 2, 3, 4, 5] have been devised which have shown promise. In our own research [3, 4, 5], we have shown that a particular approach suggested by Rome Laboratory engineers, the Adaptive Displaced Phase Centered Antenna (ADPCA) approach, provides good performance in some cases with real data. Other researchers [1, 4] have shown that the Extended Factored Approach (EFA) and the Joint-Domain Localized (JDL) approach can also provide good performance in some cases. In this research, a new methodology for constructing robust STAP schemes is proposed. In order to demonstrate the idea we use a simple model for a case with ground clutter only and we show that the resulting scheme can provide good performance in tests with measured radar data.

In section 2, we introduce the new approach and describe its application to a set of STAP algorithms. In section 3, we describe how to choose free parameters in the approach. In section 4, we discuss the application of the approach to four specific STAP algorithms. Numerical performance results are given for a measured radar data set. Conclusions are given in section 5.

2. General approach for modified scheme

Here we study a new set of space-time processing algorithms for airborne radar. In the spirit of ADPCA and other reduced-dimension algorithms, our new algorithms attempt to estimate fewer parameters than fully-adaptive approaches. In our new schemes the reduction is achieved by using a priori information that is not yet being exploited. In this report, we focus on using our knowledge on the structure of ground clutter, but other prior knowledge could also be exploited. For example, one might want to incorporate knowledge of jammers or interference from previous scans or one might have knowledge of previously detected targets. Using prior knowledge should allow our new schemes to perform well even when given only small amounts of reference data, which may have a statistical description which is slightly different from that for the cell-under-test.

A. Traditional schemes

Assume that the observations to be processed are taken from M different pulse returns received by N antenna elements from the k^{th} range cell. Each return is assumed to contain a possible signal in additive noise-plus-clutter. Denote the observation

corresponding to the i^{th} pulse at the j^{th} antenna element as x_{ij}. Each observation is a complex number corresponding to the in-phase and quadrature components of the received waveform. The observations to be processed are ordered as

$$X_k = (x_{11}, x_{21}, \ldots, x_{N1}, x_{12}, \ldots, x_{NM})^T \qquad (1)$$

where x^T denotes the transpose of the vector x.

A reasonably large set of STAP processing schemes can be described as follows. The description is broken into three parts: pre-processing, adaptive processing and post-processing. The pre-Processing can be described by

$$\tilde{X}_k(p) = (A_p \otimes B_p)^H X_k, \qquad p = 0,1,2,\ldots,P-1 \qquad (2)$$

where X_k is given in (1). In (2) A_p and B_p are scheme-dependent matrices. The adaptive processing can be described by

$$y_k(p) = S^H R_k^{-1}(p) \tilde{X}_k(p) / \Phi_p, \qquad p = 0,1,2,\ldots,P-1 \qquad (3)$$

where $$S = S_t \otimes S_s \qquad (4)$$

S_t is the scheme-dependent temporal steering vector and S_s is the scheme-dependent spatial steering vector. In (4) $\otimes$ stands for an outer product. The quantity Φ_p is the normalization needed to provide a constant false alarm rate (CFAR) in homogeneous clutter and is given by

$$\Phi_p = \sqrt{S^H R_k^{-1}(p) S} \qquad (5)$$

The post-processing is not necessary if $y_k(p)$ is the final output of interest. In this case, $|y_k(p)|$ is compared to a threshold directly to decide if target is present. If $y_k(p)$ is not

the final output of interest, we should assemble all the outputs into a vector as $Y_k = [y_k(0), y_k(1), \ldots, y_k(P-1)]^T$, then compute

$$z_{k,m} = f_m^H Y_k \tag{6}$$

typically, f_m is the m^{th} column of a $P \times P$ filter matrix F, and $z_{k,m}$ is the final output whose magnitude is compared to a threshold to make a decision.

In the traditional schemes we considered, the estimated covariance matrix is calculated as

$$R_k(p) = \frac{1}{L} \sum_{i=k-L/2-1, i \neq k,k-1,k+1}^{k+L/2+1} \tilde{X}_i(p) \tilde{X}_i(p)^H \tag{7}$$

by averaging over L range cells (assuming L is even) surrounding the k^{th} range cell excluding the cell-under-test and the two closest range cells.

B. Modified schemes

In order to use our prior knowledge of the nature of ground clutter, namely the known structure of the clutter ridge in angle-Doppler space, we use a simple model for ground clutter proposed in [1]. Assume that the clutter portion of the reference samples is Gaussian distributed with the two-dimensional power spectrum density (psd) described in [1]

$$P_c(f_t, f_s) = \sum_{d=1}^{L} \frac{\sigma_{c,d}^2}{2\pi \sigma_{ft,d} \sigma_{fs,d}} \exp\left[-\left(\frac{(f_t - f_{ct,d})^2}{2\sigma_{ft,d}^2} + \frac{(f_s - f_{cs,d})^2}{2\sigma_{fs,d}^2} \right) \right] \tag{8}$$

which is a function of normalized Doppler frequency f_t and spatial frequency f_s. The psd in (8) consists of L Gaussian-shaped humps, the d th of which is centered at $(f_t, f_s) = (f_{ct,d}, f_{cs,d})$ and has amplitude controlled by $\sigma_{c,d}^2$ and a spread in angle and

Doppler controlled by $\sigma^2_{fs,d}$ and $\sigma^2_{ft,d}$. Our approach will assume the clutter samples are described by the psd in (8) and the data will be used to estimate some of the parameters in (8). The other parameters in (8) will be fixed at values chosen to fit a wide set of measured data. Once the estimates for the parameters in (8) are found, the covariance matrix for clutter described by (8) is given by [1]

$$R_c = \sum_{d=1}^{L} \sigma^2_{c,d} C_{t,d} \otimes C_{s,d} \tag{9}$$

where $C_{t,d}$ and $C_{s,d}$ are Toeplitz matrices specified by

$$C_{t,d} = \text{Toeplitz}\left\{\left[1 \quad e^{-2(\pi\sigma_{ft,d})^2 + i2\pi f_{ct,d}} \cdots e^{-2(\pi\sigma_{ft,d}(M-1))^2 + i(M-1)2\pi f_{ct,d}}\right]\right\} \tag{10}$$

and

$$C_{s,d} = \text{Toeplitz}\left\{\left[1 \quad e^{-2(\pi\sigma_{fs,d})^2 + i2\pi f_{cs,d}} \cdots e^{-2(\pi\sigma_{fs,d}(N-1))^2 + i(N-1)2\pi f_{cs,d}}\right]\right\} \tag{11}$$

respectively.

Now we can modify the traditional schemes by using the covariance matrix in (9), possibly with slight modification, to replace the covariance matrix estimate of (7).

For our modified schemes, the covariance matrix is derived as

$$\begin{aligned} R_k(p) &= \text{E}\left\{\left(\tilde{X}_k(p) - \text{E}\left\{\tilde{X}_k(p)\right\}\right)\left(\tilde{X}_k(p) - \text{E}\left\{\tilde{X}_k(p)\right\}\right)^H\right\} \\ &= (A_p \otimes B_p)^H R_c (A_p \otimes B_p) \\ &= (A_p \otimes B_p)^H \left(\sum_{d=1}^{L} \sigma^2_{c,d} C_{t,d} \otimes C_{s,d}\right)(A_p \otimes B_p) \end{aligned}$$

$$= \sum_{d=1}^{L} \sigma_{c,d}^2 (A_p^H C_{t,d} A_p) \otimes (B_p^H C_{s,d} B_p) \qquad (12)$$

where (9) was used along with Theorem 8.8.2 and Theorem 8.8.6 in [6]. $C_{t,d}$ and $C_{s,d}$ are given in (10) and (11).

To illustrate the modified approach just described, the Sample Matrix Inversion algorithm (SMI), the Adaptive Displaced Phase-Centered Antenna algorithm (ADPCA), the Extended Factored Post-Doppler algorithm (EFA) and the Joint-Domain Localized algorithm (JDL) are used as examples. We call the new schemes modified SMI, modified ADPCA, modified EFA and modified JDL respectively.

For the modified schemes, we do not develop our covariance matrix estimate by performing averages over the adjacent range cells. Instead the covariance matrix is determined by the model parameters in (9) which are obtained from the range cell under test. Thus mismatch between the statistics of the reference data and the data from the cell under test is avoided, which can be a problem for traditional schemes in a highly non-homogeneous environment. In the traditional SMI, ADPCA, EFA and JDL schemes used in our comparison, we use a set of reference samples on either side of the cell-under-test. In our examples, 66 cells (33 on either side of the cell-under-test) are used for SMI, ADPCA and EFA. 10 cells are used for JDL (5 on each side of the cell-under-test). A covariance matrix is formed by averaging the covariance matrix estimated from each of those adjacent cells.

Obviously, the parameters for the model in (8) determine the required covariance matrix. Our tests indicate we do not need to estimate all these parameters for every range cell to achieve good performance. Our approach assumes some of the parameters are fixed at

reasonable values previously estimated. In particular, the parameters fixed are observed to have little impact on performance. We only devote computational resources to obtain the other 'key' parameters. Below is the discussion of each of the 'key' parameters and how to choose proper values for them.

3. Parameter choice

We use data that comes from the MCARM [7,8] database flight 5, acquisition 575 in our discussion. In order to obtain an estimate of the psd in the angle-Doppler domain, we apply an FFT to transform to the Doppler domain first, then we use the normalized steering vectors provided with the MCARM database to transform to the angle-Doppler domain. This would be essentially equivalent to performing a two dimensional FFT if the antenna array were a uniformly spaced linear array.

A. Slope of clutter ridge

The most important parameter of the model in (8) is the slope of the clutter ridge along which we center the Gaussian functions. The slope of clutter ridge is related to airplane's velocity which might be known directly from instruments on the aircraft. In our experiments, we have used some fast image processing algorithms to find this slope directly from data.

B. Number, amplitudes, and positions of humps

For simplicity, we fix the number of humps used and place them uniformly along the clutter ridge. If the number of humps is too small, the model cannot represent the real clutter well. On the other hand if the number of humps is too large, computational complexity increases with little performance improvement. Extensive testing indicated that using 4 or 5 humps is a good choice.

We also fix the amplitude of the humps. We found that reasonably good performance is obtained by setting the amplitude of each hump to be approximately 15% greater than the maximum value of the estimated psd. In this report, all the results shown use this choice.

C. $\sigma_{ft,d}, \sigma_{fs,d}$: parameters controlling the spread of the hump

Extensive experiments showed that spread parameters should be chosen differently for the pre-Doppler schemes (such as the modified SMI and the modified ADPCA) and the post-Doppler schemes (such as the modified EFA and the modified JDL).

For the pre-Doppler schemes, two ways are suggested to set the parameters $\sigma_{ft,d}, \sigma_{fs,d}$. One is setting a 'fixed' value for all humps. The fixed value should be set larger than that the estimated psd implies. The other method attempts to provide values that more closely match the estimated psd. In order to explain when each of these methods should be used we show some examples. We inserted a single synthetic moving target with a specified normalized Doppler frequency into a specified range cell to compare the detection performance for the two cases.

We present results which show the magnitude of the test statistic for the range cell-under-test and for surrounding range cells as in [5]. If the response at the range cell where the target is inserted is much larger than surrounding range cells, then we judge performance as being very good. We normalized all adaptive weights by a scalar (see (3) in [5]), which provides a CFAR test for homogeneous cases. The amplitude of the target is set at 0.05.

In the first example, we set $\sigma_{ft,i} = \sigma_{fs,i} = 0.1$, for $i = 1,\ldots,5$, and we inserted a single target with spatial frequency[1] 0.164 and normalized Doppler frequency 0.078, 0.156, or 0.312 in range bin 350. In a second set of results we inserted a single target in range bin 415 at the same set of spatial and Doppler frequencies. We present the results for modified ADPCA. The results are illustrated in Fig. 1.

In the second example, where we choose the spreads to more closely match what is observed in the psd estimate, we set $\sigma_{ft,i} = \sigma_{fs,i} = 0.01$, $i = 1,5$, and $\sigma_{ft,i} = \sigma_{fs,i} = 0.02$, $i = 2,3,4$. For this case, we get the performance shown in Fig. 2.

We note that for the target with normalized Doppler frequency 0.078 (whatever the range bin), the performance in the second case is much better than the first one. On the other hand, for the target with normalized Doppler frequency 0.156 and 0.312 (whatever the range bin) , the first case with 'fixed' and 'larger' $\sigma_{ft,d}, \sigma_{fs,d}$ will be better. The reason is that when target has the normalized Doppler frequency 0.078, its position is near the clutter ridge. If the spread parameters are too large, the target itself will be significantly

[1] In all the tests of this report, the spatial frequency of target is fixed at 0.164. Experiments showed that these results are representative.

suppressed. Thus, in this case, we should choose the parameters 'carefully' and use parameters which match the true parameters well. In the other cases, when the target has the normalized Doppler frequency 0.156 or 0.312, the target position is not so close to the clutter ridge. In this case it is better to use larger spread parameters to provide increased clutter suppression, since the target will not be suppressed when this is done. In practice, we can compare the relative target to clutter ridge position to a threshold to decide which way the $\sigma_{ft,d}, \sigma_{fs,d}$ parameters should be set. While the examples provided here are for modified ADPCA, further tests demonstrated that the conclusion is the same for all the other pre-Doppler processing schemes we tested.

For the post-Doppler schemes, we found that no matter where the target is in the angle-Doppler domain, the best choice for the spread parameters $\sigma_{ft,d}, \sigma_{fs,d}$ is using those that closely match the observed psd.

Four modified schemes are analyzed in next section and parameters are chosen according to the discussion in this section.

4. Performance comparison

Here, we will investigate the performance obtained when using the modified SMI, the modified ADPCA, the modified EFA and the modified JDL algorithms. Specifically we compare the performance of the modified scheme with that for the corresponding traditional scheme. The comparisons are similar to those in Fig. 1 and Fig. 2.

A. SMI

In our tests of SMI we use M=22 pulses and N=22 antennas in the adaptive processing. For the SMI scheme, we have $A_p = I_M$, $B_p = I_N$ in (2), where I_M, I_N are M×M and N×N identity matrices respectively, S_t and S_s are the target temporal and spatial response vectors respectively [1]. Post-processing is not necessary for SMI.

First, we inserted a single target with spatial frequency 0.164 and with normalized Doppler frequency of either 0.078, 0.156, or 0.312 in range bin 350. In a second set of tests, a single target with spatial frequency 0.164 and with normalized Doppler frequency of either 0.078, 0.156, or 0.312 was inserted in range bin 415. In each case the amplitude at the target was 0.05. Using modified SMI, we obtain the results in Fig. 3. Traditional SMI yielded the results in Fig. 4. For the case of range bin 350, the performance of the two schemes is close except when the target is far from the clutter ridge. In particular, the performance of the traditional SMI scheme in Fig. 3(e) is much better than that of the modified scheme in Fig. 4(e). On the other hand, the modified scheme is always much better for range bin 415 as illustrated in Fig. 3 and Fig. 4.

In order to explain the difference between the results for range bin 350 and those for range bin 415, we consider Fig. 5 which shows average energy as a function of range bin. Near range bin 350, the variation is not too great. In this case it is advantageous to average over range when estimating the covariance matrix and this leads to the good performance of traditional SMI. Since traditional SMI is optimum when the estimate of the covariance matrix is perfect, it is reasonable that we cannot outperform SMI in some cases where this is close to being true. On the other hand, Fig. 5 shows a large jump in energy near range

bin 400. So this would impact the averaging performed in the traditional schemes when a target is inserted in range bin 415. This non-homogeneous reference data leads to the poor performance of traditional SMI and in turn to the superior performance of modified SMI.

B. ADPCA

For ADPCA, the matrices A_p and B_p used in (2) are

$$A_p = \begin{bmatrix} 0_{p\times K_t} \\ I_{k_t} \\ 0_{(M-K_t-p)\times K_t} \end{bmatrix}, \qquad B_p = I_N \tag{13}$$

where the notation $0_{q\times m}$ refers to a q$\times$m matrix of zeros. In this research M is set to 128, N is set to 22 and k_t is set to 3. The A_p in (13) groups the M pulses in subgroups of size 3 with each group overlapping by 2 pulses. In the adaptive processing part, $S_t = [1 \quad -2 \quad 1]$, and S_s is the target spatial response vector. In the Post-processing part, f_m is the Doppler filter corresponding to the target Doppler frequency.

There are a number of advantages to partially adaptive schemes in general and ADPCA in particular, see [3, 4] for a discussion on these issues. In order to compare the performance of the traditional ADPCA scheme and the modified ADPCA scheme, we consider the same cases as for SMI. In addition, we also considered targets with normalized Doppler frequency of 0.039, 0.117 or 0.234. The results for modified ADPCA and traditional ADPCA are shown in Fig. 6 and Fig. 7 respectively. The modified scheme is clearly better for cases where the target has the normalized Doppler frequency 0.039 or 0.078, (when the

target is near the clutter ridge). For cases where the target has the normalized Doppler frequency 0.117 or 0.156, (where the clutter ridge is not so close to the target), the modified scheme results are significantly better for range bin 415. However, performance is about the same when the target is in range bin 350. For cases where the target has the normalized Doppler frequency 0.234 or 0.312, (where the clutter ridge is far from the target), the traditional scheme is better for range bin 350 while the schemes provide about the same performance for range bin 415. Taken collectively these results indicate the modified scheme should be used in non-stationary cases. The advantages seem to be especially clear when the target is near the clutter ridge.

C. EFA

For the EFA scheme, the pre-processing is as in (2) with

$$A_p = \left[f_{p-1}, f_p, f_{p+1} \right] \qquad B_p = I_N, \tag{14}$$

where f_{p-1}, f_p, f_{p+1} are three adjacent Doppler filters and f_p corresponds to the normalized Doppler frequency of target. The adaptive processing uses $S_t = \begin{bmatrix} 0 & 1 & 0 \end{bmatrix}^T$ and S_s set to the target spatial response vector. Only processing for a single p must be performed and so post-processing is not needed.

The results for modified EFA and traditional EFA are given in Fig. 8 and Fig. 9. The results for range bin 350 indicate that when the target is inserted far from the clutter ridge (target with normalized Doppler frequency 0.234 or larger), the modified scheme achieves significantly better performance. In the other cases, the modified scheme is slightly better. For range bin 415, the modified scheme provides better results in all cases except the case

in which the target has normalized Doppler frequency 0.117. Since we have already identified range bin 350 as an almost stationary case and range bin 415 as a highly non-stationary case, these results are reasonable. It is known that in a nearly homogeneous case, we should use the traditional scheme since in this case the estimate of the covariance matrix is a maximum likelihood estimate. In a highly non-homogeneous case, it is reasonable that the modified scheme can provide better performance.

D. JDL

For JDL the matrices in (2) should be taken as

$$A_p = \left[f_{p-1}, f_p, f_{p+1}\right], \quad B_p = [g_{q-1}, g_q, g_{q+1}], \tag{15}$$

where f_{p-1}, f_p, f_{p+1} are three Doppler filters and f_p is that filter which corresponds to the normalized Doppler frequency of target. f_{p-1} and f_{p+1} are Doppler filters corresponding to neighboring Doppler frequencies. g_{q-1}, g_q, g_{q+1} are three spatial filters and g_q is that filter which corresponds the spatial steering vector of the target. g_{q-1} and g_{q+1} are spatial filters corresponding to neighboring spatial frequencies. The steering vector S in the adaptive processing is

$$S = S_t \otimes S_s = \left[0 \quad 1 \quad 0\right] \otimes \left[0 \quad 1 \quad 0\right] \tag{16}$$

As for EFA, processing must be performed for only one p so post-processing is not needed.

We repeat the tests made for EFA for JDL to compare the performance of the modified and the traditional schemes. The results are given in Fig. 10 and Fig. 11 respectively. When the target is inserted in range bin 350, the performance of modified scheme is much worse than the traditional scheme. The problem seems to be that traditional JDL performs very well in these cases. When the target is inserted in range bin 415 far from the clutter ridge (target with normalized Doppler frequency 0.234 or 0.312), the modified scheme is better. In the other cases considered for range bin 415, the performance is about the same. Thus the performance of modified JDL is rather poor in the homogeneous case. However in most non-homogeneous cases, it performs well.

5. Conclusion

We have suggested the use of some modified schemes for adaptive airborne radar, which use the knowledge of the structure of the interference. The specific numerical results given use a model which only assumes ground clutter, while these results are obtained for a measured radar data set which includes other interference.

From the comparisons, it appears that the modified scheme can provide good performance in the cases that are traditionally considered to be difficult. It performs better in non-homogeneous cases when compared to schemes which average over range to estimate the required covariance matrix. This is reasonable since the modified schemes obtain the covariance matrix from a single range cell. However, when the target is inserted in a homogeneous environment, in most cases the traditional schemes are better.

References

1. H. Wang and L. Cai, "On adaptive spatial-temporal processing for airborne surveillance radar systems," IEEE Transactions on Aerospace and Electronic Systems, Vol. 30, pp. 660-669, July 1994.
2. J. Ward, *Space-Time Adaptive Processing for Airborne Radar*, Technical Report 1015, Lincoln Laboratory, 1995.
3. R. S. Blum, W. L. Melvin, and M. C. Wicks, "An analysis of the adaptive displaced phase centered antenna space-time processing algorithm," 1996 Radar Conference, Ann Arbor, Michigan, pp. 303-308.
4. Z. Gu, R. S. Blum, W. L. Melvin, and M. C. Wicks, "Performance Comparison of STAP Algorithms for Airborne Radar," 1997 Radar Conference, Syracuse, NY, May 1997, pp. 60-65.
5. W. L. Melvin and B. Himed, "Comparative Analysis of Space-Time Adaptive Algorithms with Measured Airborne Data", presented at the 7th International Conference on Signal Processing Applications and Technology, October 7-10, 1996.
6. F. A. Graybill, "Introduction to Matrices with Applications in Statistics", Belmont, CA: Wadsworth Publishing, 1969 (especially pp. 201-204).
* 7. D. sloper et. al., *MCARM Final Rept.*, Rome Lab tech. Rept., RL-TR-96-49, April 1996.

MCARM database web site-Rome Laboratory USAF, 'http://128.132.2.

*Although this report references the above limited report, no limited information has been extracted.

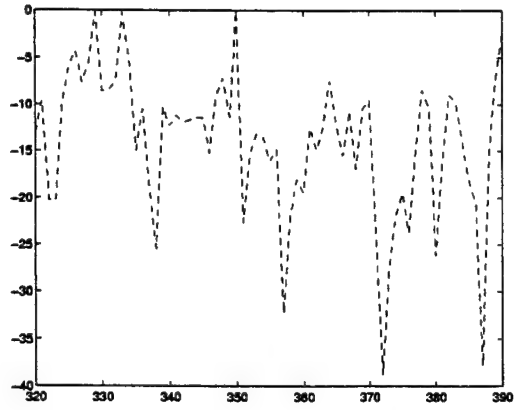

a) range bin 350, Doppler frequency 0.078

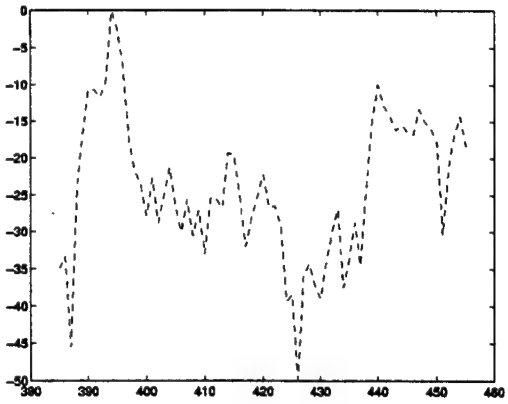

b) range bin 415, Doppler frequency 0.078

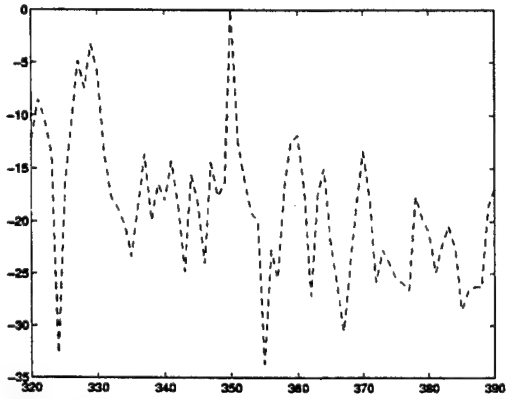

c) range bin 350, Doppler frequency 0.156

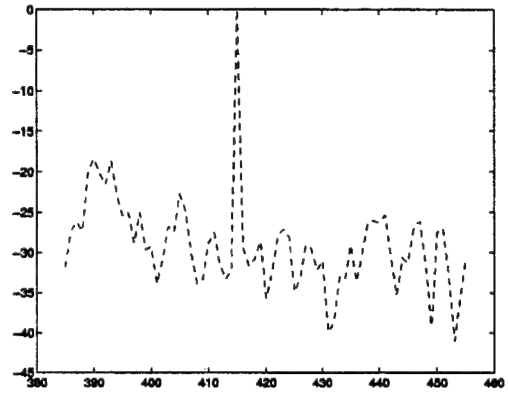

d) range bin 415, Doppler frequency 0.156

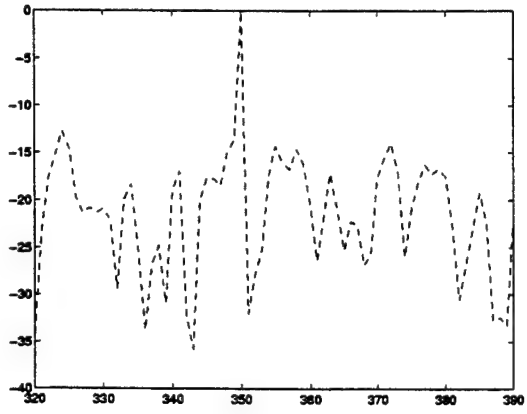

e) range bin 350, Doppler frequency 0.312

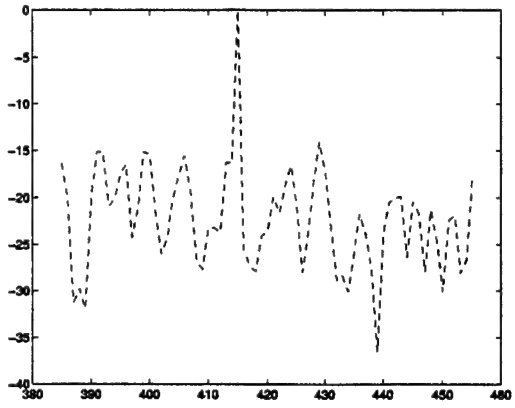

f) range bin 415, Doppler frequency 0.312

Figure 1) Performance comparison for target inserted in different range bins and with several different normalized Doppler frequencies for modified ADPCA when $\sigma_{ft,d} = \sigma_{fs,d} = 0.1, d = 1,\ldots,5.$

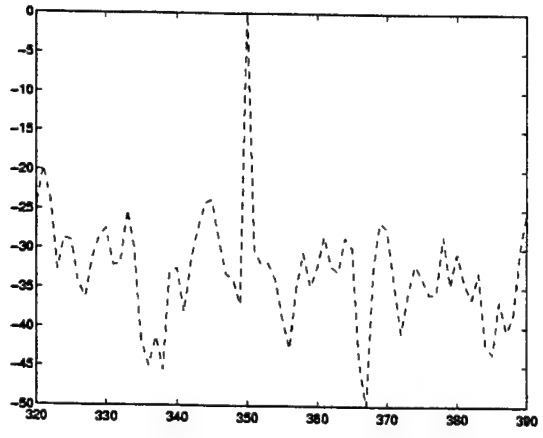

a) range bin 350, Doppler frequency 0.078

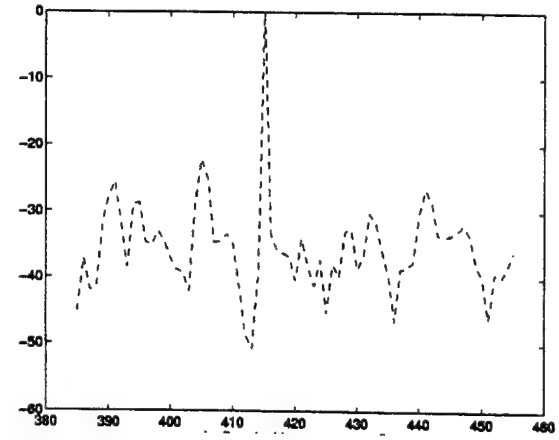

b) range bin 415, Doppler frequency 0.078

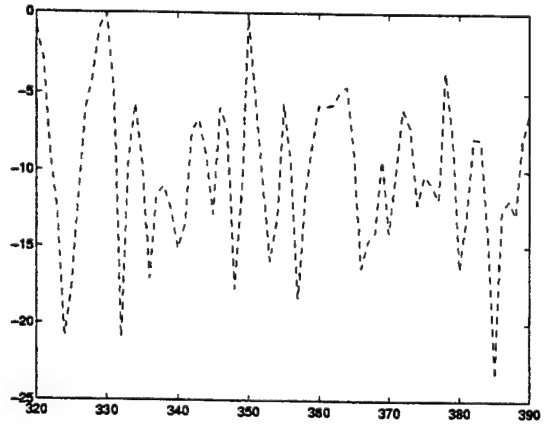

c) range bin 350, Doppler frequency 0.156

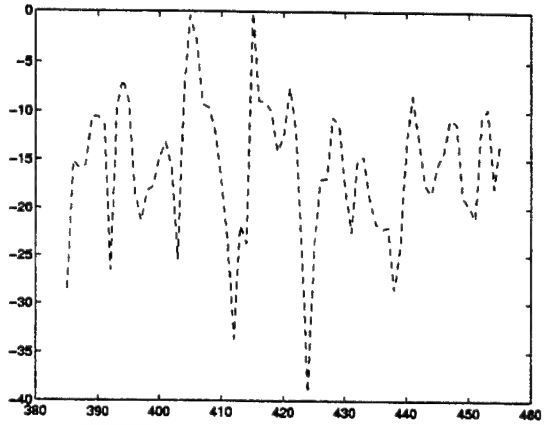

d) range bin 415, Doppler frequency 0.156

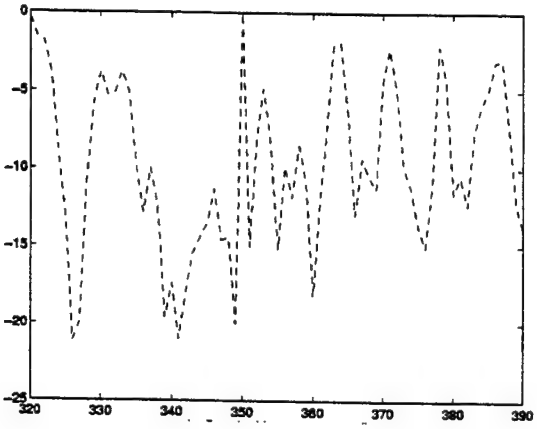

e) range bin 350, Doppler frequency 0.312

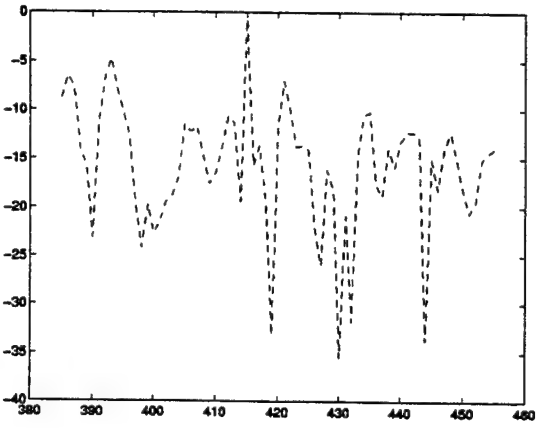

f) range bin 415, Doppler frequency 0.312

Figure 2) Performance comparison for target inserted in different range bins and with several different normalized Doppler frequencies for modified ADPCA when $\sigma_{ft,i} = \sigma_{fs,i} = 0.01$, $i = 1,5$, and $\sigma_{ft,j} = \sigma_{fs,j} = 0.02$, $j = 2,3,4$.

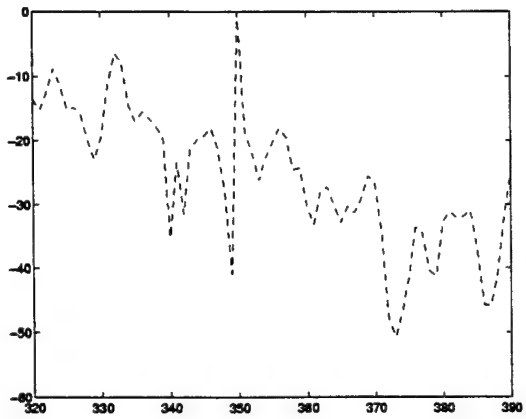

a) range bin 350, Doppler frequency 0.078

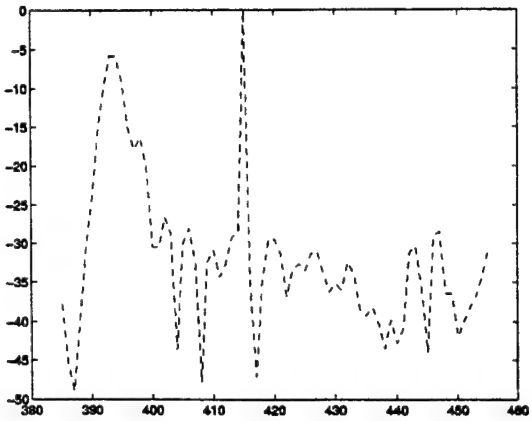

b) range bin 415, Doppler frequency 0.078

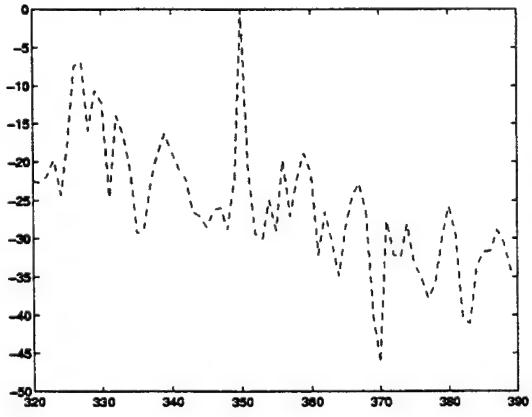

c) range bin 350, Doppler frequency 0.156

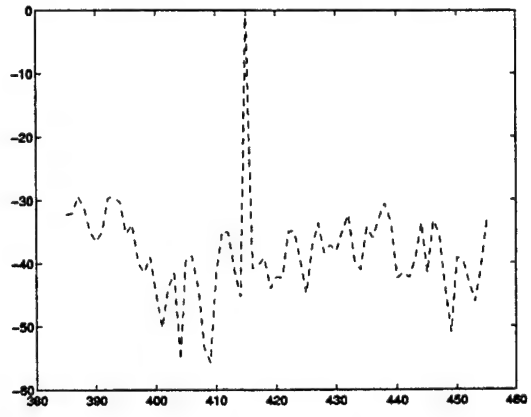

d) range bin 415, Doppler frequency 0.156

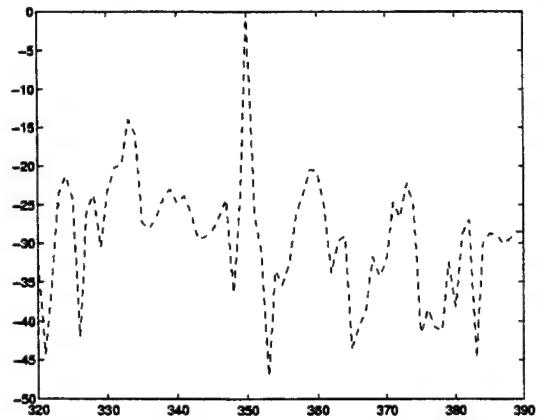

e) range bin 350, Doppler frequency 0.312

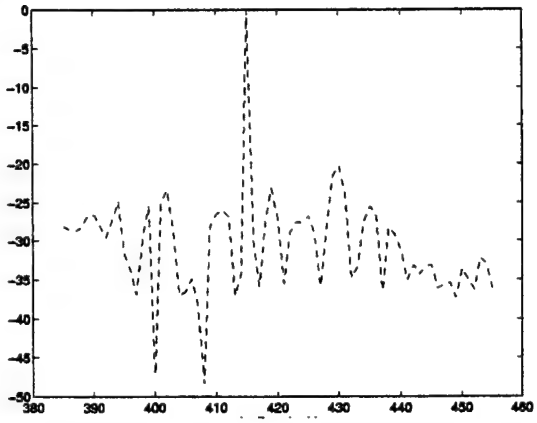

f) range bin 415, Doppler frequency 0.312

Figure 3) Performance for modified SMI when target is inserted in a particular range bin with a particular normalized Doppler frequency. In each case the normalized spatial frequency of the target is 0.164.

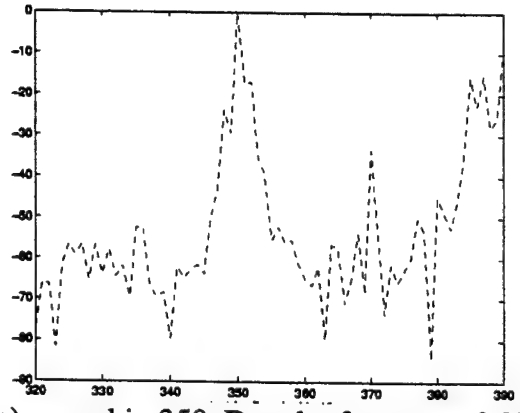

a) range bin 350, Doppler frequency 0.078

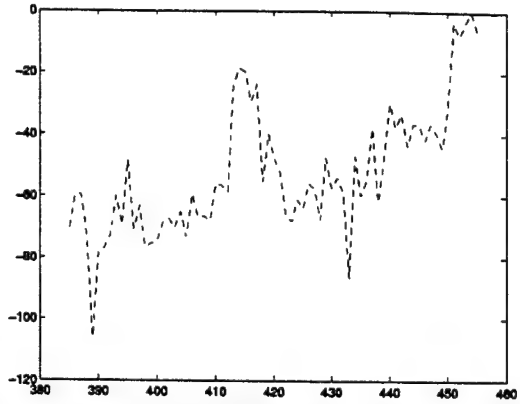

b) range bin 415, Doppler frequency 0.078

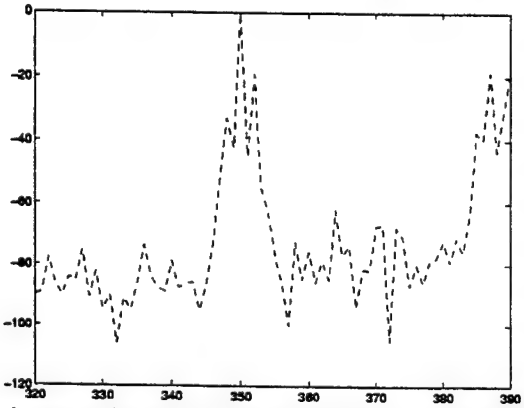

c) range bin 350, Doppler frequency 0.156

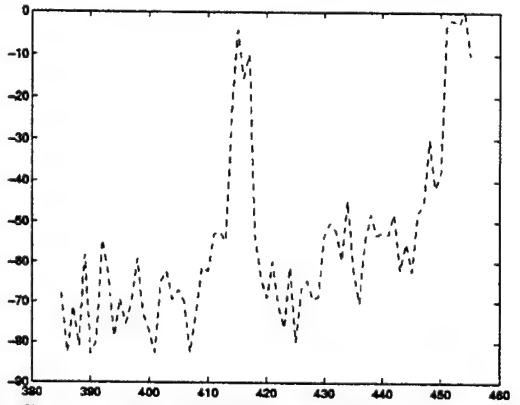

d) range bin 415, Doppler frequency 0.156

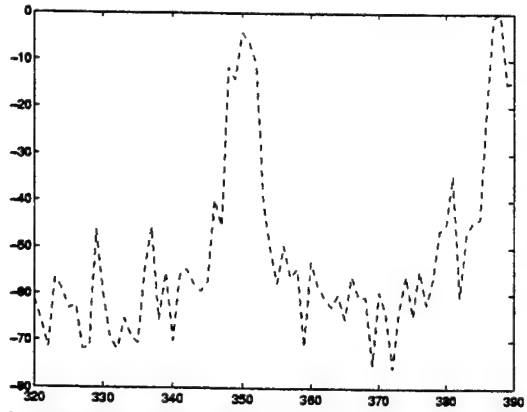

e) range bin 350, Doppler frequency 0.312

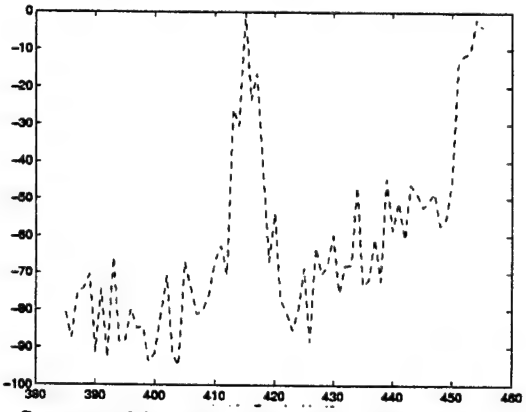

f) range bin 415, Doppler frequency 0.312

Figure 4) Performance for traditional SMI when target is inserted in a particular range bin with a particular normalized Doppler frequency. In each case the normalized spatial frequency of the target is 0.164.

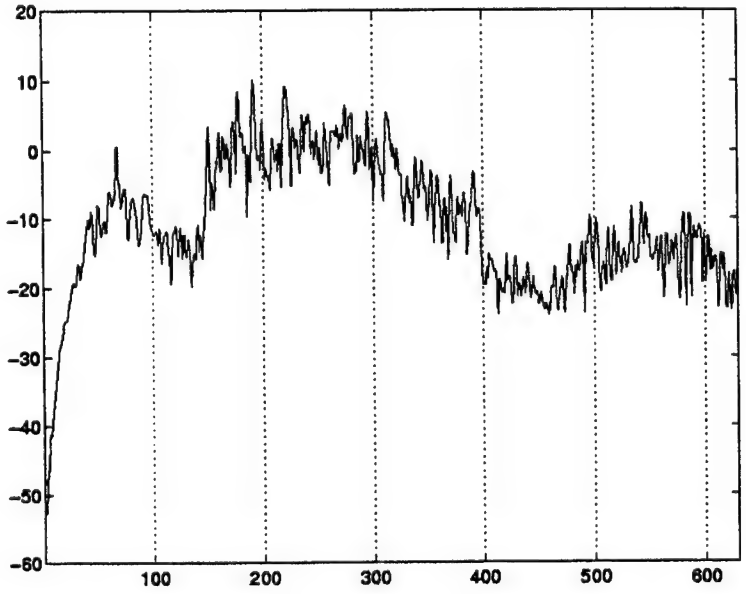

Figure 5) Average energy as a function of range bin

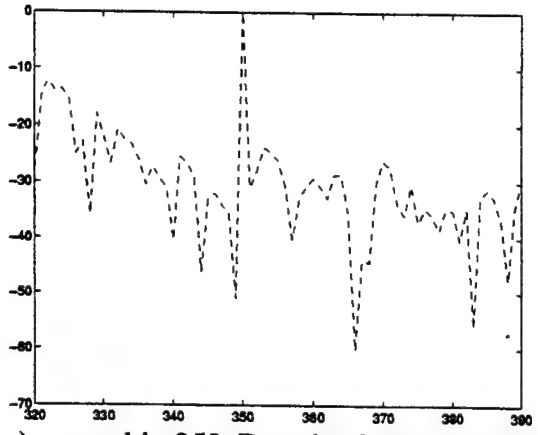

a) range bin 350, Doppler frequency 0.039

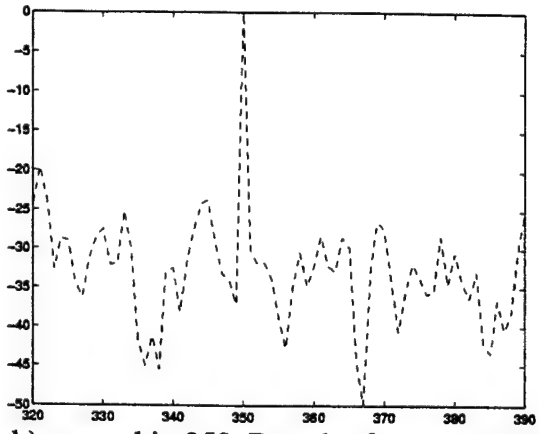

b) range bin 350, Doppler frequency 0.078

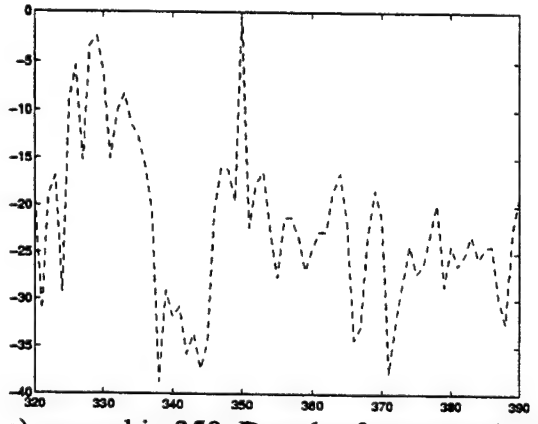

c) range bin 350, Doppler frequency 0.117

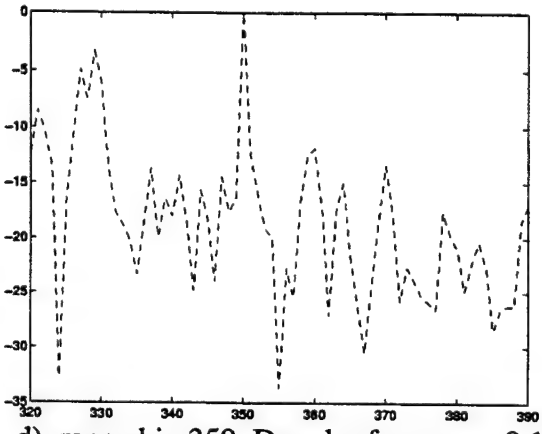

d) range bin 350, Doppler frequency 0.156

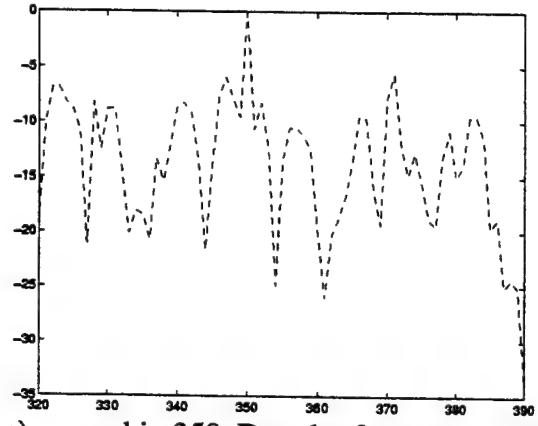

e) range bin 350, Doppler frequency 0.234

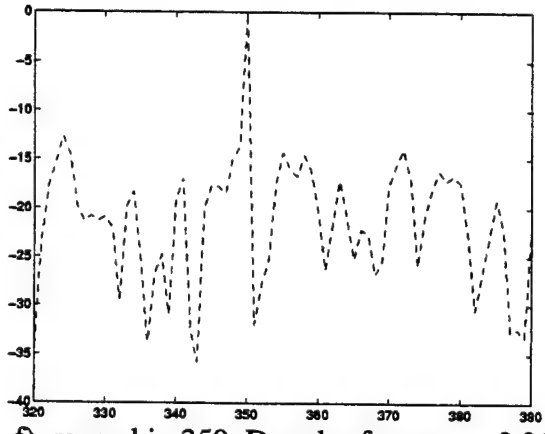

f) range bin 350, Doppler frequency 0.312

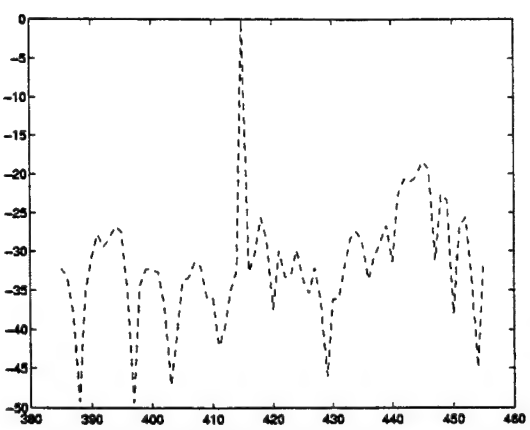
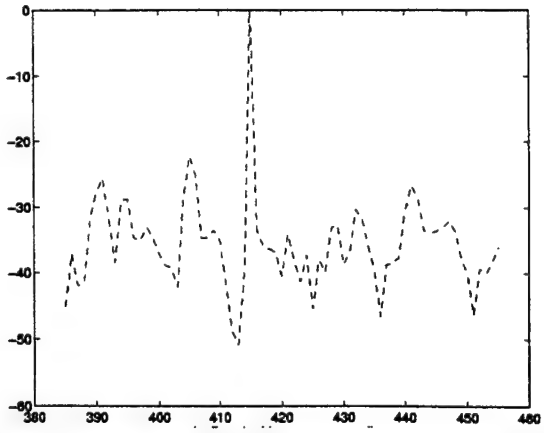

g) range bin 415, Doppler frequency 0.039 h) range bin 415, Doppler frequency 0.078

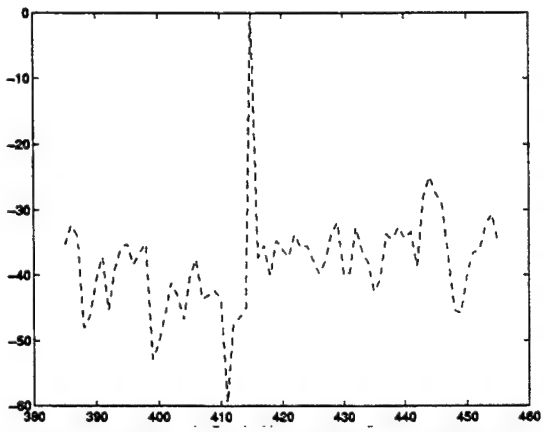
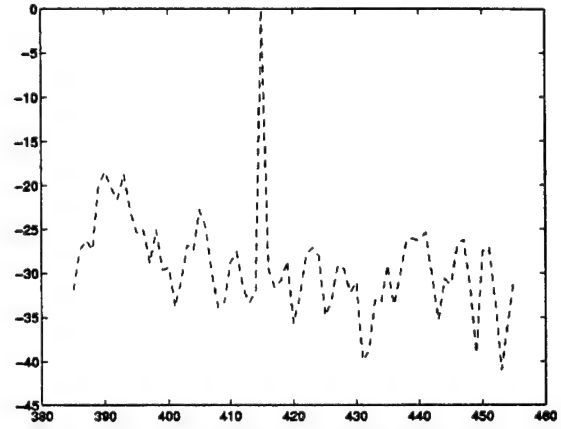

i) range bin 415, Doppler frequency 0.117 j) range bin 415, Doppler frequency 0.156

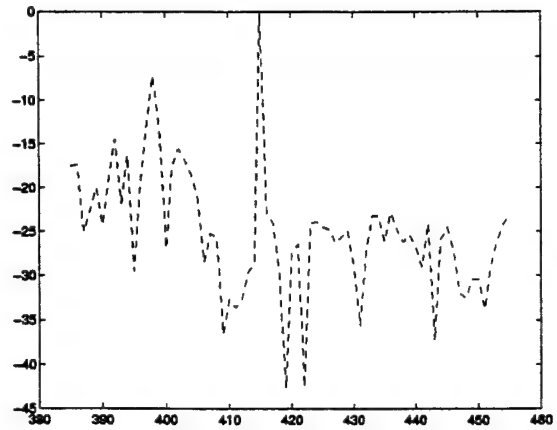
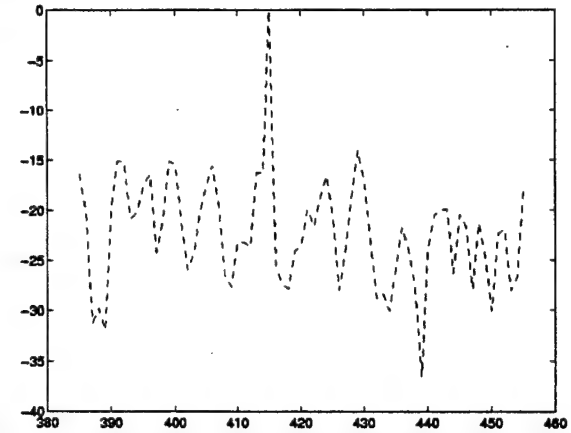

k) range bin 415, Doppler frequency 0.234 l) range bin 415, Doppler frequency 0.312

Figure 6) Performance for modified ADPCA when target is inserted in a particular range bin with a particular normalized Doppler frequency. In each case the normalized spatial frequency of the target is 0.164.

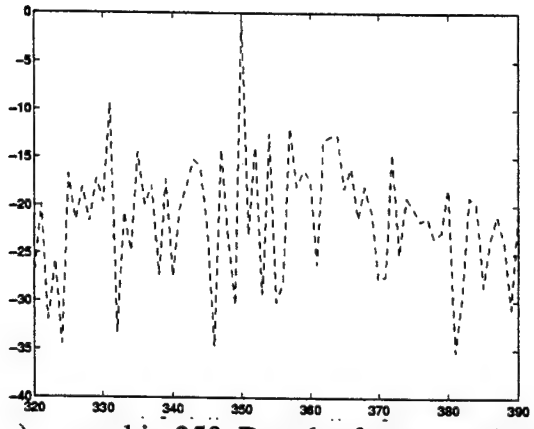

a) range bin 350, Doppler frequency 0.039

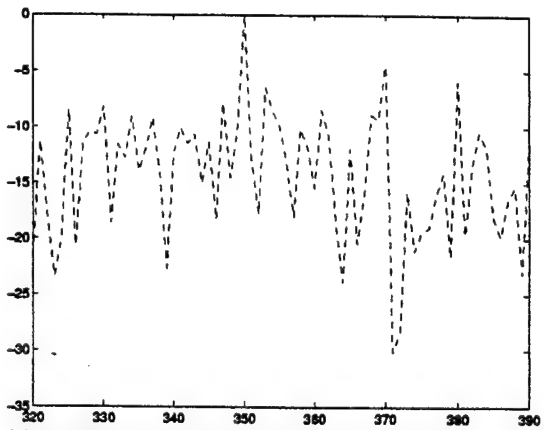

b) range bin 350, Doppler frequency 0.078

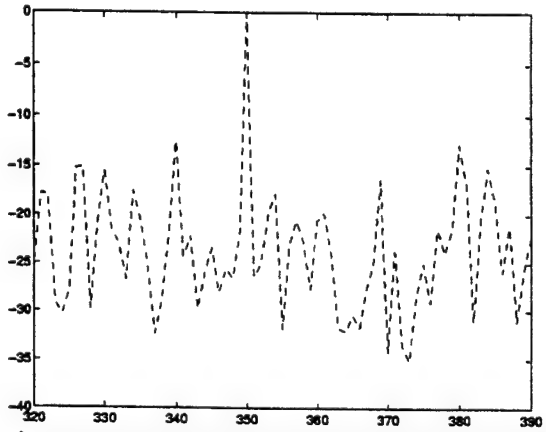

c) range bin 350, Doppler frequency 0.117

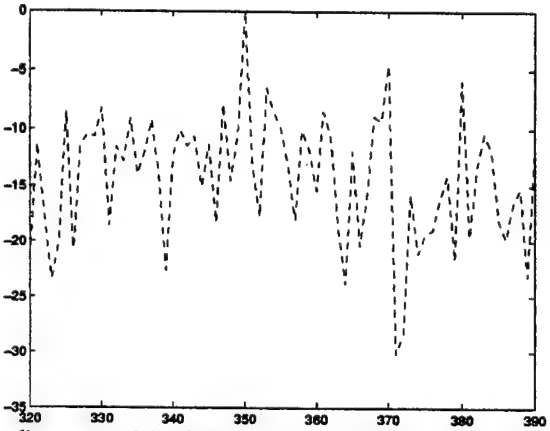

d) range bin 350, Doppler frequency 0.156

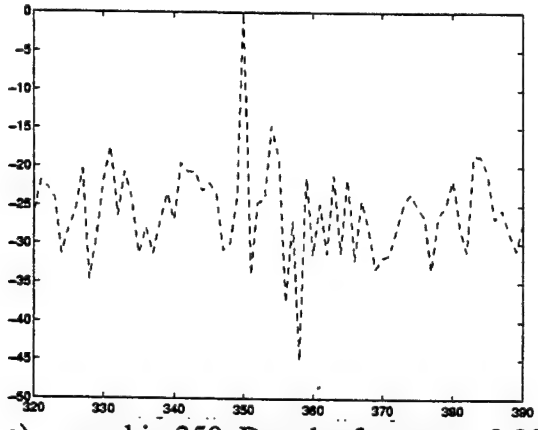

e) range bin 350, Doppler frequency 0.234

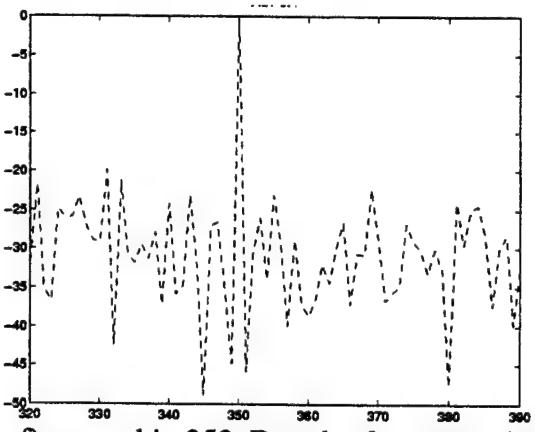

f) range bin 350, Doppler frequency 0.312

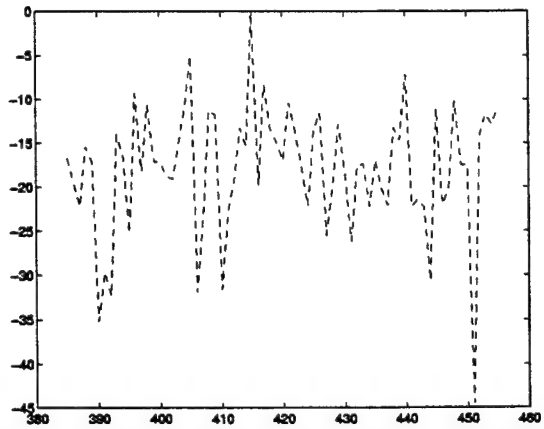

g) range bin 415, Doppler frequency 0.039

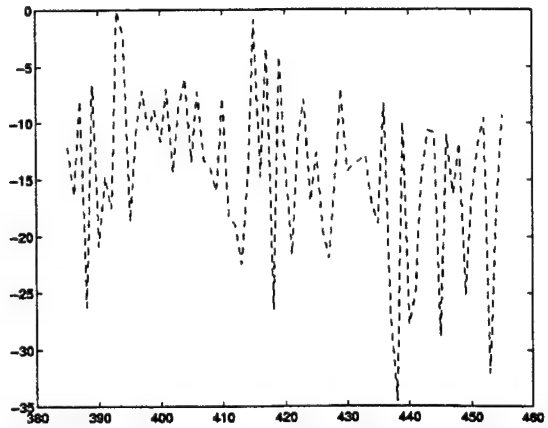

h) range bin 415, Doppler frequency 0.078

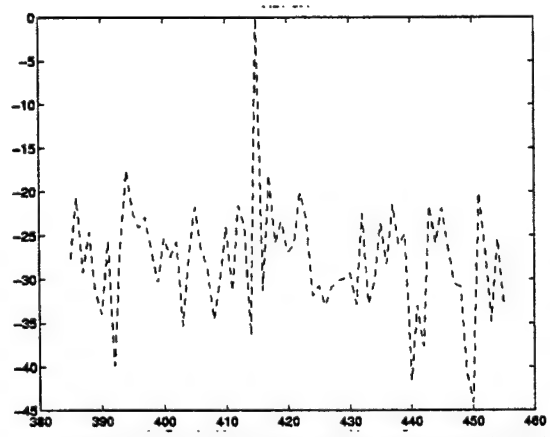

i) range bin 415, Doppler frequency 0.117

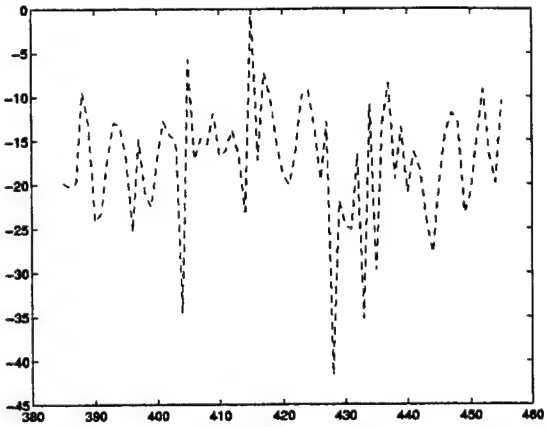

j) range bin 415, Doppler frequency 0.156

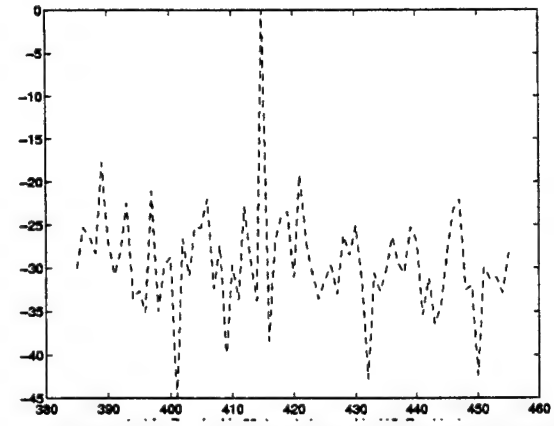

k) range bin 415, Doppler frequency 0.234

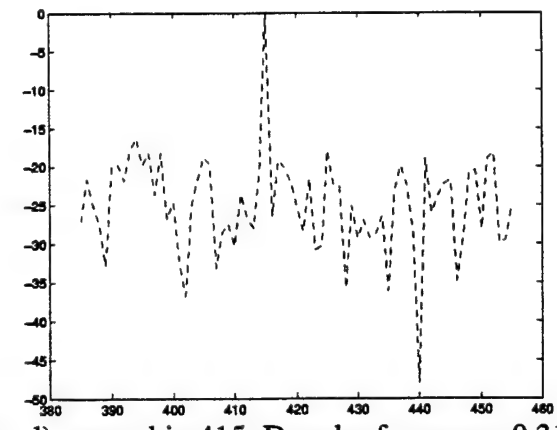

l) range bin 415, Doppler frequency 0.312

Figure 7) Performance for traditional ADPCA when target is inserted in a particular range bin with a particular normalized Doppler frequency. In each case the normalized spatial frequency of the target is 0.164.

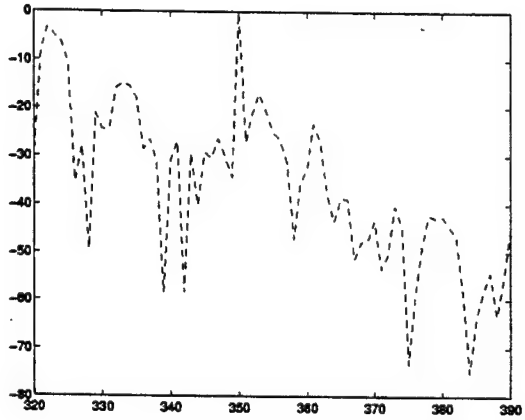

a) range bin 350, doppler frequency 0.039

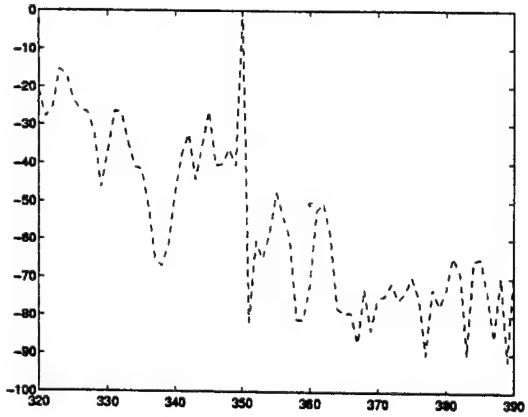

b) range bin 350, doppler frequency 0.078

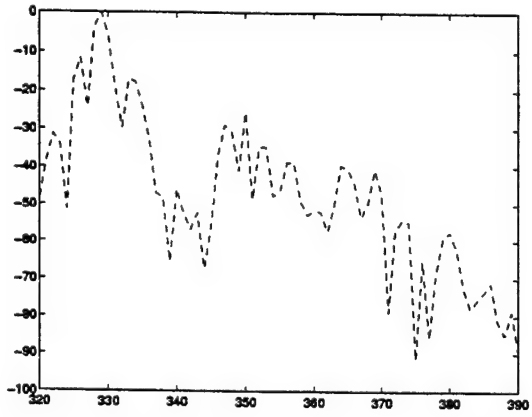

c) range bin 350, doppler frequency 0.117

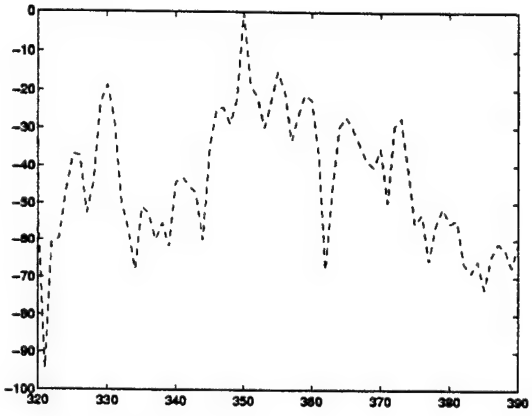

d) range bin 350, doppler frequency 0.156

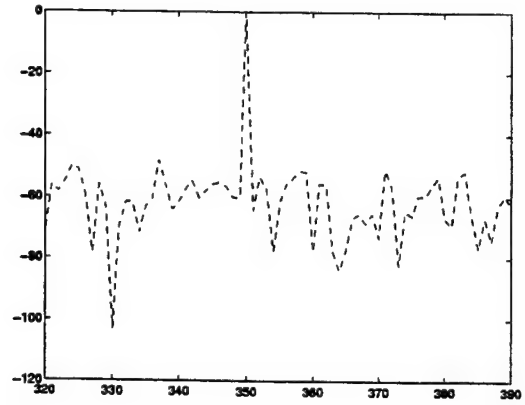

e) range bin 350, doppler frequency 0.234

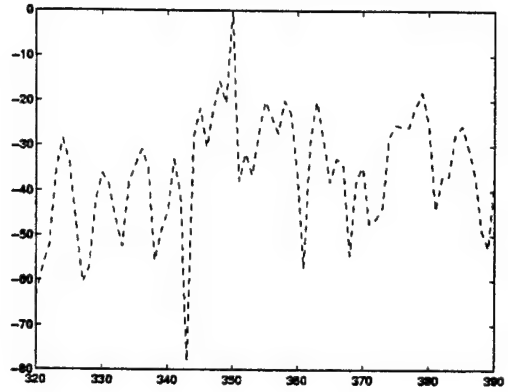

f) range bin 350, doppler frequency 0.312

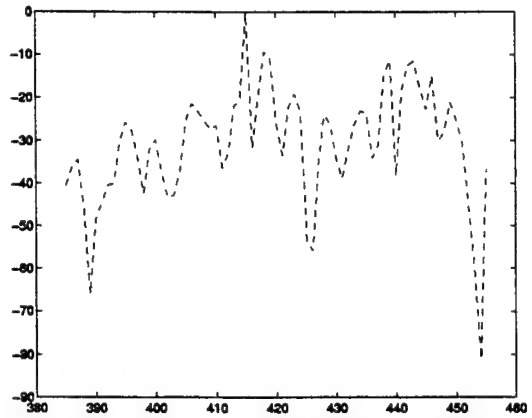

g) range bin 415, doppler frequency 0.039

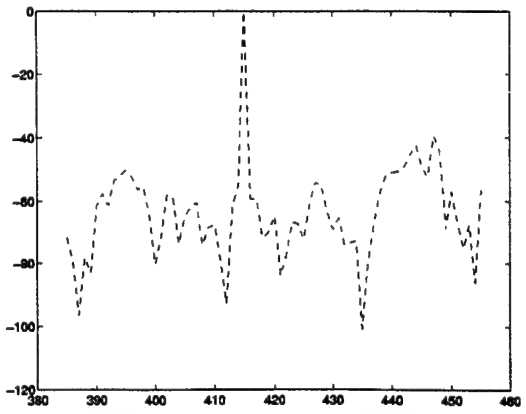

h) range bin 415, doppler frequency 0.078

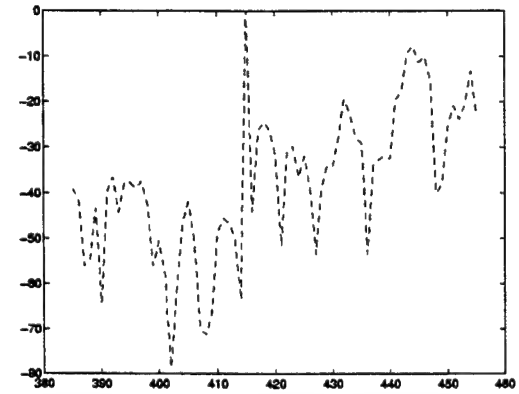

i) range bin 415, doppler frequency 0.117

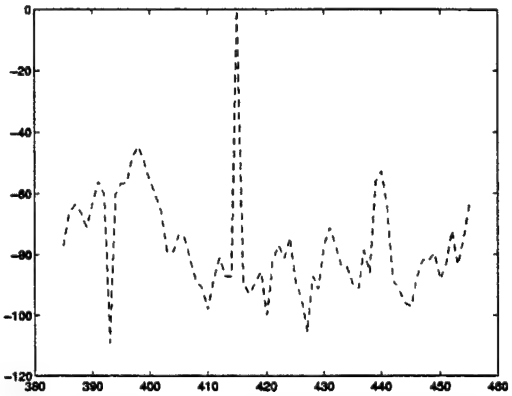

j) range bin 415, doppler frequency 0.156

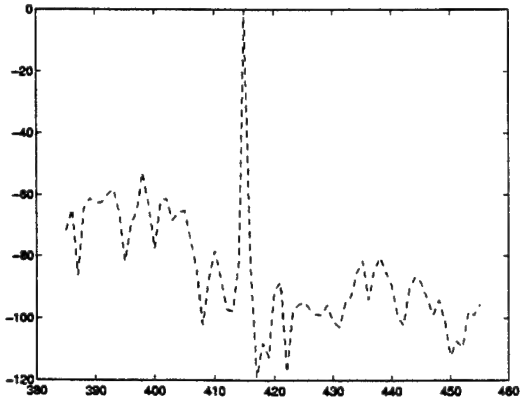

k) range bin 415, doppler frequency 0.234

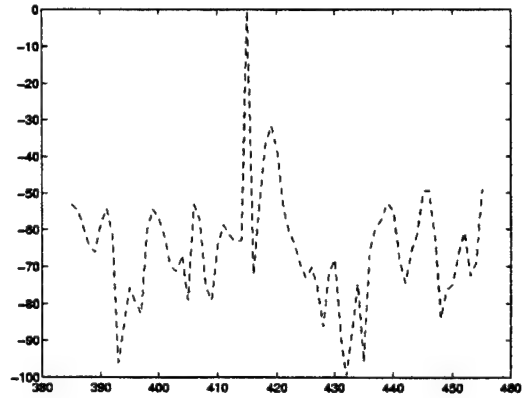

l) range bin 415, doppler frequency 0.312

Figure 8) Performance for modified EFA when target is inserted in a particular range bin with a particular normalized Doppler frequency. In each case the normalized spatial frequency of the target is 0.164.

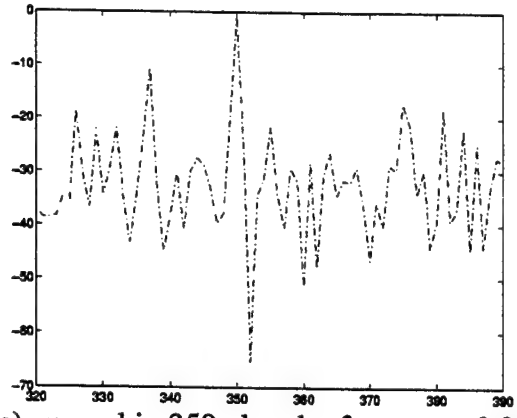

a) range bin 350, doppler frequency 0.039

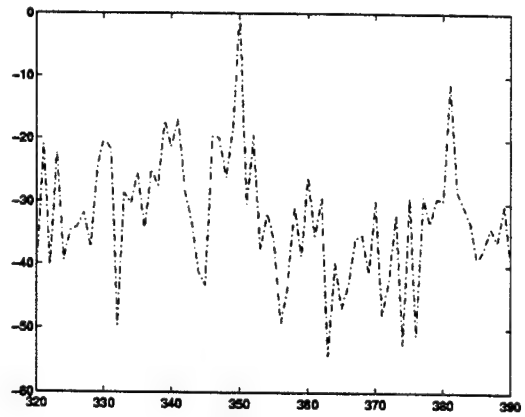

b) range bin 350, doppler frequency 0.078

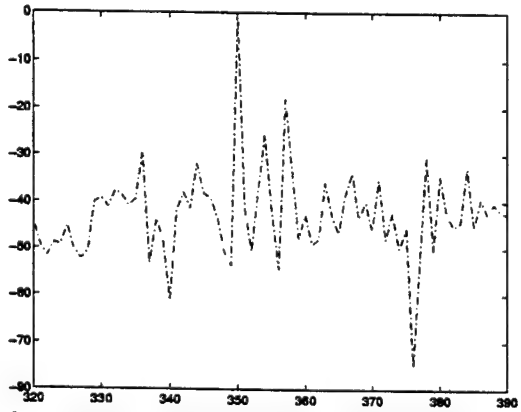

c) range bin 350, doppler frequency 0.117

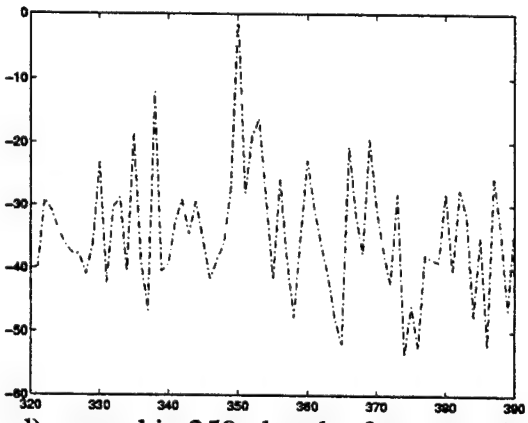

d) range bin 350, doppler frequency 0.156

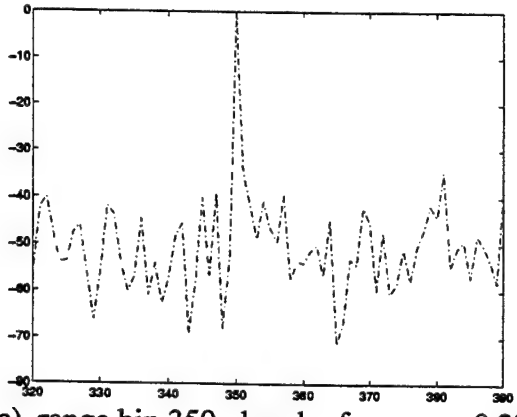

e) range bin 350, doppler frequency 0.234

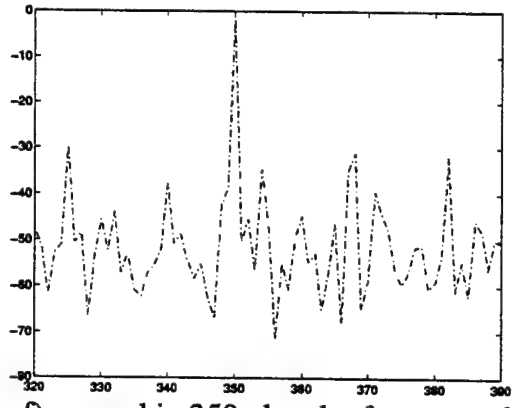

f) range bin 350, doppler frequency 0.312

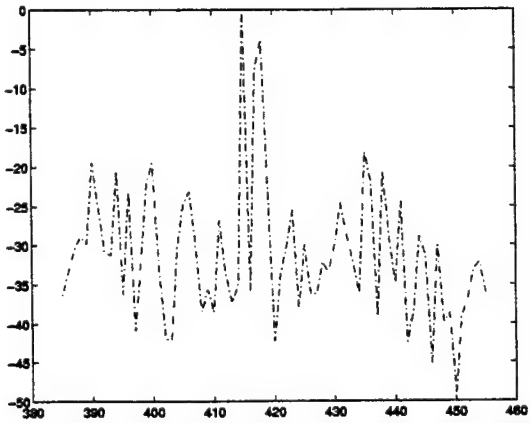

g) range bin 415, doppler frequency 0.039

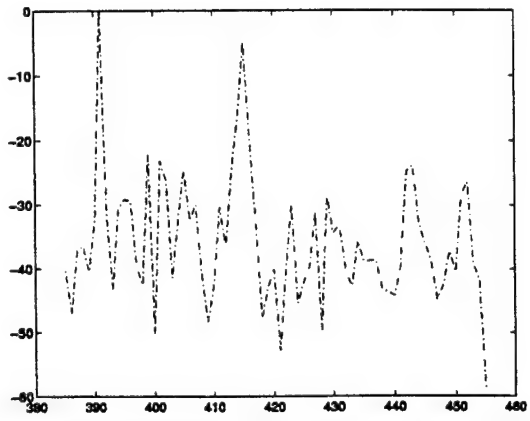

h) range bin 415, doppler frequency 0.078

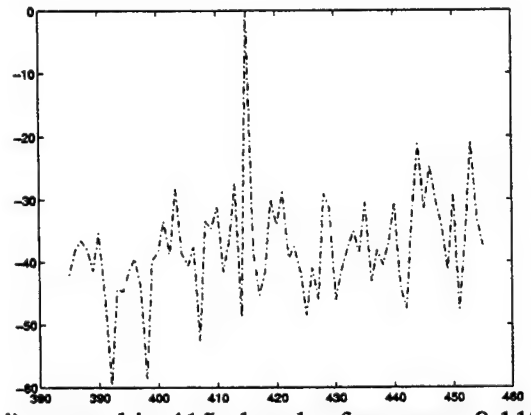

i) range bin 415, doppler frequency 0.117

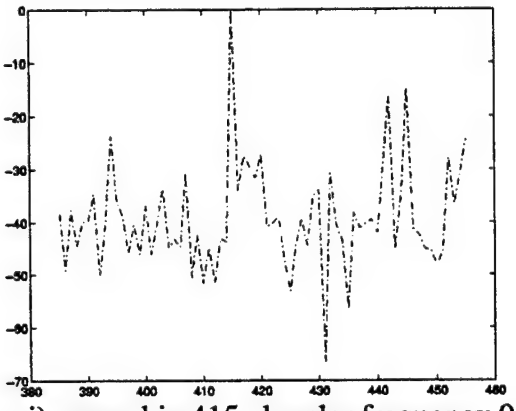

j) range bin 415, doppler frequency 0.156

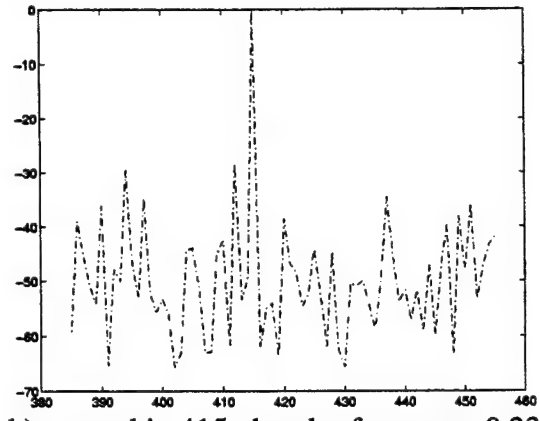

k) range bin 415, doppler frequency 0.234

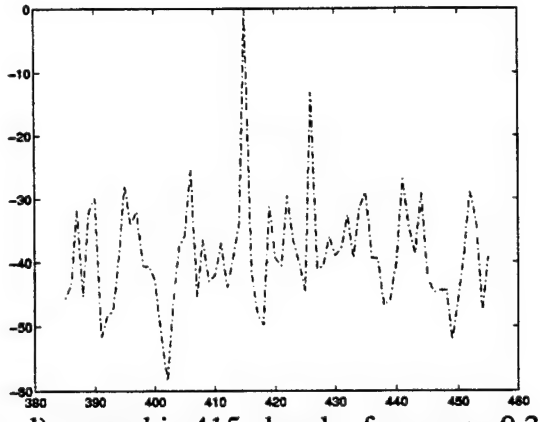

l) range bin 415, doppler frequency 0.312

Figure 9) Performance for traditional EFA when target is inserted in a particular range bin with a particular normalized Doppler frequency. In each case the normalized spatial frequency of the target is 0.164.

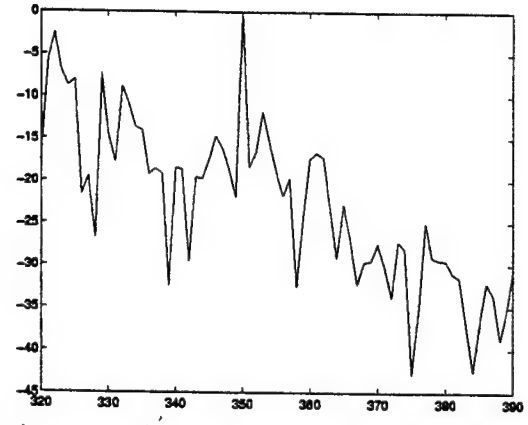

a) range bin 350, Doppler frequency 0.039

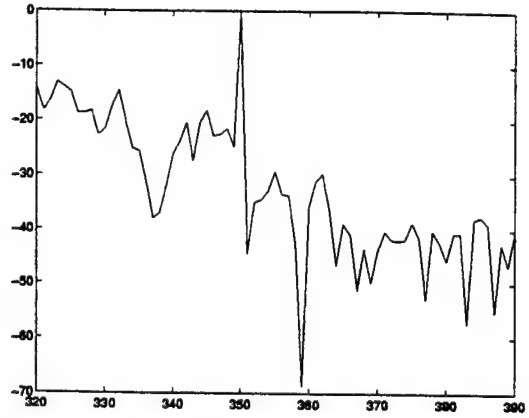

b) range bin 350, doppler frequency 0.078

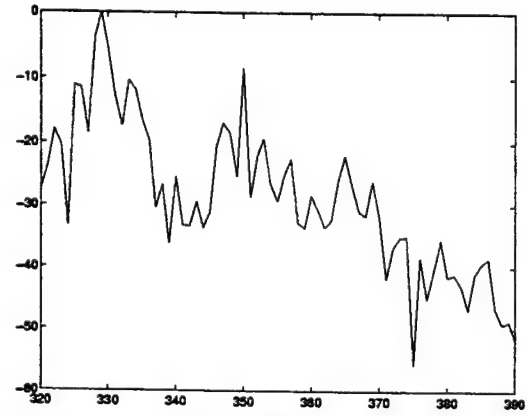

c) range bin 350, doppler frequency 0.117

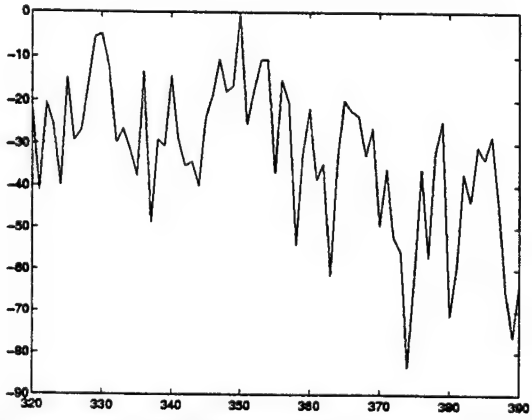

d) range bin 350, doppler frequency 0.156

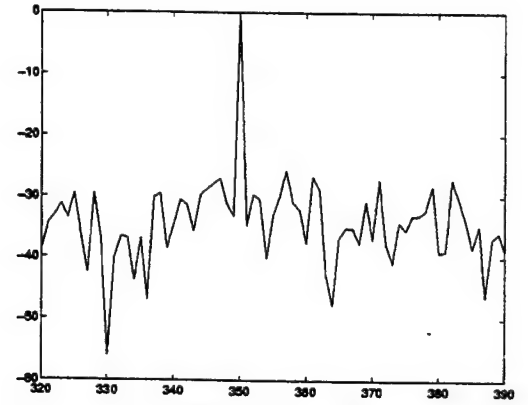

e) range bin 350, doppler frequency 0.234

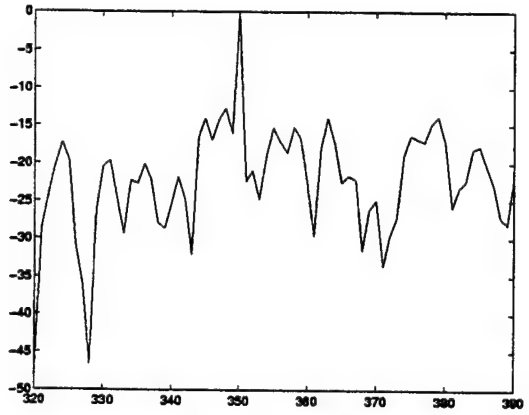

f) range bin 350, doppler frequency 0.312

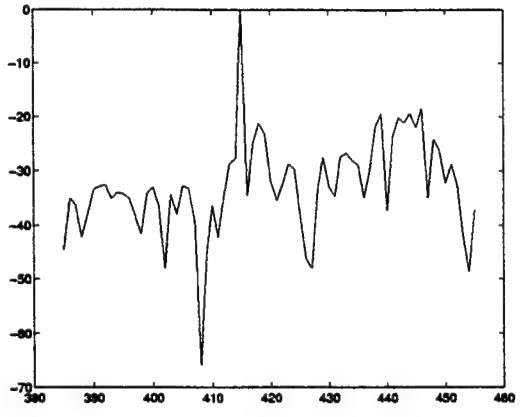

g) range bin 415, doppler frequency 0.039

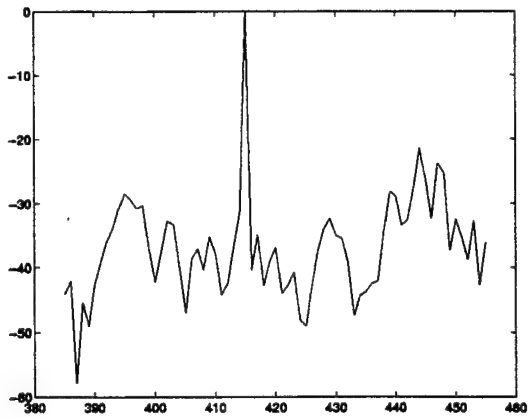

h) range bin 415, doppler frequency 0.078

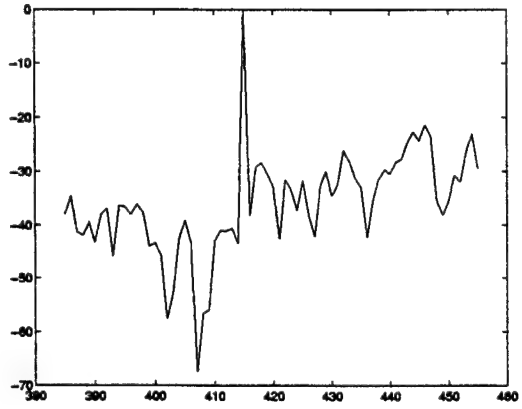

i) range bin 415, doppler frequency 0.117

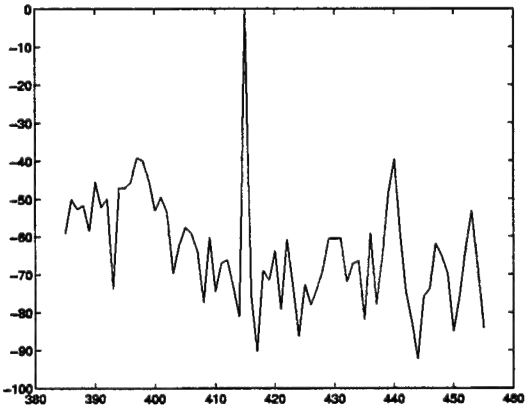

j) range bin 415, doppler frequency 0.156

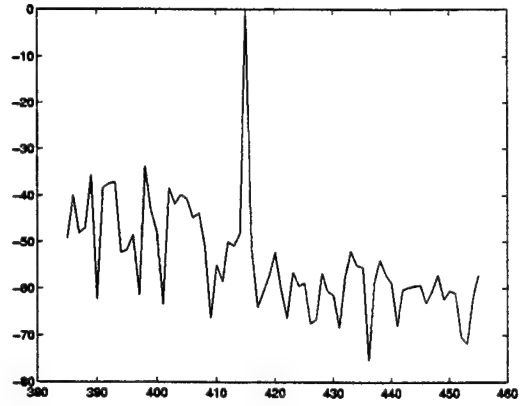

k) range bin 415, doppler frequency 0.234

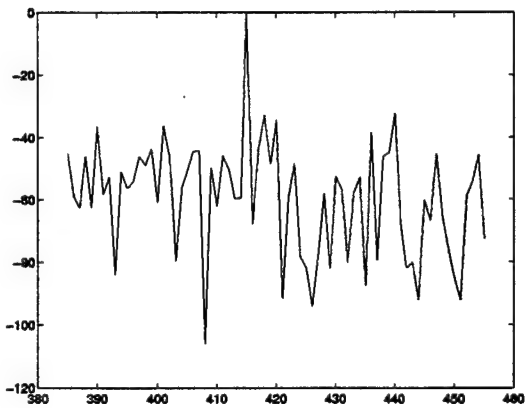

l) range bin 415, doppler frequency 0.312

Figure 10) Performance for modified JDL when target is inserted in a particular range bin with a particular normalized Doppler frequency. In each case the normalized spatial frequency of the target is 0.164.

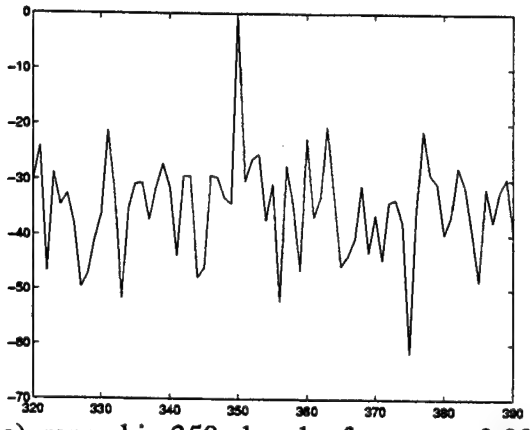

a) range bin 350, doppler frequency 0.039

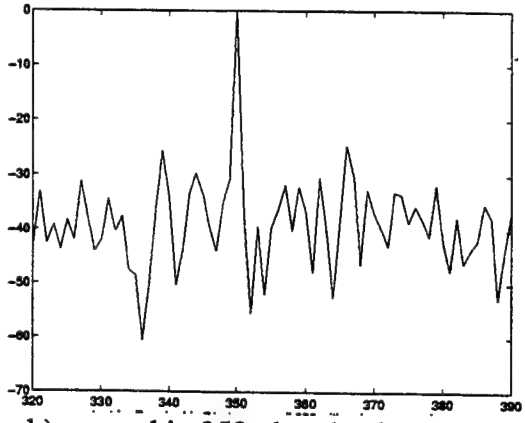

b) range bin 350, doppler frequency 0.078

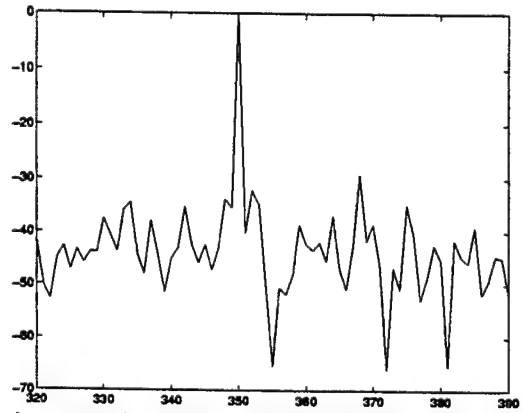

c) range bin 350, doppler frequency 0.117

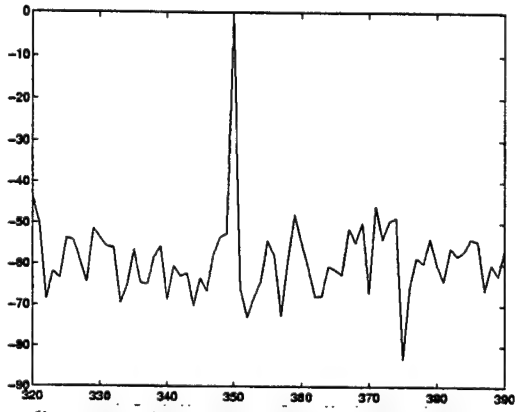

d) range bin 350, doppler frequency 0.156

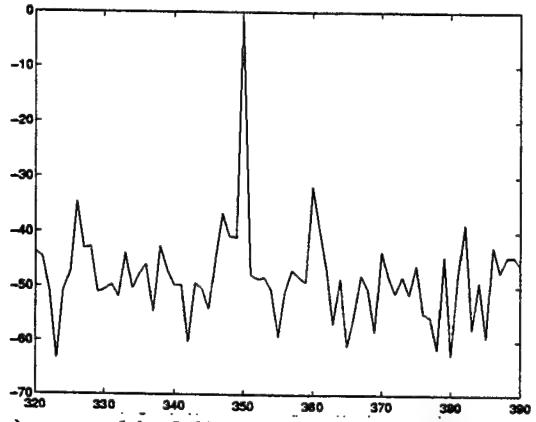

e) range bin 350, doppler frequency 0.234

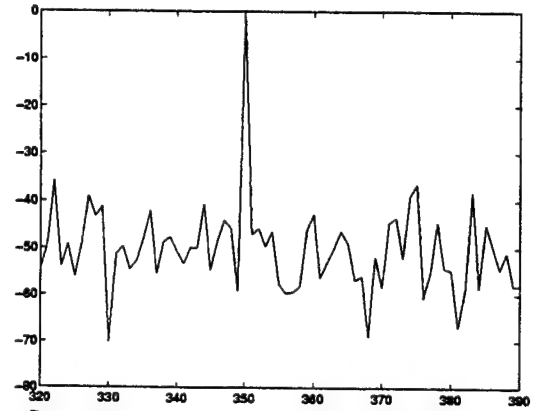

f) range bin 350, doppler frequency 0.312

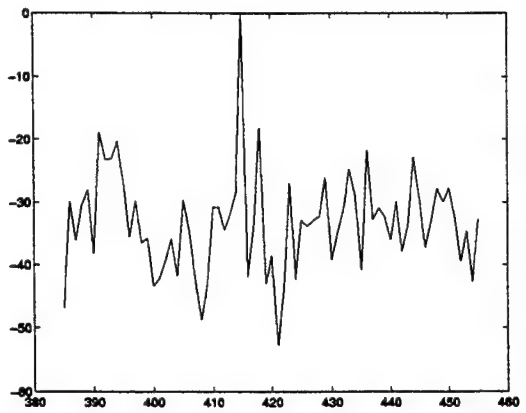

g) range bin 415, doppler frequency 0.039

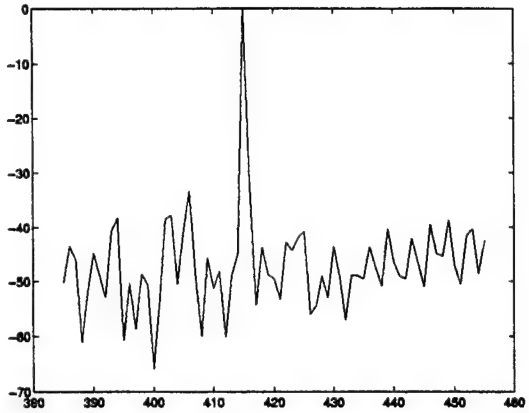

h) range bin 415, doppler frequency 0.078

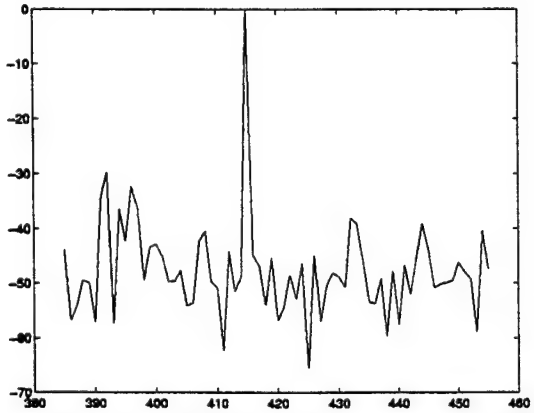

i) range bin 415, doppler frequency 0.117

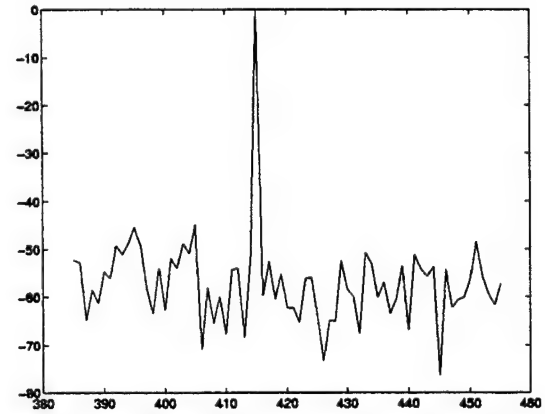

j) range bin 415, doppler frequency 0.156

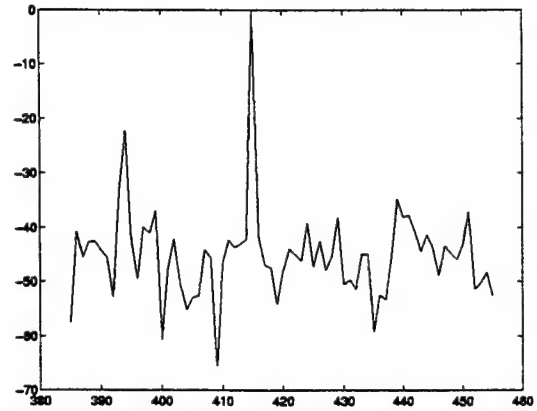

k) range bin 415, doppler frequency 0.234

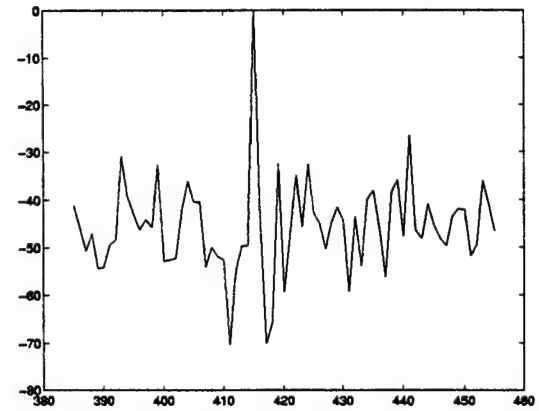

l) range bin 415, doppler frequency 0.312

Figure 11) Performance for traditional JDL when target is inserted in a particular range bin with a particular normalized Doppler frequency. In each case the normalized spatial frequency of the target is 0.164.

Chapter 3 : Performance Analysis

Applicable to both Tasks 4.1.1 and 4.1.2

Analysis of STAP Algorithms for Cases with Mismatched Statistics

Introduction

In most adaptive radar implementations, the clutter-plus-noise in the cell-under-test is characterized using samples taken from range cells that neighbor the cell-under-test. This can lead to a mismatch between the true clutter-plus-noise statistics (in the cell-under-test) and those used to design the adaptive processing scheme. Such mismatches can occur in nonhomogeneous noise-plus-clutter cases [1]. The purpose of this research is to develop analytical formulas that characterize the loss in performance due to this mismatch. These formulas should be useful as a performance metric for developing STAP schemes that are not so sensitive to mismatch. The focus is on the constant false alarm rate (CFAR) version of the sample matrix inversion (SMI) algorithm, but the analysis is extended to other algorithms also. The noise-plus-clutter, which includes clutter, jamming, and noise, is assumed to be a complex Gaussian process.

Consider a CFAR version of the SMI algorithm of the type discussed in [2,3] with the test statistic

$$\Lambda_{AMF} = \frac{\left|s^H R_e^{-1} x\right|^2}{\left|s^H R_e^{-1} s\right|} \tag{1}$$

In (1), the observed N dimensional complex vector x consists of either zero-mean complex Gaussian noise-plus-clutter with covariance matrix R_t or signal plus zero-mean complex Gaussian noise-plus-clutter with covariance matrix R_t. The signal which is added to the noise-plus-clutter is κs where s is a unit length signal vector which is completely known and κ is an unknown complex constant. The magnitude of κ sets the signal-to-noise ratio. The denominator of (1) provides the correct normalization for CFAR (for cases without mismatch). While it would be desirable to use the true

covariance[1] R_t in (1) in place of R_e, R_t is not available. Instead an estimated covariance matrix R_e is used. R_e is obtained from the maximum likelihood (ML) estimate for the case where a set of independent reference vectors $x(k)$, $k = 1,\ldots,L$ are available, all with the same distribution as the cell-under-text data x. Specifically, R_e is taken as

$$R_e = \sum_{k=1}^{L} x(k)x(k)^H \tag{2}$$

which differs from the ML estimate by a scale factor. Any scale factor modification of (2), and thus R_e, leads to the inverse of this same scale factor change in (1) which can be incorporated into the threshold (1) is compared to. Note that in practice one frequently finds R_e is not close to a scaled version of R_t, due to a variety of reasons. In fact, the expected value of R_e may differ from $L\,R_t$, which implies that even for very large L, the value of $(1/L)R_e$ will not converge to R_t. For the purpose of this paper we assume a mismatch in the reference data such that $(1/L)E\{R_e\} = R_{sd} \neq R_t$. For simplicity we assume that the reference data vectors are independent and identically distributed (iid) with a zero-mean complex Gaussian distribution with covariance matrix R_{sd}. Also, the reference data are independent from the data from the cell-under-test.

Distribution of the Test Statistic

First apply a coordinate transform, which consists of multiplication by $R_{sd}^{-1/2}$, to the observed vector from the cell-under test, the reference data vectors and to the signal vector. This transform whitens the reference data. Next, normalize the transformed signal vector so that it is again a unit vector. Then, call this transformed unit signal vector v. The operation is equivalent to scaling the signal $R_{sd}^{-1/2}s$ by dividing by $(s^H R_{sd}^{-1} s)^{1/2}$. So that signal-to-noise ratio is maintained, the transformed signal is taken to be $\beta\, v = [(s^H R_{sd}^{-1} s)^{1/2}\ \kappa]\, v$. The important parameter $|\beta|^2$ is called the signal-to-secondary

[1] This would lead to (1) being optimum [9].

noise ratio (SSNR). It plays a role similar to the role the signal-to-noise ratio plays in cases without mismatch. Next, another transformation of coordinates, which consists of multiplication by $(v, B_v^H)^H$, is made to the cell-under-test vector, the reference data vectors and to the signal vector. Here B_v *is* a matrix whose *N-1* rows consist of a set of *N* dimensional vectors which span the space orthogonal to *v*. The overall matrix $(v, B_v^H)^H$ is taken to be unitary so that the signal and noise powers are preserved. Call the transformed vector for the cell-under-test $y = (d, b^T)^T$. Here *d* is a scalar that describes the component of the vector $R_{sd}^{-1/2}x$ which lies in the direction of $R_{sd}^{-1/2}s$. On the other hand, *b* is an *N-1* dimensional vector describing the component of $R_{sd}^{-1/2}x$ that is orthogonal to $R_{sd}^{-1/2}s$. For the transformed reference vectors we employ the notation $y(k) = (d(k), b(k)^T)^T$. The transformations made have a similar flavor to those used in [4] for a similar purpose. These transformations also convert the adaptive filtering structure from the standard "direct-form" to the "generalized sidelobe canceler" form [5,6]. For generality, we could assume that the *b* and *b(k)* components are multiplied by the matrix u^H to obtain $z = u^H b$ and $z(k)= u^H b(k)$ and that *z* and *z(k), k=1,...,L* are used to form the test statistic. This allows consideration of rank reduction schemes. For cases without rank reduction, just take *u* to be an identity matrix. If rank reduction is desired then u is taken to be a column rank *M* unitary matrix where $M < N-1$. Under the assumptions outlined, we find that (1) becomes (see Appendix)

$$\Lambda_{AMF} = \frac{\left| d - \hat{r}_{zd}^H \hat{R}_z^{-1} z \right|^2}{\left| \hat{\sigma}_d^2 - \hat{r}_{zd}^H \hat{R}_z^{-1} \hat{r}_{zd} \right|} \tag{3}$$

where

$$\hat{r}_{zd} = \sum_{k=1}^{L} z(k) d(k)^H \tag{4}$$

$$\hat{\sigma}_d^2 = \sum_{k=1}^{L} d(k) d(k)^H \tag{5}$$

and

$$\hat{R}_z = \sum_{k=1}^{L} z(k)z(k)^H \tag{6}$$

Using the transformations described yields

$$E\{\hat{R}_z\} = R_m = Lu^H B_v R_{sd}^{-1/2} R_{sd} R_{sd}^{-1/2} B_v^H u = Lu^H u$$

Note that without rank reduction (u is an identity) $R_m = L\,I$, where I is an identity matrix. Now condition on z, $z(1),...,z(L)$ and note that the quantity inside the absolute value signs in the denominator of (3) can be expressed in matrix form as (as in [6] for the case without mismatch)

$$D\Sigma D^H = D\left(I - Z^H \hat{R}_z^{-1} Z\right)D^H \tag{7}$$

where

$$D = \left(d(1), d(2),..., d(L)\right)$$

and

$$Z = \left(z(1), z(2),..., z(L)\right)$$

It is possible to demonstrate (see Appendix) that the matrix Σ in (7) has rank L-M where $M \leq N-1$ ($M=N$-1 in cases with no rank reduction). Recall M is the column rank of the rank reduction matrix u. It is also possible to demonstrate (see Appendix) that $Z^H \hat{R}_z^{-1} Z$ is an idempotent projection matrix. Using this and results from [7, pp. 113-118] and [8, pp. 27-29], it follows that the denominator of (3), when conditioned on z, $z(1),...z(L)$, is a constant factor of ½ times a central chi-square distributed random variable, with $2(L-M)$ degrees of freedom. Such a random variable is denoted by $\chi^2_{2(L-M)}$. In a similar way the term in the numerator of (3), inside the $|\ \ |^2$ is

$$y_r = d - \sum_{k=1}^{L} d(k) z(k)^H R_z^{-1} z \tag{8}$$

which is zero-mean, complex Gaussian distributed when conditioned on *z, z(1),...z(L)* and assuming signal is not present. Under the same conditioning, when signal is present, y_r is complex Gaussian distributed with mean β. Under either signal absent or signal present the variance of y_r *(*same conditioning*) is*

$$Var\{y_r\} = \frac{1}{\rho} = Var\{d\} + z^H \hat{R}_z^{-1} z$$

*(*see Appendix for justification and the value of Var{d}). Next, we properly normalize (multiply by ρ*)* the numerator of (3) so it is the square of a unit-variance complex Gaussian. Conditioned on *z, z(1),...z(L),* another Theorem from [7, pp. 113-118] shows that $|\rho^{1/2} y_r|^2$ *is* a constant factor of ½ times a non-central chi-square distributed random variable with 2 degrees of freedom, $\chi_2^2(\rho|\beta|^2)$, when signal is present. When signal is absent, the same holds true with β=0. Thus, in summary, conditioned on *z, z(1),...z(L)* the test statistic in (3) is the ratio of a non-central chi-squared random variable with 2 degrees of freedom to ρ times a central chi-squared random variable with *2(L-M)* degrees of freedom

$$\Lambda_{AMF} \sim \frac{\chi_2^2\left(\rho|\beta|^2\right)}{\rho\chi_{2(L-M)}^2(0)}$$

Under the assumption that the reference data are independent from the data from the cell-under-test, the two chi-squared random variables in the numerator and denominator of Λ_{AMF} are independent. Then, from [8, p. 24-25] (with slight extension for complex quantities) the probability density function (pdf) of the test statistic is

$$f_{\Lambda_{AMF}|\rho,H_1}(\lambda|\rho) = \frac{(L-M)\rho\exp\left(-\rho|\beta^2|\right)}{(1+\rho\lambda)^{L-M+1}}\,{}_1F_1(L-M+1;1;Q) \qquad (9)$$

where

$$Q = \frac{|\beta|^2\rho^2\lambda}{1+\rho\lambda}$$

Equation (9) gives the pdf of Λ_{AMF} when conditioned on z, $z(1),\ldots z(L)$ which is equivalent to conditioning on ρ as indicated by the notation used in (9). Further the result in (9) was obtained under the signal present (H_1) hypothesis. In (9) ${}_1F_1(a;b;c)$ is used to denote the generalized hypergeometric function [8, p. 20]. The result in (9) is valid for signal absent (H_0) if one sets β=0.

To find the unconditional pdf of Λ_{AMF}, (9) must be averaged over the random fluctuations due to estimating the covariance matrix in (3). It is interesting that the loss due to this estimation enters (9) only through ρ. It is helpful to notice that ρ is directly related to the observations, as stated previously, by

$$\rho = \frac{1}{1+z^H\hat{R}_z^{-1}z} = \frac{1}{1+\xi_z^H\xi_z} \qquad (10)$$

where

$$\xi_z = \hat{R}_z^{-1/2}z$$

Thus the pdf for ρ has support for ρ between 0 and $1/Var\{d\}$ (otherwise the pdf is zero). To perform the required averaging, first note that the estimated covariance matrix in (2) is characterized by the Wishart distribution [8,9] when the reference vectors $x(k)$, $k=1,\ldots L$ are assumed to be independent and each identically distributed with zero mean and

covariance R_{sd}. The pdf for the transformed covariance matrix is also characterized by the Wishart distribution [10]

$$f_{R_z}(R) = \frac{|R_z|^{L-N+1} \exp(-tr[(u^H u)^{-1} R_z])}{\pi^{1/2(N-1)(N-2)} \Gamma(L) \cdots \Gamma(L-N+2) |u^H u|^L} \tag{11}$$

Now consider the pdf of ξ_z. Under conditioning, ξ_z *is* complex Gaussian distributed as

$$f_{\xi_z|\hat{R}_z}(\xi_z|\hat{R}_z) = \frac{|R_{tz}| \exp(-\xi_z^H R_{tz} \xi_z)}{\pi^{(N-1)}} \tag{12}$$

where

$$R_{tz}^{-1} = E\{\xi_z \xi_z^H\} = E\{\hat{R}_z^{-1/2} u^H B_v R_{sd}^{-1/2} R_t R_{sd}^{-1/2} B_v^H u \hat{R}_z^{-1/2}\}$$

Then the unconditional pdf is

$$f_{\xi_z}(\xi_z) = \iiint_{\hat{R}_z} f_{\xi_z|\hat{R}_z}(\xi_z | \hat{R}_z) f_{\hat{R}_z}(\hat{R}_z) d\hat{R}_z \tag{13}$$

where (11) and (12) are inserted. Replacing $\xi_z^H R_{tz} \xi_z$ with $tr[R_{tz}\, \xi_z \xi_z^H]$ *in (12)* further simplifies (13). Using (13) and (9), the unconditional pdf of the test statistic is

$$f_{\Lambda_{AMF}|H_1}(\lambda) = \iiint_{all \xi_j} [f_{\Lambda_{AMF}|\rho,H_1}(\lambda | \rho)]|_{\rho = 1/(Var\{d^2\} + \xi_z^H \xi_z)} f_{\xi_z}(\xi_z) d\xi_z \tag{14}$$

Distribution of ρ

It turns out that it is possible to find the distribution of ρ in (10) a different way which leads to an easier way to compute quantities like that computed in (14). To simplify things a bit, let us ignore rank reduction in the rest of this document so now we assume *M=N-1*. Now consider the random variable (*z* is a length *N-1* vector)

$$P = \frac{1}{z^H \hat{R}_z^{-1} z} = \frac{2\dfrac{z^H z}{z^H \hat{R}_z^{-1} z}}{2 z^H z} = \frac{S_1}{S_2} \tag{15}$$

Now, from (15), P is the ratio of two random variables. From [13, p 927] the first, S_1, is a central chi-squared random variable with *2(L-N+2)* degrees of freedom and S_2 is independent of S_1. The pdf of S_1 is

$$f_{S_1}(s_1) = \frac{s_1^{L-N+1}}{2^{L-N+2}\Gamma(L-N+2)} \exp\left(-\frac{s_1}{2}\right) \tag{16}$$

provided s_1 is positive, otherwise the pdf is zero. In the case without mismatch, from [7,8], the second random variable, S_2, is a central chi-squared random variable with 2(N-1) degrees of freedom. In cases with mismatch the distribution for S_2 is more complicated as we now demonstrate by extending some results from [17]. Since *z* is complex Gaussian with zero mean and covariance matrix

$$R_{MM} = B_v R_{sd}^{-1/2} R_t R_{sd}^{-1/2} B_v^H$$

we can write

$$\Pr\left[z^H z \le y\right] = \int_{z^H z \le y} \frac{1}{\pi^{N-1}\left|R_{MM}\right|} \exp\left(-z^H R_{MM}^{-1} z\right) dz$$

By factoring $R_{MM}=\Xi\Xi^H$ and defining $a=\Xi^{-1}z$ we find

$$\Pr\left[z^H z \le y\right] = \int_{a^H \Xi^H \Xi a \le y} \frac{1}{\pi^{N-1}} \exp\left(-a^H a\right) da$$

Now by forming an *N-1* by *N-1* unitary ($\psi^H \psi = I$) matrix of eigenvectors ψ such that $\psi^H (\Xi^H \Xi) \psi = \Phi$ where Φ is diagonal with elements $\phi_1, \phi_2, \ldots, \phi_{N-1}$ along the diagonal and defining $w = \psi^H a = (w_1, \ldots, w_{N-1})^T$ we obtain

$$\Pr\left[z^H z \le y\right] = \int_{w^H \Phi w \le y} \frac{1}{\pi^{N-1}} \exp\left(-w^H w\right) dw = \Pr\left(\sum_{j=1}^{N-1} \phi_j \left|W_j\right|^2 \le y\right)$$

Note that the eigenvalues $\phi_1, \phi_2, \ldots, \phi_{N-1}$ of $\Xi^H \Xi$ are exactly the same as those of R_{MM} *[17]*. Thus the distribution of S_2 is the same as the distribution of

$$2\sum_{j=1}^{N-1} \phi_j \left|W_j\right|^2$$

where the W_js are independent and identically distributed zero-mean and unit-variance complex Gaussian random variables and $\phi_1, \phi_2, \ldots, \phi_{N-1}$ are the eigenvalues of R_{MM}. Thus S_2 has characteristic function (t is the frequency variable)

$$E\left\{\exp\left\{it2\sum_{j=1}^{N-1} \phi_j \left|W_j\right|^2\right\}\right\} = \prod_{j=1}^{N-1} \int_{w_j=-\infty}^{\infty} \frac{1}{\pi} \exp\left(-\left|w_j\right|^2\right) \exp\left(it2\phi_j \left|w_j\right|^2\right) dw_j$$

$$= \prod_{j=1}^{N-1} \int_{w_j=-\infty}^{\infty} \frac{1}{\pi} \exp\left(-\left|w_j\right|^2 \left(1 - 2it\phi_j\right)\right) dw_j = \prod_{j=1}^{N-1} \left(1 - 2it\phi_j\right)^{-1}$$

(17)

where $i = \sqrt{-1}$. By expanding (17) into a partial fraction expansion one finds the pdf of S_2. First assume that all the eigenvalues are distinct so (17) becomes, after partial fraction expansion

$$\prod_{j=1}^{N-1}\frac{1}{1-2it\phi_j}=\sum_{j=1}^{N-1}\frac{b_j}{1-2it\phi_j} \tag{18}$$

with

$$b_j=\phi_j^{N-2}\prod_{k=1,k\neq j}^{N-1}\left(\phi_j-\phi_k\right)^{-1}$$

So the pdf for S_2 is (a mixture of chi-squared random variables with 2 degrees of freedom, each scaled by ϕ_j)

$$f_{S_2}(s_2)=\sum_{j=1}^{N-1}\frac{b_j}{2\phi_j}\exp\left(-\frac{s_2}{2\phi_j}\right) \tag{19}$$

as long as s_2 is positive (the pdf is zero otherwise). If any of the eigenvalues are repeated, this is easy to handle. If a particular $\phi_j=\phi$ is repeated r times this leads to replacing r terms on the right hand side of (18) with (the new partial fraction expansion)

$$\sum_{j=1}^{r}\frac{B_j}{(1-2it\phi)^j}$$

and thus these terms contribute a weighted sum (weighted by B_j) of chi-squared random variables with different degrees of freedom, each scaled by ϕ, or in equation form they contribute

$$\sum_{j=1}^{r}B_j\frac{\left(\frac{s_2}{\phi}\right)^{j-1}}{2^j\Gamma(j)\phi}\exp\left(-\frac{s_2}{2\phi}\right) \tag{20}$$

to (19) as long as s_2 is positive (the pdf is zero otherwise). Using (19) and (20) as appropriate one can find the pdf of S_2.

Now returning to (15) we find

$$f_P(p) = \int_{s_2=0}^{\infty} s_2 f_{S_1}(ps_2) f_{S_2}(s_2) ds_2 \tag{21}$$

for p ≥0. (21) is derived in the Appendix. For example, if no eigevalues are repeated (21) becomes from (16) and (19)

$$\begin{aligned}
f_P(p) &= \int_{s_2=0}^{\infty} s_2 \frac{(ps_2)^{L-N+1} \exp(-ps_2/2)}{2^{L-N+2}\Gamma(L-N+2)} \sum_{j=1}^{N-1} \frac{b_j}{2\phi_j} \exp\left(-\frac{s_2}{2\phi_j}\right) ds_2 \\
&= \frac{2^{L-N+3}\Gamma(L-N+3)}{2^{L-N+2}\Gamma(L-N+2)} \sum_{j=1}^{N-1} \frac{b_j p^{L-N+1}}{2\phi_j (p+1/\phi_j)^{L-N+3}} \times \\
&\int_{s_2=0}^{\infty} \frac{((p+1/\phi_j)s_2)^{L-N+2}}{2^{L-N+3}\Gamma(L-N+3)} \exp\left(-\frac{s_2}{2}(p+1/\phi_j)\right)(p+1/\phi_j) ds_2 \\
&= \frac{2^{L-N+3}\Gamma(L-N+3)}{2^{L-N+2}\Gamma(L-N+2)} \sum_{j=1}^{N-1} \frac{b_j p^{L-N+1}}{2\phi_j (p+1/\phi_j)^{L-N+3}} = \sum_{j=1}^{N-1} \frac{(L-N+2) b_j p^{L-N+1}}{\phi_j (p+1/\phi_j)^{L-N+3}}
\end{aligned} \tag{22}$$

where we used the normalization of a chi-squared pdf. If an eigenvalue ϕ is repeated r times then (16), (20) and (21) lead to a result with terms like

$$\begin{aligned}
&\int_{s_2=0}^{\infty} s_2 \frac{(ps_2)^{L-N+1} \exp(-ps_2/2)}{2^{L-N+2}\Gamma(L-N+2)} \sum_{j=1}^{r} \frac{B_j}{2^j \Gamma(j)\phi} \left(\frac{s_2}{\phi}\right)^{j-1} \exp\left(-\frac{s_2}{2\phi}\right) ds_2 = \\
&\sum_{j=1}^{r} \frac{2^{L-N+j+2}\Gamma(L-N+j+2)}{2^{L-N+2}\Gamma(L-N+2)} \frac{B_j p^{L-N+1}}{2^j \Gamma(j)\phi^j (p+1/\phi)^{L-N+j+2}} \times \\
&\int_{s_2=0}^{\infty} \frac{((p+1/\phi)s_2)^{L-N+j+1}}{2^{L-N+j+2}\Gamma(L-N+j+2)} \exp\left(-\frac{s_2}{2}(p+1/\phi)\right)(p+1/\phi) ds_2 \\
&= \sum_{j=1}^{r} \frac{2^{L-N+j+2}\Gamma(L-N+j+2)}{2^{L-N+2}\Gamma(L-N+2)} \frac{B_j p^{L-N+1}}{2^j \Gamma(j)\phi^j (p+1/\phi)^{L-N+j+2}} \\
&= \sum_{j=1}^{r} \frac{B_j (L-N+j+1)! p^{L-N+1}}{(j-1)!(L-N+1)!\phi^j (p+1/\phi)^{L-N+j+2}}
\end{aligned} \tag{23}$$

for the terms corresponding to a repeated eigenvalue. Using (22) and (23) allows one to find a closed form expression for the pdf of P in any given case. One must simply substitute the terms in (23) into (22) in replacement of the terms in (22) that correspond to repeated eigenvalues.

Now we can use the distribution of P to find the distribution of ρ. First consider the pdf of $R = 1/P$ which is (using standard transformation of random variable techniques)

$$f_R(r) = f_P\left(\frac{1}{r}\right)\frac{1}{r^2} \tag{24}$$

which applies for positive r (otherwise the pdf is zero). Then the pdf of $Y=Var\{d\}+R$ is

$$f_Y(y) = f_R(y - Var\{d\}) = \left(\frac{1}{y - Var\{d\}}\right)^2 f_P\left(\frac{1}{y - Var\{d\}}\right) \tag{25}$$

for y between $Var\{d\}$ and infinity. Finally $\rho = 1/Y$ so[2]

$$\begin{aligned} f_\rho(\rho \mid H_0) &= f_\rho(\rho \mid H_1) = \frac{1}{\rho^2} f_Y\left(\frac{1}{\rho}\right) \\ &= \left(\frac{1}{1 - Var\{d\}\rho}\right)^2 f_P\left(\frac{\rho}{1 - Var\{d\}\rho}\right) \end{aligned} \tag{26}$$

for $0<\rho<1/Var\{d\}$, otherwise the pdf is zero.

[2] In this case the pdf of ρ is the same under H_0 and H_1, but in cases considered later this is not true. This is the reason for the notation used in (26).

A Consistency Check

Note that in the case without mismatch ($R_{sd} = R_t$) we have $\phi_1 = \phi_2 = \ldots = \phi_{N-1} = 1$ and so (19) becomes (20) with $r=N-1$ and $B_1=B_2=\ldots=B_{N-2}=0$, $B_{N-1}=1$ and so in this case S_2 becomes a chi-squared random variable with $2(N-1)$ degrees of freedom. Under this condition the random variable P is a ratio of two chi-squared random variables and from [8] we find P is an F random variable with pdf (similar to (9))

$$f_P(p) = \frac{L!\,p^{(L-N+1)}}{(L-N+1)(N-2)!(1+p)^{L+1}} \tag{27}$$

since

$${}_1F_1(L+1; L-N+2; 0) = 1$$

Equation (27) applies for p between 0 and infinity (otherwise the pdf is zero). Now applying (24), (25), and (26) we can use the transformation to R and Y and finally ρ for $Var\{d\}=1$ to obtain (for $0<\rho<1$)

$$f_\rho(\rho|H_0) = f_\rho(\rho|H_1) = \frac{L!\,\rho^{L-N+1}(1-\rho)^{N-2}}{(L-N+1)!(N-2)!} \tag{28}$$

which matches the result in [3] as expected. As a second check, consider the case without mismatch again. We note that in this case (23) applies with $\phi_1 = \phi_2 = \ldots = \phi_{N-1} = 1$ and $r=N-1$ *and* $B_1=B_2=\ldots=B_{N-2}=0$, $B_{N-1}=1$. So we evaluate (23) under these conditions and we obtain (27) and ultimately (28) which matches the result in [3] as expected.

Probability of detection and false Alarm

The distributions of ρ found in the last section lead to an easier way, as compared to (14), to derive the detection and false alarm probabilities. The approach is similar to that taken in [3] for cases without mismatch. Conditioned on ρ, we have already shown (see discussion between (8) and (9)) that our test statistic has exactly the same form as the one

in [3, equation (27)] and so by the same arguments given there we find that the false alarm probability conditioned on ρ is

$$P_{FA|\rho} = \frac{1}{(1+\tau\rho)^{L-N+1}} \tag{29}$$

where τ is the threshold (3) is compared to[3]. It is interesting that this is exactly the expression for a scalar CFAR case with *L-N+1* reference samples (Kelly has discussed this in [14]). The unconditional false alarm probability is

$$P_{FA} = \int_0^{1/Var\{d\}} \frac{1}{(1+\tau\rho)^{L-N+1}} f_\rho(\rho \mid H_0) d\rho \tag{30}$$

where (26) should be inserted. The expression in (30) can be evaluated by numerical integration. Under H_1, the detection probability conditioned on ρ is obtained from [3,equation (33)] as

$$P_{D|\rho} = 1 - \frac{1}{(1+\tau\rho)^{L-N+1}} \sum_{m=1}^{L-N+1} \frac{(L-N+1)!}{(L-N+1-m)!m!} (\tau\rho)^m G_m\left(\frac{|\beta|^2\rho}{1+\tau\rho}\right) \tag{31}$$

where

$$G_m(y) = \exp(-y) \sum_{k=0}^{m-1} \frac{y^k}{k!}$$

as defined in [3]. Using (26) and (31) gives the unconditional probability of detection as

[3] The same threshold is compared to (1).

$$P_D = \int_0^{1/Var\{d\}} P_{D|\rho} f_\rho(\rho \mid H_1) d\rho \qquad (32)$$

Effects of Mismatch: Numerical results

Now we wish to investigate the effects of mismatch and at the same time we check the correctness of (30) and (32). For the case with mismatch (26) implies that performance is sensitive to how much

$$Var\{d\} = v^H R_{sd}^{-1/2} R_t R_{sd}^{-1/2} v \quad (33)$$

differs from unity. Further, (22) and (23) indicate that performance is also sensitive to how much the eigenvalues of

$$R_{MM} = B_v R_{sd}^{-1/2} R_t R_{sd}^{-1/2} B_v^H \qquad (34)$$

differ from unity. *Var{d}* and the eigenvalues of R_{MM} are the only parameters which effect performance[4] so we present results for various values of these parameters. We compare calculated results using (30) and (32) to Monte carlo simulations using 50,000 trials.

Consider the specific case of *N=4, L=8* and a probability of false alarm of *0.01*. Similar results are obtained in other cases. First consider the case with the eigenvalues of R_{MM} fixed at $C=[\phi_1, \phi_2, \phi_3]$. The results in Fig. 1 show that the probability of detection generally increases as Var{d} decreases with C fixed. This is reasonable since *1/Var{d}* measures the SNR of *d* and any signal energy will end up in *d*. Note the excellent agreement between the curves produced by (30) and (32) and the "points" produced by the Monte carlo simulations. In Fig. 2, Var{d} is fixed and C is varied. We see that

[4] Of course performance also depends on N and L as indicated in (22) and (23), leading to a dependence in ρ similar to that in (27).

increasing any eigenvalue, ϕ_j, is similar to increasing Var{d}. This is reasonable since each eigenvalue can be thought of as the noise-plus-clutter power from unwhitened noise-plus-clutter in a particular one-dimensional subspace. Clearly increasing noise-plus-clutter power should lead to a decrease in performance. Again, there is excellent agreement between the calculated and simulated results. In the results in Fig. 1 and Fig. 2 the threshold of the test is changed each time Var{d} or C is changed so that the probability of false alarm is fixed at 0.01. This provides an easy to interpret result.

In practice, both probability of detection and probability of false alarm will be altered due to mismatch so now we consider changes in false alarm probability. Here we fix the threshold at the value needed to achieve the correct probability of false alarm, 0.01, for the case without mismatch, Var{d}=1 and C=[1,1,1]. Fig. 3 gives results for fixed C and Fig. 4 gives results for fixed Var{d}. The results indicate that increasing Var{d} or any of the components of C leads to an increase in the probability of false alarm. This can be expected based on the interpretations of Var{d} and C in the last paragraph. Increasing either of these is like increasing the effective noise-plus-clutter power.

Now we consider an airborne radar example where ground clutter produces a clutter ridge in the two dimensional spatial-Doppler power spectral density (psd). For simpilicity, we consider R_t and R_{sd} modeled by the simple model described in [11]. This model places Gaussian humps along a line in the angle-Doppler plane to model the clutter ridge as shown in the psd in Fig. 5. The equation for this psd is

$$P_c(f_t, f_s) = \sum_{d=1}^{L} \frac{\sigma_{c,d}^2}{2\pi\sigma_{ft,d}\sigma_{fs,d}} \exp\left[-\left(\frac{(f_t - f_{ct,d})^2}{2\sigma_{ft,d}^2} + \frac{(f_s - f_{cs,d})^2}{2\sigma_{fs,d}^2}\right)\right]$$

which is a function of doppler frequency f_t and spatial frequency f_s. This psd consists of L Gaussian-shaped humps, the d th of which is centered at $(f_t, f_s) = (f_{ct,d}, f_{cs,d})$ and has amplitude controlled by $\sigma_{c,d}^2$ and a spread in angle and doppler controlled by

$\sigma^2_{fs,d}$ and $\sigma^2_{ft,d}$. The choices of the parameters used in the above equation are given in Table 1. The extra hump in Fig. 5 is inserted just in either the psd for the cell-under-test (corresponds to altering R_t *[11]*) or in the psd for the reference data (corresponds to altering R_{sd} *[11]*). This extra hump models mismatch, possibly due to some discrete scatterers. The target is located near the extra hump to have maximum effect. The performance results are shown in Fig. 6 for several different choices of target location and extra hump location. For each different choice for the location of the extra hump, the threshold of the test is changed to maintain the false alarm probability of 0.01. In all cases, if the hump is added in the reference data performance improves, but if the hump is added to the cell-under-test data performance degrades. This simple example illustrates the use of our equations in an airborne radar application.

One can explain the results in Fig. 1 through Fig . 6 by considering the changes in the pdf of ρ caused by changes in var{d} or C. Any of the decreases in Var{d} or ϕ_j causes the mass in the pdf of ρ to move towards larger values of ρ. Due to the decreasing nature of the function multiplying the pdf of ρ in the integrand of (30), this causes a decrease in the probability of false alarm. It is possible to apply similar analysis to explain changes in probability of detection also.

Extension to a more general class of Tests

Consider the class of tests considered in [12] which compare Λ_{AMF} to

$$\gamma\left[1+\alpha x^H R_e^{-1} x\right] \tag{35}$$

If α=0 this is the test we considered previously with $\tau=\gamma$. If $\alpha=1$ then this becomes the Generalized Likelihood Ratio (GLR) test [4]. In [12] α is called a sensitivity factor. The only difference between the above formula and (2) in [12] is due to the missing *1/L* in our

(2) (compare to (3) in [12]). Applying the same transformations as before yields that this is equivalent to comparing the simplified test statistic in (3) to the threshold

$$\frac{\gamma}{1-\gamma\alpha}\left[(1-\alpha)+\frac{\alpha}{\rho}\right] \tag{36}$$

This means we can find the probability of false alarm and the probability of detection for this more general class of tests by using (29) through (32) with τ replaced by the quantity in (36).

It is of interest to extend the results to other STAP algorithms. One extension is considered in the next section,

Steering and Covariance Mismatch

Now consider the case where both the steering vector and the covariance matrix have mismatch. This case provides performance for ADPCA for cases with covariance matrix mismatch. Consider the test in (1) when the steering vector is q, but were the true signal vector that is observed is the vector κs. As in the previous case, first apply a coordinate transform, which consists of multiplication by $R_{sd}^{-1/2}$, to the observed vector from the cell-under test, the reference data vectors and to the signal and steering vectors. Next, normalize the transformed signal vector so that it is again a unit vector. Call the transformed unit signal vector ν. So that signal-to-noise ratio is maintained, the transformed signal is taken to be $[(s^H R_{sd}^{-1} s^{1/2})\ \kappa]\ \nu$. Similarly, call the normalized transformed steering vector q_u. Next, another transformation of coordinates, which consists of multiplication by $(q_u, B_q^H)^H$, is made to the cell-under-test vector, the reference data vectors and to the signal and steering vectors. Here B_q *is* a matrix whose *N-1* rows consist of a set of N dimensional vectors that span the space orthogonal to q_u. The matrix $(q_u, B_q^H)^H$ is taken to be unitary. Denote the transformed vector for the cell-

under-test by $y = (d, z^T)^T$. Here d is a scalar that describes the component of the vector $R_{sd}^{-1/2}x$ which lies in the direction of q_u. On the other hand, z is an $N-1$ dimensional vector describing the component of $R_{sd}^{-1/2}x$ which is orthogonal to q_u. For the transformed reference vectors employ the notation $y(k) = (d(k), z(k)^T)^T$. Under the assumptions outlined, we again obtain (3). Further, the previous observations about (3) still hold, except that, under H_1, the expected value of y_r given z, $z(1)$, $z(2),\ldots,z(L)$ is now

$$E\{y_r \mid H_1\} = \left(\frac{q^H R_{sd}^{-1} s}{\sqrt{q^H R_{sd}^{-1} q}} \right) \kappa \tag{37}$$

and so

$$\Lambda_{AMF} \sim \frac{\chi_2^2\left(\rho \left| \frac{q^H R_{sd}^{-1} s}{\sqrt{q^H R_{sd}^{-1} q}} \right|^2 |\kappa|^2 \right)}{\rho \chi_{2(L-M)}^2(0)} \tag{38}$$

Thus the result in (38) is similar to the previous result (see the distribution of Λ_{AMF} just prior to (9)), but with a different effective value of β. The results like (9) and (15) still hold (with β set as suggested by (38)) and in fact (26) still gives the correct distribution of ρ under H_0 if we define

$$R_{MM} = B_q R_{sd}^{-1/2} R_t R_{sd}^{-1/2} B_q^H$$

However (26) does not give the correct distribution of ρ under H_1. Now, since q and s don't point in the same direction, only part of the signal goes into d, while the other part goes into z. Thus, under H_1 we find $S_2 = 2\, z^H z$ contains signal which alters the results given by (19) and (20) and thus (22) and (23). This is the key difference in this case. The signal in z also changes the effective SSNR. As we see in (38) the effective value of SSNR is reduced from $|\beta|^2$ to

$$|\beta|_{qs}^2 = |E\{y_r \mid H_1\}|^2 = \left(\frac{|q^H R_{sd}^{-1} s|^2}{q^H R_{sd}^{-1} q} \right) |\kappa|^2 = |\beta|^2 \cos^2(\theta)$$

which might be called the SSNR in the subspace spanned by the steering vector. Here $cos(\theta)$ is defined by this equation using the previous definition of $|\beta|^2=|\kappa|^2(s^H R_{sd}^{-1} s)$. For simplicity we take

$$\cos(\theta) = \frac{q^H R_{sd}^{-1} s}{\sqrt{q^H R_{sd}^{-1} q}\sqrt{s^H R_{sd}^{-1} s}}$$

where an unimportant possible complex multiple has been ommitted [3]. Now the part of $|\beta|^2$ which was lost went into z and is

$$|\mu_z|^2 = |E\{z \mid H_1\}|^2 = |\beta|^2 \sin^2(\theta) = |B_q R_{sd}^{-1/2} s|^2 |\kappa|^2$$

which could be called the SSNR in the subspace orthogonal to the steering vector.

The signal entering z changes the distribution of S_2. Thus, we now consider the distribution of S_2 (the distribution of S_1 is still given by (16)). Again we extend some results in [17]. Under H_1 z is Gaussian with mean $\mu_z = B_q R_{sd}^{-1/2} \kappa s$ and covariance matrix R_{MM}. Thus, we can write

$$\Pr[z^H z \le y] = \int_{z^H z \le y} \frac{1}{\pi^{N-1} |R_{MM}|} \exp\left(-(z-\mu_z)^H R_{MM}^{-1} (z-\mu_z)\right) dz$$

By factoring $R_{MM}=\Xi\Xi^H$ and defining $a=\Xi^{-1}z$ and $\mu_a = \Xi^{-1}\mu_z$ we find

$$\Pr[z^H z \le y] = \int_{a^H \Xi^H \Xi a \le y} \frac{1}{\pi^{N-1}} \exp\left(-(a-\mu_a)^H (a-\mu_a)\right) da$$

Now by forming an *N-1* by *N-1* unitary ($\psi^H \psi = I$) matrix of eigenvectors ψ such that $\psi^H (\Xi^H \Xi) \psi = \Phi$ where Φ is diagonal with elements $\phi_1, \phi_2, \ldots, \phi_{N-1}$ along the diagonal and defining $u = \psi^H a$ and $\omega = \psi^H \mu_a = (\omega_1, \ldots, \omega_{N-1})^T$ we obtain

$$\Pr\left[z^H z \le y\right] = \int_{u^H \Phi u \le y} \frac{1}{\pi^{N-1}} \exp\left(-(u-\omega)^H (u-\omega)\right) du$$

$$= \int_{(w+\omega)^H \Phi (w+\omega) \le y} \frac{1}{\pi^{N-1}} \exp\left(-w^H w\right) dw = \Pr\left(\sum_{j=1}^{N-1} \phi_j \left| W_j + \omega_j \right|^2 \le y \right)$$

where $w = u - \omega$. Again, we note that the eigenvalues $\varphi_1, \varphi_2, \ldots, \varphi_{N-1}$ of $\Xi^H \Xi$ are exactly the same as those of R_{MM} *[17]*.

Thus the distribution $S_2 = 2\, z^H z$ is the same as the distribution of

$$2 \sum_{j=1}^{N-1} \phi_j \left| W_j + \omega_j \right|^2 \qquad (39)$$

where as before the W_js are independent and identically distributed zero-mean and unit variance complex Gaussian random variables. In (39) $(\omega_1, \ldots, \omega_{N-1})^T = \psi^H \Xi^{-1} B_v R_{sd}^{-1/2} \kappa s$. Also, as before $\phi_1, \phi_2, \ldots, \phi_{N-1}$ are the eigenvalues of R_{MM}. Now the characteristic function for S_2 must be, using (39)

$$E\left\{\exp\left(it2\sum_{j=1}^{N-1}\phi_j\left|W_j+\omega_j\right|^2\right)\right\}=$$

$$\prod_{j=1}^{N-1}\int_{w_j=0}^{\infty}\frac{1}{\pi}\exp\left(-\left|w_j\right|^2\right)\exp\left(it2\phi_j\left|w_j+\omega_j\right|^2\right)dw_j=$$

$$\prod_{j=1}^{N-1}\int_{x=-\infty}^{\infty}\int_{y=-\infty}^{\infty}\exp\left(2it\phi_j\left[\left(x+\omega_{Rj}\right)^2+\left(y+\omega_{Ij}\right)^2\right]\right)\frac{1}{\pi}\exp\left(-\left(x^2+y^2\right)\right)dxdy$$

$$=\prod_{j=1}^{N-1}\int_{x=-\infty}^{\infty}\frac{1}{\sqrt{\pi}}\exp\left(-\left(x+\mu_{Rj}\right)^2\left(1-2it\phi_j\right)\right)dx$$

$$\int_{y=-\infty}^{\infty}\frac{1}{\sqrt{\pi}}\exp\left(-\left(y+\mu_{Ij}\right)^2\left(1-2it\phi_j\right)\right)dy$$

$$\exp\left(2it\phi_j\left|\omega_j\right|^2\right)\exp\left(\left[\mu_{Rj}^2+\mu_{Ij}^2\right]\left(1-2it\phi_j\right)\right)$$

$$=\prod_{j=1}^{N-1}\left(1-2it\phi_j\right)^{-1}\exp\left(\frac{2it\phi_j\left|\omega_j\right|^2}{1-2it\phi_j}\right)$$

(40)

where $\omega_j = \omega_{Rj} + i\omega_{Ij}$ and $\mu_j = \mu_{Rj} + i\mu_{Ij}$ are suitably chosen to make (40) true (pick the cross terms in the quadratic in the exponential to match). Now note from (40), that if all $\phi_j = 1$ and $\omega_j = 0$ (this occurs without mismatch, where $R_{sd}=R_t$ and $s=q$) then (40) implies that S_2 is central chi-squared with $2(N-1)$ degrees of freedom as suggested by the known result for the case without mismatch. If there is mismatch in covariance, but no mismatch in steering vector, then $\omega_j = 0$ and (40) matches (17). Suppose there is no mismatch of covariance matrix $R_{sd}=R_t$ but that there is a mismatch in steering vector so $s \neq q$. Then from (40), S_2 has a noncentral chi-squared pdf with $2(N-1)$ degrees of freedom, which is denoted by $\chi 2_{(N-1)}(|\omega|^2)$. Thus $R=1/P$ has an F distribution [8]

$$f_{R|H_1}(r \mid H_1) = \frac{L! r^{N-2} \exp(-|\omega^2|)}{(L-N+1)!(N-2)!(1+r)^{L+1}} {}_1F_1\left(L+1; N-1; \frac{|\omega|^2 r}{1-r} \right)$$

The pdf of ρ can be found using (25), (26) and the series expansion for ${}_1F_1$ in [8] to be

$$f_{\rho|H_1}(\rho \mid H_1) = \frac{L!(1-\rho)^{N-2} \rho^{L-N+1} \exp(-|\omega^2|)}{(L-N+1)!(N-2)!} {}_1F_1\left(L+1; N-1; |\omega|^2 \rho\right)$$

$$= \exp(-|\omega^2|) \sum_{m=0}^{\infty} \frac{1}{m!} |\omega^2|^m \frac{(L+1+m)!}{(L+1-N)!(N+m-2)!} \rho^{L-N+1} (1-\rho)^{N+m-2}$$

which checks with (30) from [3] which is appropriate for this case.

To invert (40) to obtain a pdf (in the general case) it is useful [17] to expand (40) in terms of $\theta = 1/(1 - 2it\zeta)$ by rewriting (40) as

$$E\left\{ \exp\left(it2 \sum_{j=1}^{N-1} \phi_j |W_j + \omega_j|^2 \right) \right\} =$$

$$\exp\left(-\left[\frac{1-\theta}{2} \right] \sum_{j=1}^{N-1} \frac{2|\omega_j|^2}{1-\theta\left(1-\frac{\varsigma}{\phi_j}\right)} \right) \prod_{j=1}^{N-1} \frac{\varsigma\theta}{\phi_j} \left(1 - \left(1 - \frac{\varsigma}{\phi_j} \right) \theta \right)^{-1} \qquad (41)$$

$$= \theta^{N-1} \sum_{j=0}^{\infty} e_j \theta^j$$

By canceling θ^{N-1} from both sides of (41), the coefficients of the expansion can be found by using the standard formula for Taylor series. They can be expressed as

$$e_0 = \left[\exp\left(-\sum_{j=1}^{N-1} |\omega_j|^2 \right) \right] \prod_{j=1}^{N-1} \frac{\varsigma}{\phi_j} \tag{42}$$

$$e_r = \frac{1}{2r} \sum_{j=0}^{r-1} B_{r-j} e_j \quad \text{for } r>0 \tag{43}$$

$$B_r = \sum_{j=1}^{N-1} 2\left(1-\frac{\varsigma}{\phi_j}\right)^r + r\sum_{j=1}^{N-1}\left(\frac{2|\omega_j|^2\varsigma}{\phi_j}\right)\left(1-\frac{\varsigma}{\phi_j}\right)^{r-1} \tag{44}$$

Now note that (41) says we can represent the distribution of S_2 as

$$f_{S_2}(s_2) = \sum_{j=0}^{\infty} e_j \frac{\left(\frac{s_2}{\varsigma}\right)^{N-2+j}}{2^{N-1+j}\Gamma(N-1+j)\varsigma} \exp\left(-\frac{s_2}{2\varsigma}\right) \tag{45}$$

which is a mixture of central chi-squared pdfs. In (45), we set $\zeta=1$ if all the $\phi_j \geq 1$. Otherwise we set $\zeta = \min_j \phi_j$. Now use (16), (21) and (45) to find that the pdf of p is

$$f_P(p) = \int_{s_2=0}^{\infty} s_2 \frac{(ps_2)^{L-N+1}\exp(-ps_2/2)}{2^{L-N+2}\Gamma(L-N+2)} \times \sum_{j=0}^{\infty} e_j \frac{\left(\frac{s_2}{\varsigma}\right)^{N-2+j}}{2^{N-1+j}\Gamma(N-1+j)\varsigma} \exp\left(-\frac{s_2}{2\varsigma}\right) ds_2 \tag{46}$$

which simplifies to

$$f_P(p)=\sum_{j=0}^{\infty} e_j \frac{p^{L-N+1}2^{L+j+1}\Gamma(L+j+1)}{2^{L+1+j}\Gamma(L-N+2)\Gamma(N-1+j)\left(p+1/\varsigma\right)^{L+j+1}}\times$$

$$\int_{s_2=0}^{\infty}\frac{\left(\left(p+1/\varsigma\right)s_2\right)^{L+j}\exp\left(-\left(p+1/\varsigma\right)\left(\frac{s_2}{2}\right)\right)}{2^{L+j+1}\Gamma(L+j+1)\varsigma^{N-1+j}}\left(p+1/\varsigma\right)ds_2$$

$$=\sum_{j=0}^{\infty} e_j \frac{p^{L-N+1}\Gamma(L+j+1)}{\Gamma(L-N+2)\Gamma(N-1+j)\left(p+1/\varsigma\right)^{L+j+1}\varsigma^{N-1+j}}$$

(47)

for p ≥0. Using (47) in (26) provides the desired distribution for ρ under H_1. Then (29), (30), (31) and (32) provide the probability of false alarm (using the previously found pdf for ρ under H_0) and detection.

Now note that if $\phi_1 = \phi_2 = \ldots = \phi_{N-1} = 1$ (which occurs if $R_{sd} = R_t$, thus no mismatch) then $e_0 = 1$ and $e_j = 0, j \neq 0$ from (42), (43), and (44). In this case (45) becomes a $2(N-1)$ central chi-squared pdf as required and (47) matches with (27).

Steering and Covariance Mismatch:

An Explanation for the good performance of ADPCA

We have performed numerical studies for cases with steering vector mismatch similar to those in Fig. 1 through 6. These results illustrate that performance varies with $Var\{d\}$ and ϕ_j, $j=1,2,\ldots,N-1$ in a manner similar to that shown in Fig. 1 through 6. Also $|\beta|_{qs}^2$ plays a role similar to that played by $|\beta|^2$ (SSNR) in Fig. 1 through 6. Finally, ω is a new parameter for the case with steering vector mismatch, but it is easy to understand the role of ω. An increase in any component of ω generally leads to decreases in probability of

detection and no change to probability of false alarm. Since ω is a transformation of the signal that is orthogonal to the steering vector this is reasonable.

Probably, the most interesting aspect of the results is that steering vector mismatch can sometimes offset covariance matrix mismatch. In fact, this appears to explain the good performance of ADPCA which was observed in pervious studies. Recall that one key aspect of ADPCA is that it does not use the optimum steering vector for the case where the covariance matrix is exactly known. Instead, it uses a steering vector that can whiten clutter that was not completely whitened after multiplication by the inverse of the estimated covariance matrix. Some examples of cases where steering vector mismatch offsets covariance matrix mismatch are provided in Fig. 7. In each case we see the probability of detection curve for the case of both steering and covariance matrix mismatch is above the curve for the case with just covariance matrix mismatch. We note that this does not always occur. In Fig. 8, we show cases where the probability of detection curve for the case of both steering and covariance matrix mismatch is below the curve for the case with just covariance matrix mismatch.

In fact, it is easy to explain one case where steering vector mismatch can sometimes offset a covariance matrix mismatch. Consider the case where L is very large so that R_e is very close to R_t in the case without covariance matrix mismatch and R_e is very close to R_{sd} in the case with mismatch. Now recall that R_e is used in the test statistic in (1) and that if L is very large the denominator of (1) is close to a constant which can be considered part of the threshold that is chosen to set the required false alarm probability. Now it is easy to imagine that one can choose a mismatched q that can make $q^H R_{sd}^{-1}$ closer to the optimum value of $s^H R_t^{-1}$ than $s^H R_{sd}^{-1}$ is. In fact, this is exactly the case shown in Fig. 6.

Conclusion

We would like to continue studying mismatch in order to develop STAP schemes that are robust to mismatches. We believe this is an important practical issue that deserves attention and that significant advanced can be made through such research. We believe this is clearly demonstrated by the results given in this report.

References

1. W. L. Melvin and B. Himed, ``Comparative Analysis of Space-Time Adaptive Algorithms with Measured Airborne Data", *presented at the 7th International Conference on Signal Processing Applications and Technology*, October 7-10, 1996.

2. W. S. Chen and I. S. Reed, "A new CFAR detection test for radar", *Digital Signal Processing*, Vol. 4, Oct. 1991, pp. 198-214.

3. F. Robey, D. Fuhrmann, E. Kelly, and R. Nitzberg, ``A CFAR adaptive matched filter detector", *IEEE Transactions on Aerospace and Electronic Systems*, Vol. 28, No.1, Jan. 1992, pp. 208-216.

4. E. J. Kelly, ``An adaptive detection algorithm," *IEEE Transactions on Aerospace and Electronic Systems*, AES-22, March 1986, pp. 115-127.

5. J. S. Goldstein and I. S. Reed, ``Subspace selection for partially adaptive sensor array processing," *IEEE Transactions on Aerospace and Electronic Systems*, AES-33, April 1997, pp. 539-544.

6. J. S. Goldstein and I. S. Reed, ``A tutorial on space-time adaptive processing," *IEEE Presented at the 1997 IEEE National Radar Conference*, May 1997.

7. A. D. Whalen, Detection of signals in noise, Academic Press. Inc. , Orlando, Florida, 1971.

8. R. J. Muirhead, Aspects of multivariate statistical theory, John Wiley & Sons, New York, NY, 1982.

9. J. S. Reed, J. D. Mallett, and L. E. Brennan, ``Rapid convergence rate in adaptive arrays," *IEEE Transactions on Aerospace and Electronic Systems*, AES-10, No. 6, Nov. 1974, pp. 853-863.

10. J. Capon and N. R. Goodman, "Statistical analysis based on a certain multivariate complex Gaussian distribution," *Proc. IEEE*, Vol. 58, Oct. 1970, pp. 1785-1786.

11. H. Wang and L. Cai, ``On adaptive spatial-temporal processing for airborne surveillance radar systems", *IEEE Transactions on Aerospace and Electronic Systems*, Vol. 30, July 1994, pp. 660-669.

12. S. Z. Kalson, ``An adaptive array detector with mismatched signal rejection", *IEEE Transactions on Aerospace and Electronic Systems*, Vol. 28, Jan. 1992, pp. 195-207.

13. S. Haykin, Adaptive Filter Theory, third edition, Prentice Hall, Upper Saddle River, New Jersey, 1996.

14. E. J. Kelly, ``Performance of an adaptive detection algorithm: Rejection of unwanted signals," *IEEE Transactions on Aerospace and Electronic Systems*, AES-25, March 1989, pp. 122-133.

15. L. Cai, and H. Wang ``Further results on adaptive filtering with embedded CFAR", *IEEE Transactions on Aerospace and Electronic Systems*, Vol. 30, Oct. 1994, pp. 1009-1020.

16. E. J. Kelley, Adaptive detection in non-stationary interference, Part III. Technical Report 761, M.I.T. Lincoln laboratories, Lexington, MA, Aug. 1987.

17. N. L. Johnson and S. Kotz, Distributions in Statistics: Continuous Univariate Distributions-2, Houghton Mifflin Company, Boston, MA, 1970.

Appendix

Simplification of Λ_{AMF}

Apply the transformations and normalizations as required to (1). Then use the Frobenius relation [4] in (1) to obtain

$$\Lambda_{AMF} = \frac{\left|\left(\hat{\sigma}_d^2 - r_{zd}^H R_z^{-1} r_{zd}\right)^{-1} d - r_{sd}^H \; R_z^{-1}\left(\hat{\sigma}_d^2 - r_{zd}^H R_z^{-1} r_{zd}\right)^{-1} z\right|^2}{\left\|\left(\hat{\sigma}_d^2 - r_{zd}^H R_z^{-1} r_{zd}\right)\right\|^{-1}}$$

Simplification of this (multiply numerator and denominator by the scalar equal to the square of the inverse of the denominator) gives (3).

Rank Of C

Defining

$$B = \left(b(1), b(2), \ldots, b(L)\right)^H$$

and assuming L>M and that B is full column rank (this occurs with probability 1) gives

$$Z^H \hat{R}_z^{-1} Z = \left(u^H B\right)^H \left[\left(u^H B\right)\left(u^H B\right)^H\right]^{-1} \left(u^H B\right)$$

Now noting that the column rank of u is M, implies that the rank of all of the three matrices in the product above must be M and so the product must have rank M [8, Appendix]. Thus multiplication by $Z^H \hat{R}_z^{-1} Z$ projects onto an M dimensional space. Similarly $I - Z^H \hat{R}_z^{-1} Z$ (I is an L by L identity matrix) projects onto an L-M dimensional space.

Idempotence

By direct calculation

$$\left(Z^H \hat{R}_z^{-1} Z\right)\left(Z^H \hat{R}_z^{-1} Z\right) = \left(Z^H \hat{R}_z^{-1} Z\right)$$

Variance of y_r

Using (8), the independence of d,*d(1),...,d(L),* and conditioning on *z, z(1),...,z(L) gives*

$$Var\{y_r\} = Var\{d\} + E\left\{\left|\sum_{k=1}^{L} d(k) z(k)^H \hat{R}_z^{-1} z\right|^2\right\}$$

$$= Var\{d\} + E\{d(k)^2\} z^H \hat{R}_z^{-1} \hat{R}_z \hat{R}_z^{-1} z = Var\{d\} + E\{d(k)^2\} z^H \hat{R}_z^{-1} z$$

since d*(1), ..., d(L)* are iid. Also

$$Var\{d\} = v^H R_{sd}^{-1/2} R_t R_{sd}^{-1/2} v$$

and

$$E\{d(k)^2\} = 1$$

Derivation of (21)

$$\Pr\left(p < \frac{S_1}{S_2} \le p + dp\right) = f_P(p)dp = \int_0^\infty \left(\int_{ps_2}^{(p+dp)s_2} f_{S_1 S_2}(s_1, s_2) ds_1 \right) ds_2 dp$$

$$= \int_0^\infty f_{S_1 S_2}(ps_2, s_2) s_2 ds_2 dp = \int_0^\infty f_{S_1}(ps_2) f_{S_2}(s_2) s_2 ds_2 dp$$

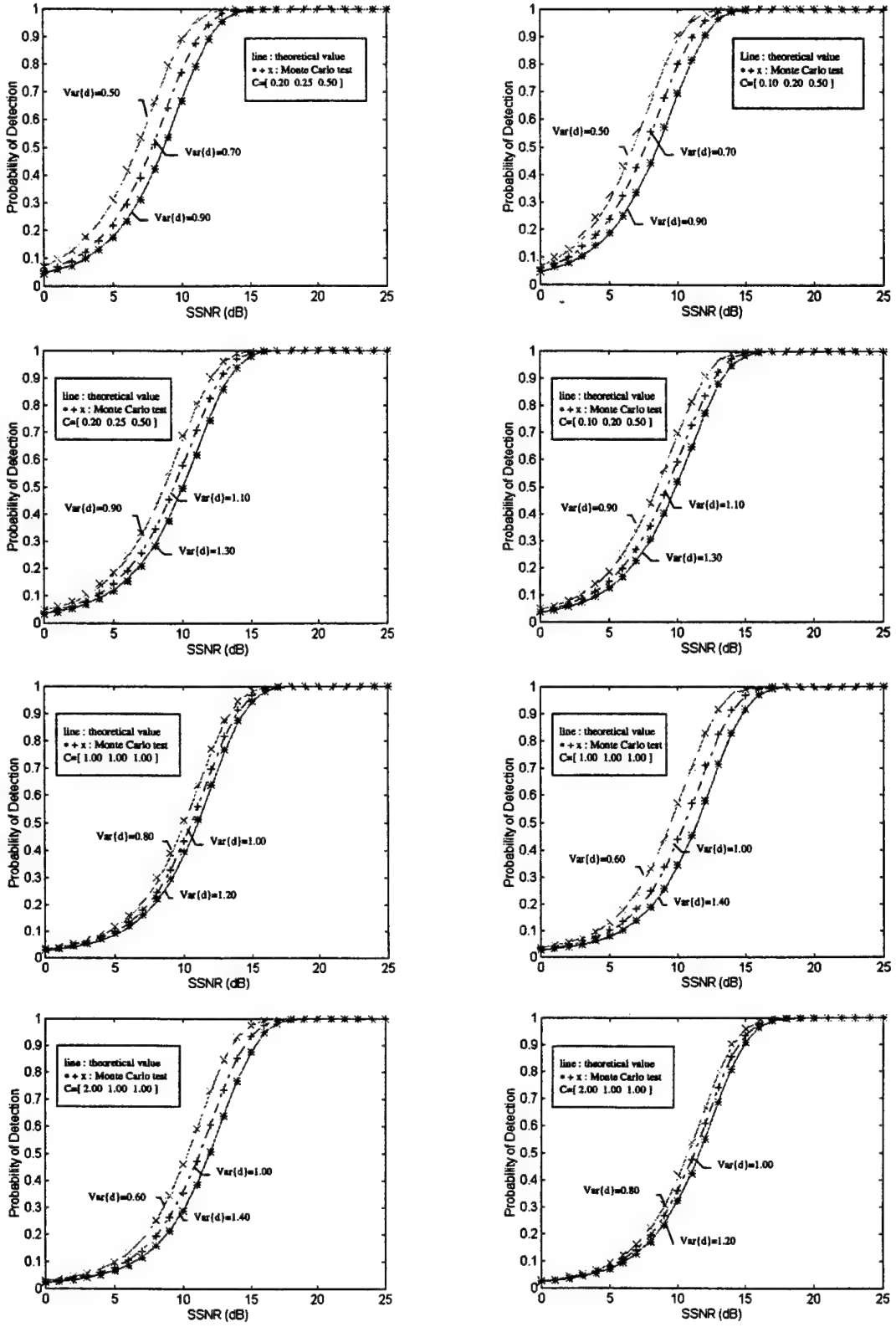

Fig. 1. Probability of detection variation with Var{d}.

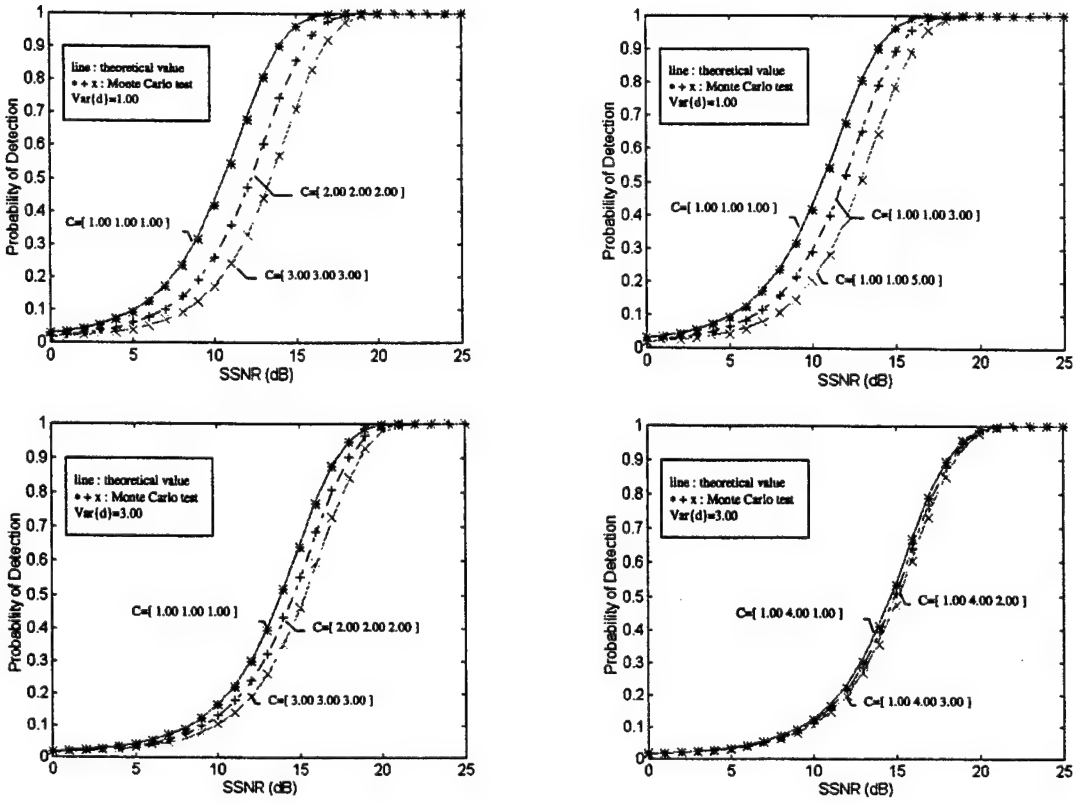

Fig. 2. Probability of detection variation with C=[ϕ_1 , ϕ_2 , ϕ_3].

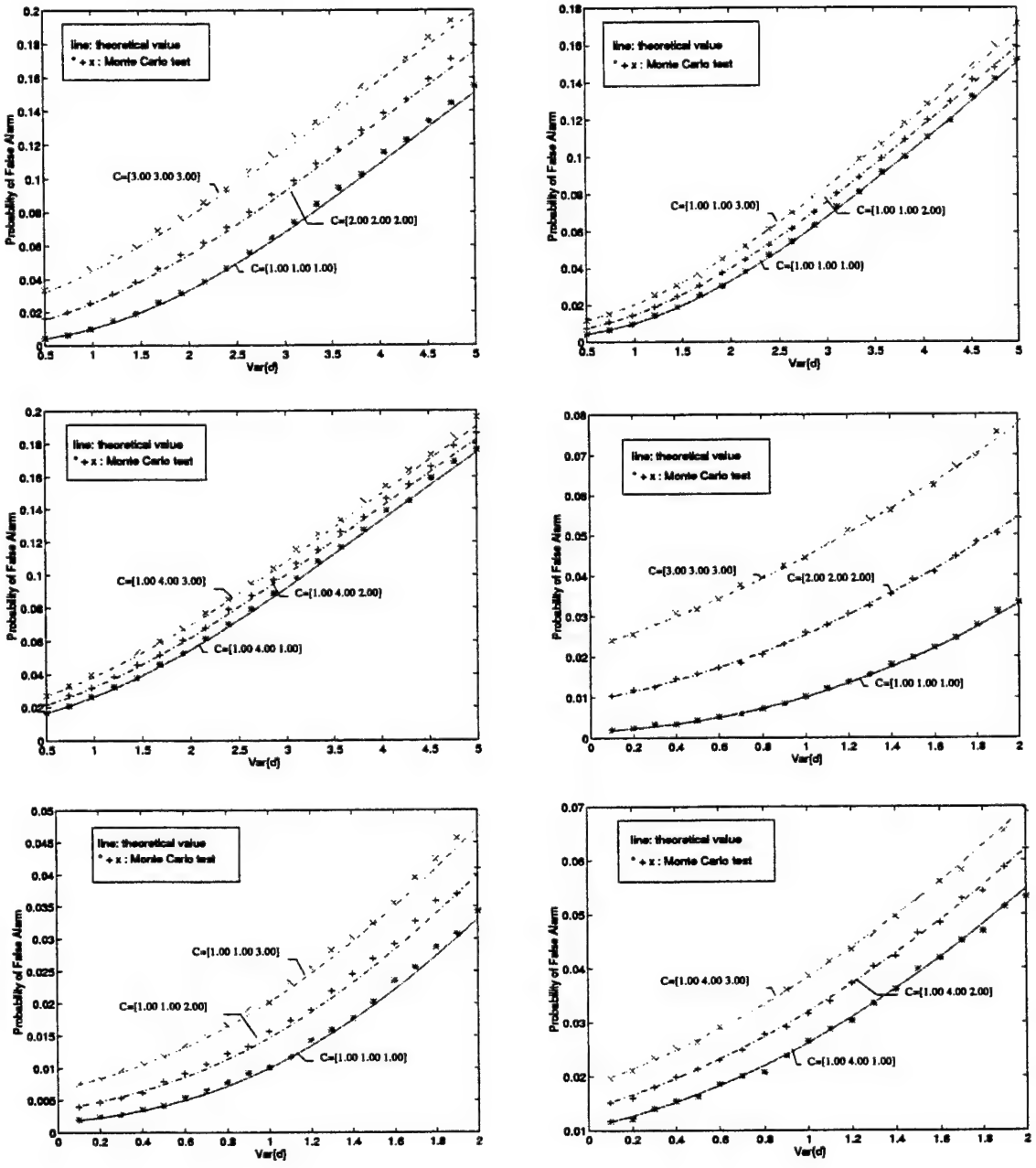

Fig. 3. Probability of false alarm variation with Var{d}.

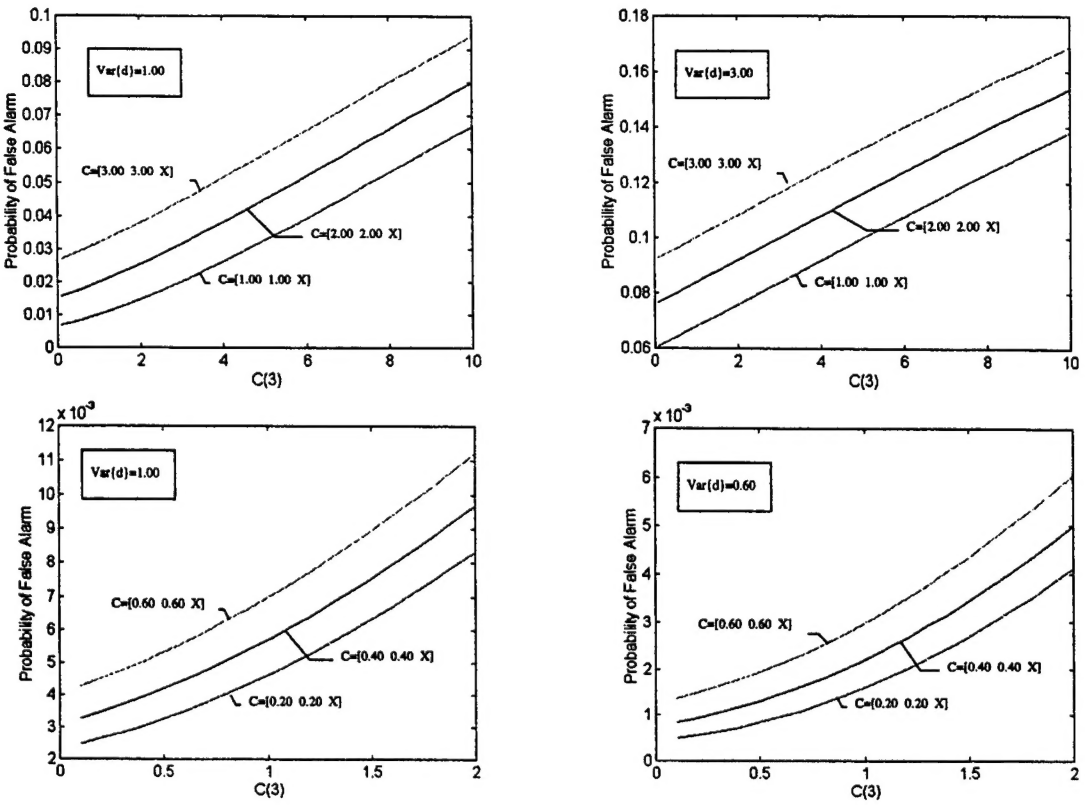

Fig. 4. Probability of false alarm variation with C.

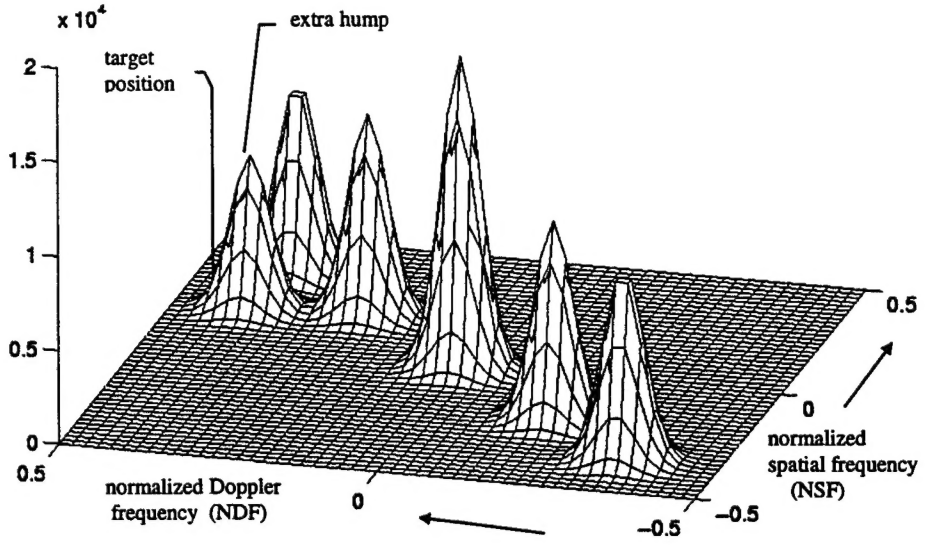

Fig. 5. Power spectral density of a simple model [17] for ground clutter and mismatch (extra hump).

Table 1. Parameters of the power spectral density model in Fig.

d	$f_{ct,d}$	$f_{cs,d}$	$\sigma_{ft,d}$	$\sigma_{fs,d}$	$\sigma_{c,d}$
1	-0.35	-0.35	0.03	0.03	8.00
2	-0.20	-0.20	0.03	0.03	8.00
3	0.00	0.00	0.03	0.03	9.98
4	0.20	0.20	0.03	0.03	8.00
5	0.35	0.35	0.03	0.03	8.00
extra hump	0.38	0.18	0.03	0.03	7.00

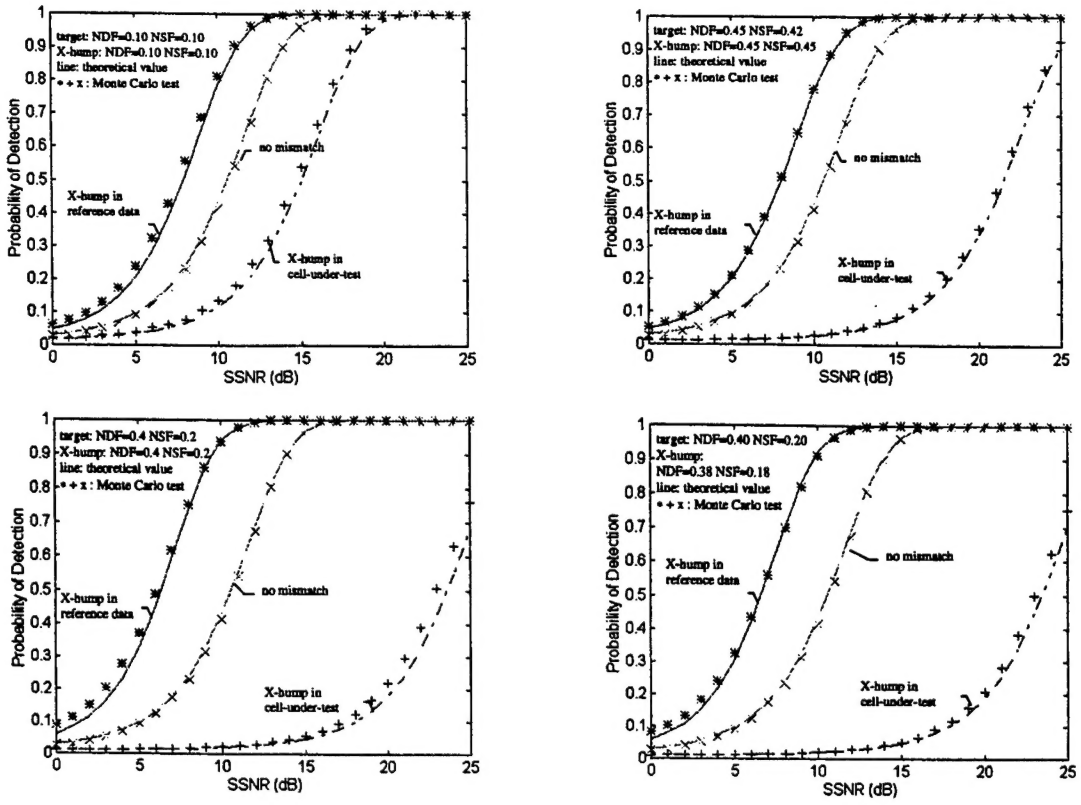

Fig. 6. Performance variation for an airborne radar example

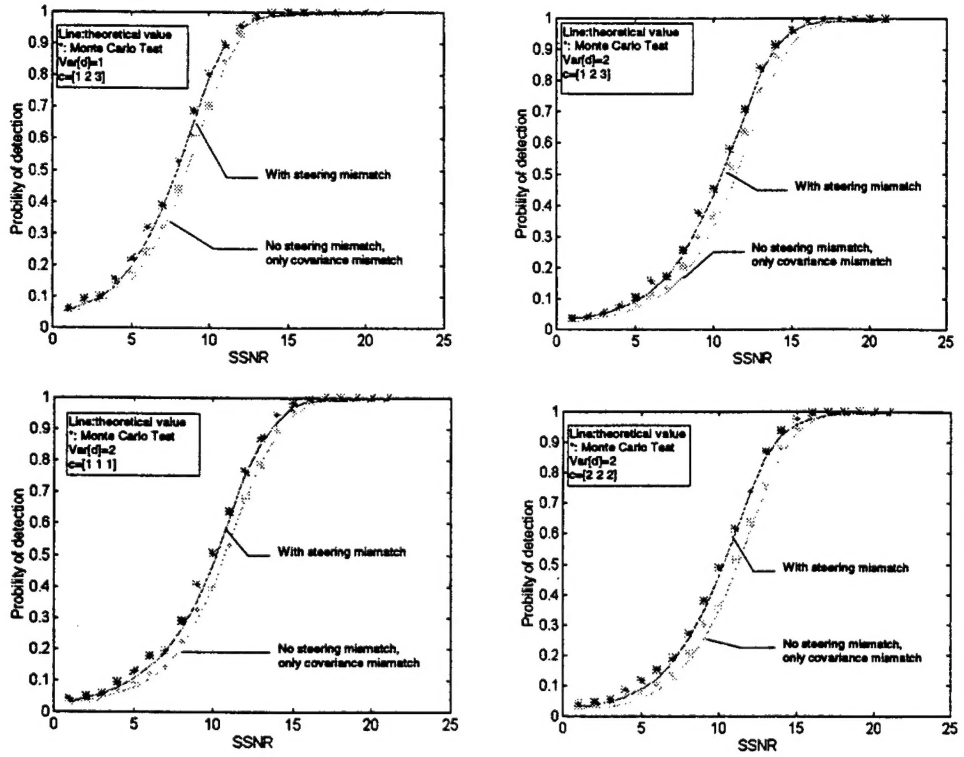

Fig. 7. Probability of detection variation with steering mismatch (offset).

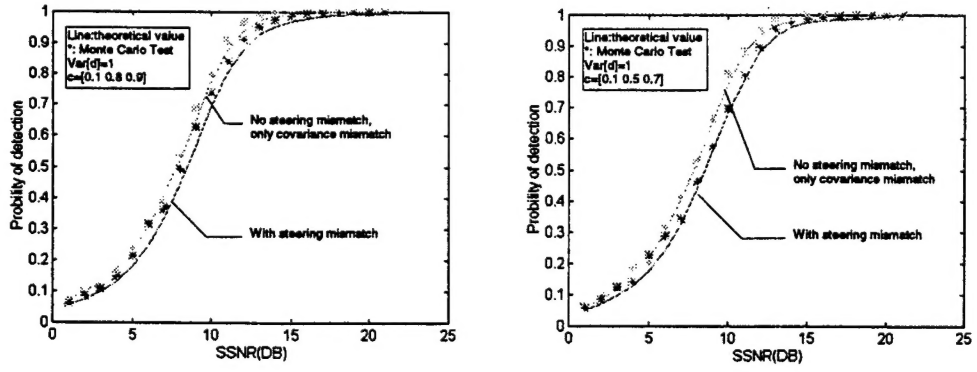

Fig. 8. Probability of detection variation with steering mismatch (not offset).

*U.S. GOVERNMENT PRINTING OFFICE: 2001-610-055-10061